IKE Institut für Kernenergetik und Energiesysteme

Development of a fast running multidimensional thermal-hydraulic code to be readily coupled with multidimensional neutronic tools, applicable to modular High Temperature Reactors

Abu Sayed Md. Kamal Hossain

February 2011, IKE 6-208

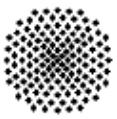

Universität Stuttgart

IKE Institut für Kernenergetik und Energiesysteme

Development of a fast running multidimensional thermal-hydraulic code to be readily coupled with multidimensional neutronic tools, applicable to modular High Temperature Reactors

Von der Fakultät Energie-, Verfahrens- und Biotechnik der
Universität Stuttgart zur Erlangung der
Würde eines Doktor-Ingenieurs (Dr.-Ing.)
genehmigte Abhandlung

Vorgelegt von

Abu Sayed Md. Kamal Hossain
geboren in Barisal, Bangladesch

Hauptberichter : Prof. G. Lohnert, Ph.D.
Mitberichter : Prof. Dr.-Ing. J. von Wolfersdorf

Tag der Einreichung: 17.06.2010
Tag der mündlichen Prüfung: 15.12.2010

ISSN 0173 6892
February 2011, IKE 6-208

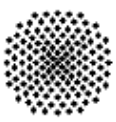

Universität Stuttgart

I dedicate this work to my late father,
who passed away during my PhD work,
may God bless his soul, and to my mother

Acknowledgements

I would like to express my deepest gratitude to my supervisor Prof. G. Lohnert for his continuous guidance throughout my research work at Institut für Kernenergetik und Energiesysteme(IKE), Universität Stuttgart. I also express my warm and sincere heartfelt thanks for every discussion that I had with him, the confidence he had shown and the vast amount of patience he had with me.

I would like to thank Prof. Dr.-Ing. J. von Wolfersdorf (Institut für Thermodynamik der Luft-und Raumfahrt, Universität Stuttgart) for his support during this work and accepting to become the co-supervisor for my thesis.

I would like to thank Prof. Dr.-Ing. E. Laurien (Institut für Kernenergetik und Energiesysteme, Universität Stuttgart) for advice and support that he showed me during my time at IKE.

Special thanks go to Dr. W. Bernnat (Institut für Kernenergetik und Energiesysteme, Universität Stuttgart), who has always guided me throughout my work; without him, my PhD work and my whole career would have been totally different.

I would like to thank Dr. M. Buck (Institut für Kernenergetik und Energiesysteme, Universität Stuttgart), who always guided me throughout this code development; without him, this code development might not be possible.

The development, validation and applications of this safety analysis codes have always been a teamwork at IKE. I thank Mr. Bürger, Mr. Pfister, Dr. Ben Said, Ms. Meier, Mr. Conti, Mr. Lapins, Mr. Bader, and all the others who have contributed to this work.

Finally, I would like to thank my family for giving me constant strength and encouragement to perform this dissertation.

Abstract

Modular High Temperature Reactors (HTRs) are considered as one of the most promising next generation reactors which will fulfil the future energy demand. The inherent safety is the most attractive feature of this type of reactor along with simplicity in design, operation and maintenance. Since the reactor is safe during any accident conditions without the actuation of any external safety systems, it is considered to be an inherently safe reactor. With its offered inherent safety features, the reactor responses solely from the reactor's physical properties, hence any dangerous situation will be avoided.

The inherent safety feature of this reactor depends entirely on the correct design of this reactor. The power density in the core, radius and height of the core, properties of the materials used and its configuration must be chosen in such a way that the decay heat produced in the core during any accident can be released to the surrounding by natural heat transfer phenomena without any help of external safety features. In addition, possible reactivity insertions into the core are limited such that the corresponding temperature increases of the fuels stay always below the fuel's temperature design limit. Along with its inherent safety feature, the reactor must be designed such a way that it offers a competitive economics.

The objective of this endeavour is to develop a fast running/multidimentional code which can be used to analyze, design and safety related issues in modular high temperature reactors. The program shall be generally applicable for modular HTRs (e.g pebble fuel, block fuel elements). Operational conditions with forced cooling as well as accident situations with heat removal by conduction and natural circulation shall be covered. Coupling to a reactor physics code shall be provided to account for the feedback of neutronics and thermal-hydraulics. Emphasis is on capturing essential effects resulting from three-dimensional features (e.g. single control rod withdrawal, power distribution with block-type fuel elements) rather than on a high level of detail, in order to keep computation times reasonably low. In general, we strive for a quick-turn analysis that provides enough insight to make informed decisions that can not wait for the extensive time it takes to conduct in-depth, detailed analyses, e.g. with large CFD models.

The porous media approach is applied. The time dependent mass and energy conservation equations and simplified steady-state momentum conservation equations (dominance of friction) are solved for the cooling gas along with the time dependent energy conservation equation for the solid. An appropriate set of constitutive equations (e.g. effective heat conductivity of solid, pressure drop, heat transfer coefficient, etc.) is applied. A finite-volume method is used for the spatial discretisation. A fully implicit method with adaptive time step selection is applied for the temporal integration in transient problems. The capability of the program for simulating both pebble bed and block fuel reactors are demonstrated by calculating two benchmark problems. The capability of the program to couple with a

neutronics system is shown by coupling the program with a point kinetics model. Finally, the tool is verified by calculating an experimental benchmark problem.

Kurzfassung

Modulare Hochtemperaturreaktoren (HTR) stellen eine vielversprechende Option für die nächste Generation von Reaktoren dar, um den zukünftigen Anforderungen an die Energieerzeugung gerecht zu werden. Die inhärenten Sicherheitseigenschaften sowie die Einfachheit der Auslegung, des Betriebes und der Wartung sind die wesentlichen ansprechenden Eigenschaften dieses Reaktortyps. Da der Reaktor unter jeglichen Unfallsszenarios auch ohne Aktivierung des Reaktorschutzsystems als sicher gilt, wird er als inhärent sicher bezeichnet.

Die inhärente Sicherheit hängt vollständig von der richtigen Auslegung des Reaktors ab. Die Leistungsdichte im Kern, Kernradius und -höhe, sowie Materialeigenschaften und -anordnung müssen so gewählt werden, dass die Nachzerfallswärme des Kernes in jeder Unfallsituation durch natürliche Wärmeübertragungsmechanismen ohne Hilfe externer Sicherheitssysteme an die Umgebung abgeführt werden kann. Auẞerdem ist der Reaktor so ausgelegt, dass bei maximaler möglicher externer Reaktivitätszufuhr die Brennstofftemperatur immer unter der maximalen Auslegungstemperatur liegt. Zusätzlich zu seinen inhärenten Sicherheitseigenschaften muss der Reaktor jedoch auch so ausgelegt sein, dass er wirtschaftlich konkurrenzfähig ist.

Ziel dieser Arbeit ist es ein schnell rechnendes/multidimensionales Programm zu entwickeln, das zur Analyse der Auslegung und sicherheitsrelevanter Fragestellungen in Hochtemperaturreaktoren eingesetzt werden kann. Der Code soll allgemein für modulare HTR (Kugel-Typ, Block-Typ) anwendbar sein. Sowohl Betriebszustände mit erzwungener Konvektion als auch Unfallsituationen sollen abgedeckt werden. Die Kopplung an einen Reaktorphysik-Code soll bereitgestellt werden um den Rückwirkungen von Neutronik und Thermohydraulik Rechnung zu tragen. Besonderes Augenmerk liegt eher auf der Abbildung der wesentlichen Effekte, die aus dreidimensionalen Eigenschaften resultieren (z.B. Auswurf eines einzelnen Kontrollstabs, Leistungsverteilung mit Block-Typ Brennelementen), als auf einem hohen Detaillierungsgrad um die Rechenzeit in einem vernünftigem Rahmen zu halten. Generell streben wir eher eine Strategie zur Analyse mit kurzen Rechenzeiten an, das jedoch ausreichenden Einblick gibt um informationsgestützte Entscheidung zu treffen, die nicht auf eine tiefgreifende Detailanalyse warten kann, wie das z.B. bei groẞen CFD Modellen der Fall wäre.

Es wird der Ansatz des porösen Mediums verwendet. Die zeitabhängigen Kontinuitäts- und Energieerhaltungsgleichungen, sowie vereinfachte Impulsgleichungen (reibungsdominiert) werden für das Kühlgas gelöst. Gleichzeitig werden zeitabhängige Energieerhaltungsgleichungen für den Feststoff gelöst. Zusätzlich wird ein Satz konstitutiver Gesetzmäẞigkeiten (z. B. effektive Wärmeleitfähigkeit im Feststoff, Druckabfall, Wärmeübergangskoeffizient) verwendet. Für die räumliche Diskretisierung wird die Methode der Finiten Volumina verwendet. Eine vollständige implizite Methode mit adaptiver Zeitschrittsuche wird für die Zeitintegration

transienter Probleme angewendet. Die Leistungsfähigkeit des Programms zur Simulation von Kugeltyp-, sowie Blocktypreaktoren wird durch die Berechnung zweier verschiedener Benchmarkproblemstellungen demonstriert. Die Möglichkeit zur Kopplung des Programms an ein Neutroniksystem wird durch Kopplung an ein Punktkinetikmodell gezeigt. Abschließend wird das Werkzeug noch durch Berechung eines experimentellen Benchmarkproblems verifiziert.

Contents

List of Tables

List of Figures

Nomenclature

Latin Symbols

A	m^2	surface area
c_p	J/kg K	specific heat capacity
D	m	core diameter
d	m	pebble diameter
d_h	m	hydraulic diameter
g	m/s^2	gravitational constant
h	J/kg	specific enthalpy
k	-	neutron multiplication factor
L	m	length
n	neutrons/m^3	neutron density
p	Pa	pressure
P	MW	power
$\dot{q}$	W/m^3	power density
R	m	core radius
r	m	radius
T	$^\circ C$	Temperature
u	m/s	velocity
V	m^3	volume

Greek Symbols

ε	-	porosity
ϵ	-	emissivity coefficient
λ	W/m K	conductivity
ρ	kg/m^3	density
μ	kg/m s	dynamic viscosity
ψ	-	pressure drop coefficient
α	W/m^2K	convective heat transfer coefficient
σ	W/m^2K^4	Stefan-Boltzmann constant
η	-	neutron reproduction factor
β	-	delayed neutron fraction
ϕ	neutrons/m^2 s	neutron flux

Indices

eff	effective
s	solid
avg	average
nu	nuclear
conv	convective
p	particle
g	gas
rad	radiation
r	radial
z	axial

Abbreviations

HTR	High Temperature Reactor
HTGR	High Temperature Gas Reactor
GIF	Generation IV International Forum
GFR	Gas Cooled Fast Reactor
VHTR	Very High Temperature Reactor
CFD	Computational Fluid Dynamics
KTA	Nuclear Safety Standards Commission of Germany
VDI	Association of German Engineers
RPV	Reactor Pressure Vessel
RCCS	Reactor Cavity Cooling System

Dimensionless Number

Nu	Nusselt Number = $\frac{\alpha \cdot d}{\lambda}$
Pr	Prandtl Number = $\frac{c_p \mu}{\lambda}$
Re	Reynold Number = $\frac{\rho u d}{\mu}$
Sc	Schmidt Number = $\frac{\mu}{\rho d}$

Chapter 1

Introduction

The world energy demand is increasing sharply with increasing population and an increasing standard of living. According to an International Energy Outlook (IEO) 2007 report, the total world energy consumption is projected to be increasing by 57% by 2030 if the present laws and policies remain unchanged [14]. If the present energy mix remains the same and if it is simply expanded proportionally to meet the future demand, the adverse effects due to the production of greenhouse gas on global climate change will be intensified. To fulfill the future demand without producing the adverse effects on the global climate, energy supply must be increased in the total energy mix which comes from safe, clean, and cost effective energy sources.

Since the first commercial reactor started to operate in 1950s, world's attention was focused on peaceful purposes of nuclear fission energy especially on power generation. Nowadays, 438 nuclear power plants are operating around the globe and producing 16% of the total electricity production (see figure 1.1). This is the biggest portion of the total electricity production that comes from non-greenhouse-gas-producing sources [49].

At this moment, at least a quarter of the total electricity production comes from nuclear power plant for sixteen countries and for the case of France and Lithuania; it is more than 75% of its total electricity. Belgium, Bulgaria, Hungary, Slovakia, South Korea, Sweden, Switzerland, Slovenia and Ukraine use one third or more while Japan, Germany and Finland use more than a quarter of their power from nuclear energy. For the US, almost one fifth of the total power is produced by nuclear plants [14].

Due to the continuous depletion of the fossil fuel, the rise of oil price, the intention to reduce the greenhouse emission and energy security for continuous economical growth, nuclear energy is seen as an obvious part of the total energy mix. Both developed and developing countries believe that a greater use of nuclear energy is required for secured future energy. If the nuclear energy can be presented as safer and more secure along with environmental benefits it already offers, it could

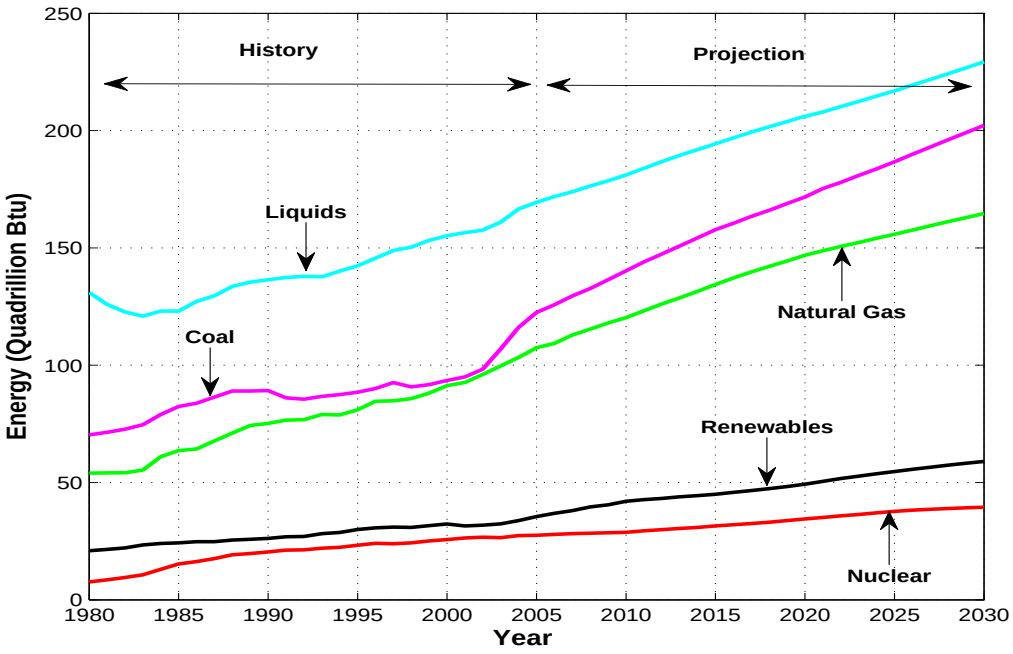

(a)

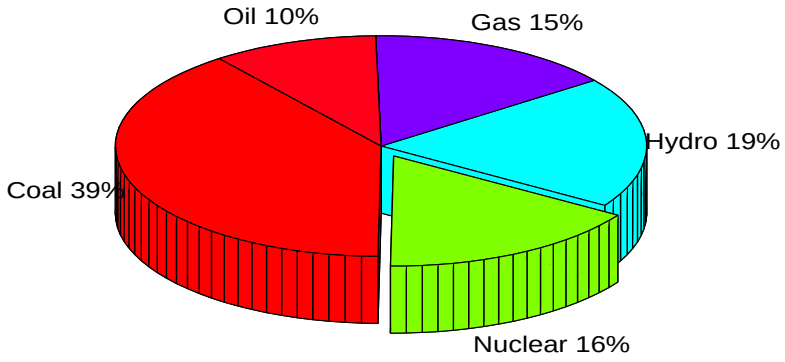

(b)

Figure 1.1: World projected energy consumption and electricity production: (a) World marketed energy use by fuel type (b)Present electricity production by fuel type [14]

attract even more people and it's use can be expanded into some more areas (e.g. production of hydrogen, process heat, desalination of sea water, etc).

To provide all the mentioned benefits, significant research and development is required on next generation nuclear systems. After realizing the need, ten countries - Argentina, Brazil, Canada, France, Japan, the Republic of Korea, the Republic of South Africa, Switzerland, the United Kingdom, and the United States- have agreed on a framework for international cooperation in research for a future generation of nuclear energy systems, known as Generation IV [49]. The objective of the Generation IV is concentrated not only on nuclear reactor and its energy systems but also on the entire fuel cycle from ore extraction to final waste disposal. The goals of the Generation IV research and development are focused on four areas:

- Manageable nuclear waste, effective fuel utilization, and increased environmental benefits.
- Competitive economics.
- Recognized safety performance.
- Secure nuclear energy systems and nuclear materials.

Considering the above mentioned goals, the following six nuclear systems are selected by the Generation IV International Forum (GIF) as 4th generation nuclear systems [49]. The importance of the gas cooled High Temperature Reactor (HTR) in the future nuclear energy systems are very clear from Table 1.1 where two of the selected six Generation IV systems are gas cooled (GFR, VHTR).

By considering the inherent safety features, environmental impact (robust fuel

Table 1.1: Generation IV reactors selected by GIF.

Generation IV System	**Acronym**
Gas-Cooled Fast Reactor System	GFR
Lead-Cooled Fast Reactor System	LFR
Molten Salt Reactor System	MSR
Sodium-Cooled Fast Reactor System	SFR
Supercritical-Water-Cooled Reactor System	SCWR
Very-High-Temperature Reactor System	VHTR

with no significant radioactive release), sustainability (high efficiency, potential suitability for various fuel cycles), economics (simplifications arising from safety features), the European Union (EU) is also working on HTRs since 1990 [19]. From

April 2005, the EU commission has started a new four years long project know as RAPHAEL (ReActor for Process Heat and Electricity) on Very High Temperature Reactors (VHTR) which is proposed by the European High Temperature Reactor Technology Network (HTR-TN). 33 organizations form 10 European countries are participating on this RAPHAEL project. The goal of the RAPHAEL project is to develop technologies for industrial production of VHTR and for all type of modular HTR.

The modular HTR is a concept which had been introduced by Reutler and Lohnert [39]. They observed that the problems arise in large HTR power plants during construction as well as during operation are related to the physical size of the large reactor core. They have also shown that by limiting the thermal power to around 200 MW, the maximum fuel temperature can be guaranteed below the critical value for all possible type of accidents. The modular HTR is a very promising reactor which is suitable for all possible plant sides and can be used for any sized plants for the production of process steam and electricity [39]. This small reactor can be connected in series for getting the required large power output while keeping the inherent safety features of small high temperature reactors. Figure 1.2 shows the axial section and passive decay heat removal systems of the HTR-Module reactor development by Interatom GmbH, Federal Republic of Germany [30] [31].

Modular high temperature reactors are designed in such a way that they offer inherent safety features. The term "Inherent safety" is a specialized term used by Lohnert [30] for describing the safety features of the HTR-Module. Due to these safety features, the reactor itself can react during accident conditions without the actuation of the active systems in such a way that no dangerous situations can occur. These safety features are governed by physical properties of the reactor components and don't depend on the external safety features. So, at any condition, whether the external safety systems are activated or not, these safety features can't fail.

In high temperature modular reactors, maximum fuel temperature is not permitted to exceed 1600 °C at any circumstances, even in the case of failure of all shutdown systems or even the failure of all reactor cavity cooling systems. In high temperature reactor, TRISO coated fuel particles are used which show structural integrity and do not release any fission products at very high temperature and burn-up. General Atomics showed that the coatings of the TRISO particle don't degrade until 2000°C for GT-MHR fuel where TRISO particle are mixed with a carbonaceous matrix and bonded into cylindrical fuel compacts [29]. Schenk has shown that no fission product release takes place below 1600°C and for a time span less than 500 hours for TRISO particle embedded in spherical fuel [43]. So, by limiting the maximum fuel temperature to 1600°C, it is assured that no release of radioactive fission product would take place even in the most extreme accident cases.

In order to limit the maximum temperature to 1600°C, the power density, the ge-

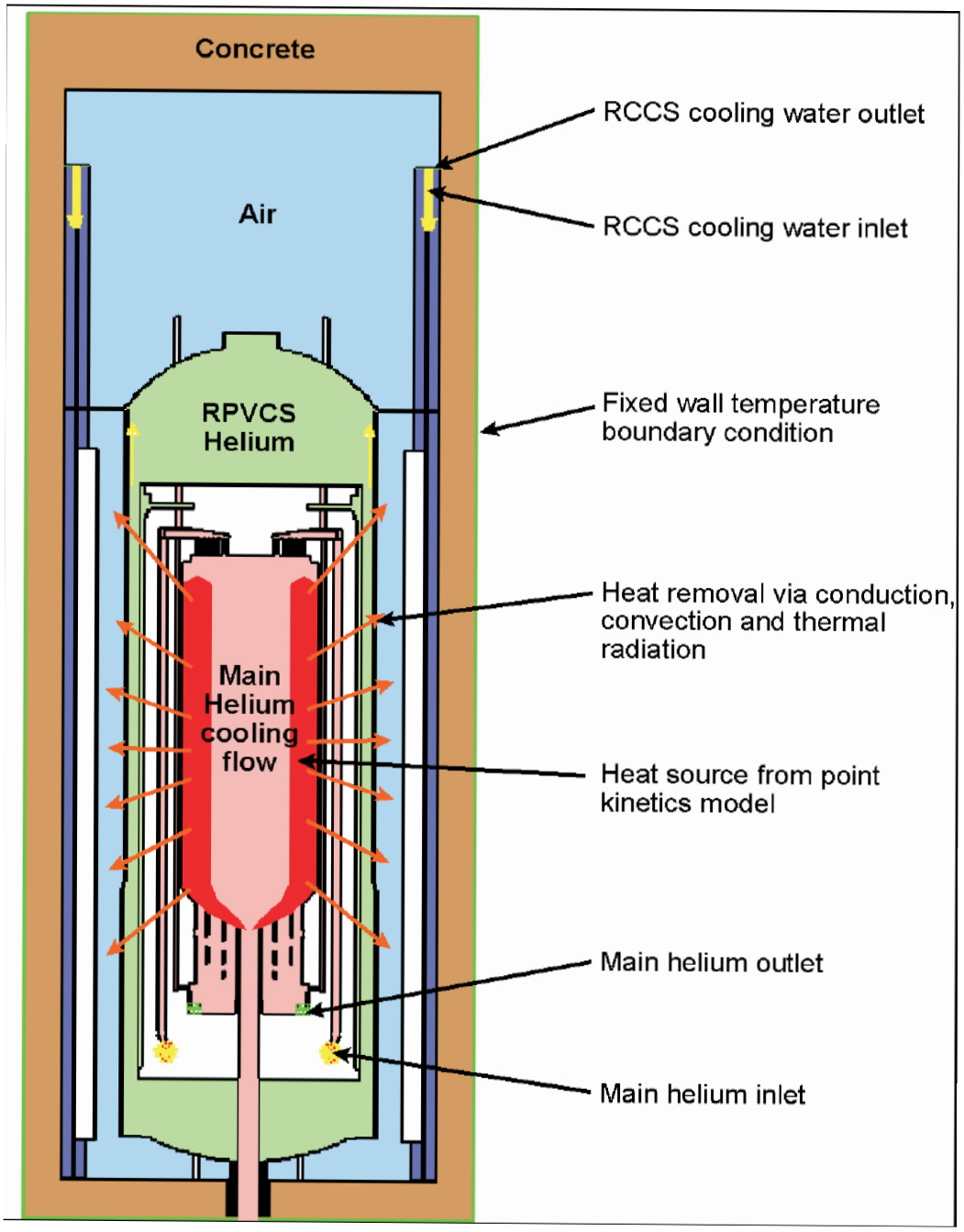

Figure 1.2: Axial section of a Modular High Temperature Reactor (PBMR) showing different components and the principle of the passive decay heat removal.

ometry (core height, radius), surrounding components, the materials used must be chosen in such a way that the decay heat produced inside the core during any accident can be released to the surroundings by natural phenomena of heat transfer. Reutler and Lohnert also showed that the only way of increasing the reactor power is by increasing the reactor height since the radius of the core is quite fixed by the requirement of the reactor shutdown system. The height of the reactor core is also fixed by the core pressure drop and attainable axial power distribution [39].So, by proper selection of geometry, power, materials; the inherent safety feature for removing decay heat during any accident can be achieved. Even in the case of a reactivity insertion accidents (e.g. withdrawing of all control rods quickly), the above mentioned criterion for fulfilling the inherent safety of the reactor can be ensured. In this case, the reactor power and the temperature starts to increase with increasing inserted reactivity. But, due to the negative reactivity coefficient of fuel and moderator, the maximum temperature does not go beyond the limiting value of 1600°C and inherent safety of the reactor can be achieved.

1.1 Objectives of the present work

For design and development of next generation high temperature reactors (HTRs), reliable simulation of heat transfer and fluid flow, coupled with neutronics inside the reactor is very essential. Among several thermal-hydraulic tools available and mostly used for designing and safety analysis of HTRs, the tool THERMIX/KONVEK developed by Jülich Research Center, Germany is very popular and well recognized [4] [35]. An in-house version of THERMIX/KONVEK (with some improvements and extended applicability for various HTRs designs, coupled with neutronics code system ZIRKUS) is routinely used also at the Institute of Nuclear Technology and Energy Systems (IKE) [7] [41]. THERMIX/KONVEK is a two-dimensional code. For designing the next generation HTRs, increasing requirements concerning accuracy and applicability are arising. The computing capacities which are nowadays available also allow us addressing three-dimensional situations that could arise from geometrical conditions, non-axisymmetric feeding or disposal of fuel pebbles, non-axisysmetric burn-up in block type fuel reactor, etc (for details, see chapter 2).

Commercial computational fluid dynamics (CFD) codes could in principle be used as a basis for this. This was demonstrated, e.g. by Becker and Laurien [5], who used the CFD code CFX4. However, application of CFD codes bears some problems in view of our objectives. They are usually quite time consuming (considering set-up of problem and calculation). The problem can be overloaded by modeling physical mechanisms and details that are not important and required, although they must resort to simplifying assumption (e.g. porous media approach in the pebble bed) anyway. Another problem is that they represent a black box (usually no access to the source code), which makes modifications and, e.g. coupling with neutronics quit impossible. On the other hand, application of CFD codes is fully

adequate for special applications, e.g. to sub-assemblies which can be fully resolved to clarify specific questions, e.g. on friction, heat transfer, mixing of hot and cold gas.

Concerning fast-running tools like THERMIX/KONVEK, 3D capabilities are presently not available. In the endeavor of developing a 3D thermal hydraulic tool, extension of the available legacy code was initially also considered. However, in view of previous experience concerning difficulties to adapt new variants, and to extend the models (due to the code structure, programming style, input handling, etc.), it was decided to base the development of the new 3D model (later on being named TH3D) on an already available code from Light Water Reactor (LWR) safety research at IKE.

The overall objectives of this endeavor are to develop a three-dimensional thermal-hydraulics tool, which could be used for multidimensional thermal hydraulic analysis and would offer the followings features:

- Applicability to simulate 3-D geometry.
- Capability to couple with a neutronics tool to get the feedback of neutronics and thermal hydraulics.
- Provide physical description adequate enough to answer questions arising from design and safety consideration.
- Fast running; simulation time is short enough to get a quick turn analysis of a design change or parameter studies.
- applicability to various HTR designs, including pebble bed and block fuel elements.

1.2 Outline of the present work

In chapter 2, the development of possible three dimensional problems in modular HTRs are described in details. The importance of considering three dimensional thermal hydraulics with respect to neutronics feedback is also described in the same chapter. In order to get the accurate thermal hydraulic behavior of modular HTRs, some parameter (e.g. porosity, emissivity, mass flow rate, etc) must be considered very carefully. In chapter 3, the factors that influence the thermal hydraulics of modular HTRs most and its level of influence are described.

The mathematical/physical model of TH3D which is a set of partial differential equations is described in chapter 4. The constitutive equations which are required to solve the partial differential equations are also described in this chapter. In order to calculate accurate fuel and moderator temperature, a detailed fuel model

for pebble fuel is implemented in TH3D. The detailed fuel model and its implementation procedures are described in chapter 4. Numerical methods used for discretization of the partial differential equations and for time integration are also described also in this chapter.

In chapter 5, the capabilities of TH3D for simulating pebble bed and block fuel elements are demonstrated. Two benchmarks oriented to pebble bed and block fuel reactors are simulated and the obtained results are compared with some recognized thermal hydraulic codes. The capability of TH3D for simulating three dimensional problems is demonstrated by simulating a situation where three neighboring control rods where withdrawn while other rods were kept at nominal operational position. The neutronics and thermal hydraulics consequences of withdrawing three control rods are described in this chapter too.

In order to get the neutronics/thermal hydraulics feedback, TH3D is coupled with a point kinetics model. The point kinetics model is described in chapter 6. The thermal hydraulic parameters that influence the neutronics feedback are also described in this chapter. In order to show the capability of TH3D being capable to be coupled with a neutronics model, a very fast transient case is simulated where all control rods are withdrawn very quickly. The results of this coupling are also presented in the same chapter.

In the validation process, an experimental benchmark is calculated. The benchmark is defined for nominal operation and for two transient cases. For all three cases, calculated results were compared with experimental data and are presented in chapter 7.

Chapter 2

Three Dimensional Problems In HTRs

Uniform power distribution is highly desirable in the reactor core for getting possible uniform outlet coolant temperature as well as for getting uniform burn-up of the fuel during reactor operation. Several measures are considered during a reactor design for getting an even distribution of neutron flux and that the uniform power distribution in the reactor core. Due to the leakage of the neutrons at the core boundaries, neutron flux is lower at the boundaries than at the center. For minimizing the ratio of the peak flux at the core center to the flux at the boundaries of the core, reactor core is generally surrounded by reflectors; higher enriched fuel is used at the boundaries of the core or for suppressing the peak flux at some region, neutron poisons are used though this option is least desirable. Despite the above mentioned measures, the neutron flux and the power density in the reactor core may vary in radial, axial, and in theta direction. If the variation in theta direction is relatively small, the reactor can be considered as cylindrically symmetric and a 2D consideration for simulating thermal hydraulics of the reactor is sufficient. But there are some situations when the variations in the theta direction become significant and the reactor geometry is no longer cylindrically symmetric and the 3D consideration of the geometry becomes a necessity for getting an accurate thermal hydraulics feedback. The following sections describe the situations, by any one of those, could create significant theta directional neutron flux/power density variations.

2.1 Non-axisymmetric Geometry

If the geometrical condition of the reactor can't be treated as cylindrically symmetric, 3D geometrical consideration becomes the only way to address this non-symmetric situation. Though most of the high temperature reactors (e.g. THTR, Modular HTR, PBMR, HTR-10, etc) can be considered as cylindrically symmetric from geometric point of view, there are rectors (e.g. AVR) which are cylindrically non-symmetric. The following figure 2.1 shows the top view of the AVR reactor

core when the core is empty and the horizontal section of the reactor. It is clearly visible from figure 2.1 that the core is not cylindrically symmetric due to the presence of the graphite structures inside the reactor core. No heat is produced in the graphite structure regions and due to presence of the control rods inside these graphite structures, power density in these regions and its surroundings is different. In this case, cylindrically symmetric power density consideration could be misleading and can't be justified. If the power density in the four graphite structural region is identical, power density in the reactor core is symmetric for every 90° cut of the reactor. So, for getting a reasonable and justified thermal hydraulic feedback of the reactor, at least a 90° cut/slice of the reactor needs to be considered.

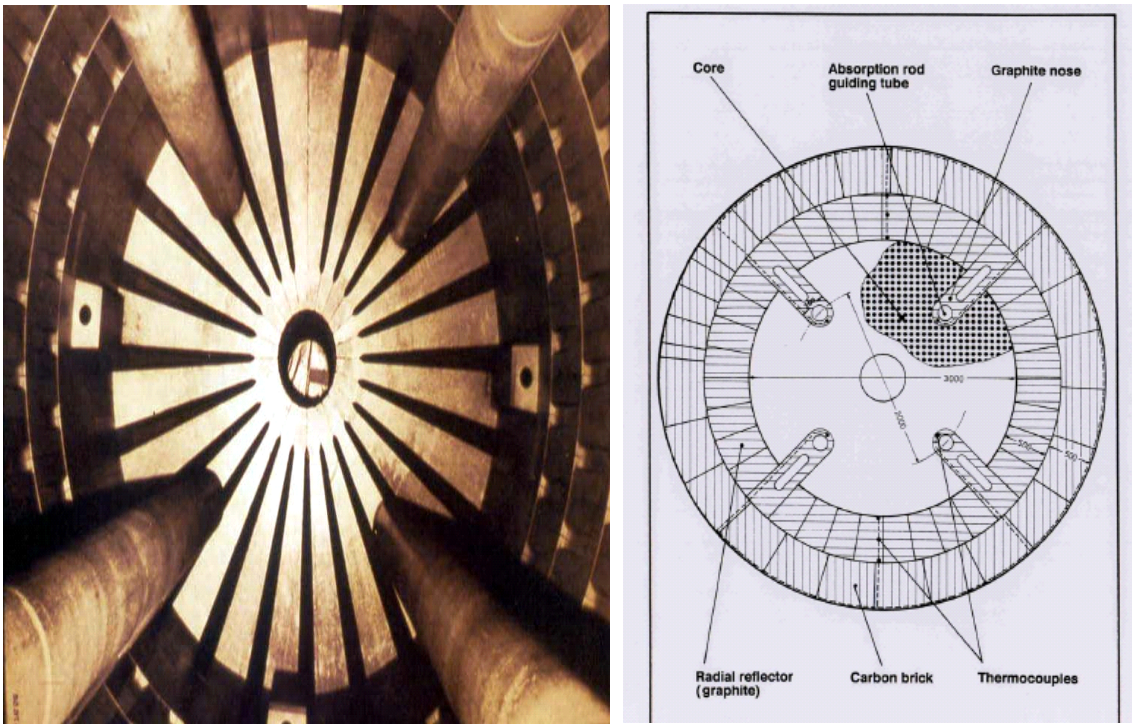

Figure 2.1: View of the empty core (left) and horizontal section of the AVR reactor.

2.2 Non axisymmetric fueling/defueling

Non-axisymmetric power distribution can be created from fueling/defueling operation of the pebble bed fuel reactors where fueling/defueling is done during the reactor's operation. In pebble bed reactors, fuel pebbles are extracted from the defueling chute at the bottom of the core and depending on the burn-up condition, integrity of the pebble, it is further used to the reactor core through the fueling chute

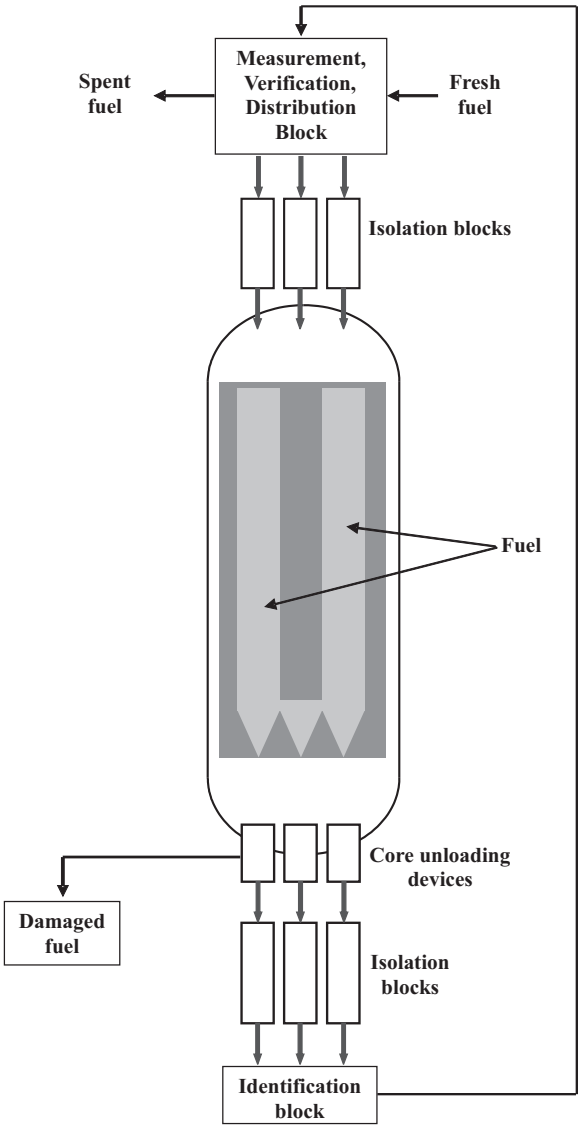

Figure 2.2: Fueling/defueling in PBMR reactor.

at the top of the reactor or send to the fuel storage tank (see figure 2.2). The number of fueling and defueling chutes varies from reactor to reactor (e.g. AVR, THTR and HTR-Module have single defueling chute and PBMR has three defueling chutes while PBMR and THTR have three and nine fueling chutes respectively). Non-axisymmetric fueling/defueling could occur from the malfunction of any of the fueling/defueling chutes which consequently produces non-axisymmetric power distribution in the reactor core.

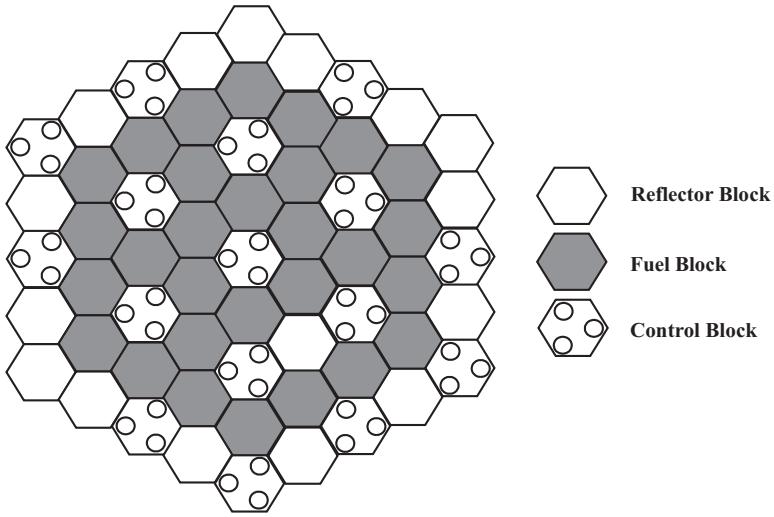

Figure 2.3: Core layout of HTTR showing fuel, reflector and control blocks.

2.3 Non-axisymmetric enrichment/burnup

Non-axisymmetric power distribution which stems from different enrichment or burnup is observed in the reactor core especially for block type reactors. The following figure shows the core layout of the HTTR reactor. Here, the gray blocks represent fuel blocks, solid white blocks represent reflector blocks and white blocks with holes represent the control blocks. The arrangement of the fuel blocks for this type of reactors can't be considered as cylindrically symmetric. Due to the high absorption of neutron in the region of control blocks, the neutron flux and thus the power density at the vicinity of the control blocks are smaller than at the vicinity of fuel blocks. So, the power density profile of the core can't be considered as cylindrically symmetric. This is a 3D situation which requires 3D thermal hydraulics/neutronics calculation for getting accurate temperature profile and power densities. Moreover enrichment and burnup is different between neighboring fuel blocks due to the yearly exchange of fuel blocks which leads to spectrum changes in neighboring fuel blocks and strong flux gradients is observed. So, a 3D thermal hydraulic/neutronics analysis is essential for getting a more accurate temperature profile in the reactor.

2.4 Non-axisymmetric Control Rod Operation

Control rods are used for controlling fission chain reaction by absorbing incident neutrons. Generally, all control rods are combined into control rod assemblies and inserted into control blocks (block fuel reactors) or into side reflectors (pebble bed reactors). Control rods are moved downward or upward depending on the desired neutron flux. During nominal operation, all control rods are kept almost at the

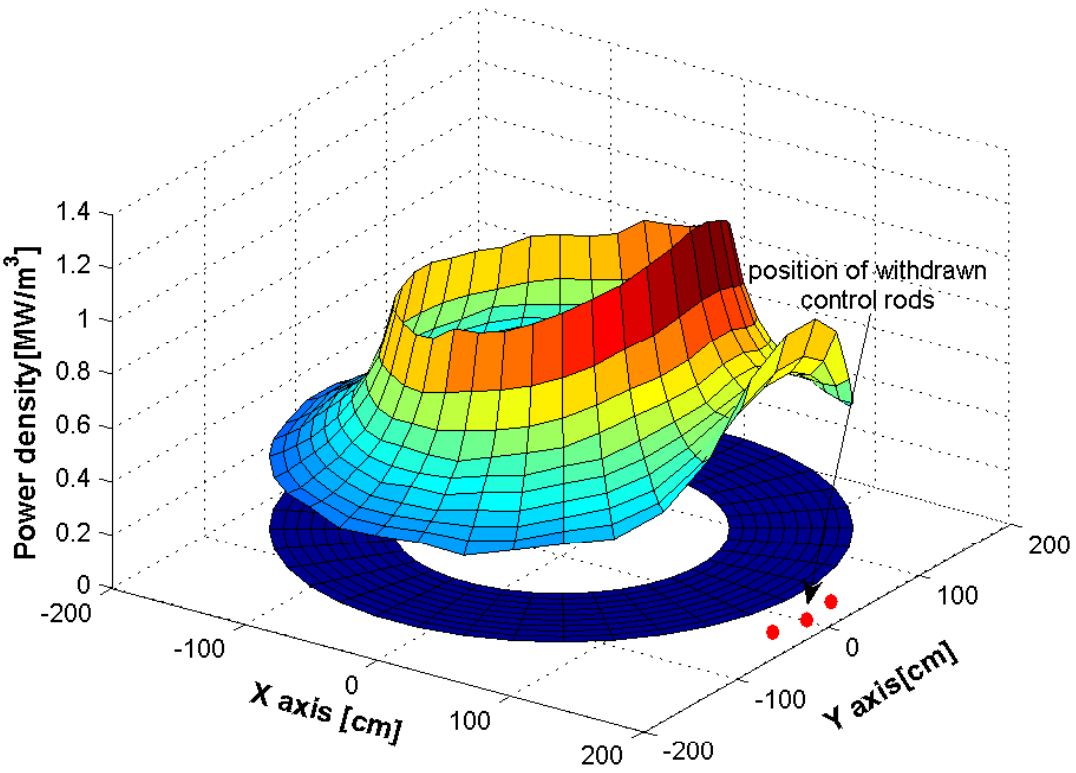

Figure 2.4: PBMR-400 power density at the top of the core during partial withdrawn of control rods.

same level for getting a smooth power distribution. But situations could arise when a single control rod or few neighboring control rods are not working and lead to a partial withdrawal or insertion of the control rod. The following figure 2.4 shows the power density for the PBMR-400 reactor at the top of the core when three neighboring control rods were withdrawn while other rods were inserted at some depth from the top of the reactor core. The withdrawal process increases the thermal flux and that the power density at the outer boundary of the core and this effect propagates up to inner reflector due to the small width of the annular core. This is a 3D situation which can't be considered as cylindrically symmetric and at least a 180° cut/slice of the reactor must be considered for getting the correct results.

2.5 Partial blockage of helium channels

This is a situation which could take place in a high temperature gas cooled reactor using block type fuel elements. This is a case where higher temperatures could

be observed locally due to the blockage of some coolant channels during nominal operation of the reactor. The blockage of the coolant channels could be the result of a possible deformation of the flow channels due to the high operating temperature, possible displacement of the fuel blocks during coolant flow, etc. Figure 2.5 shows a FA1 type fuel block used in HTGR showing the blocked and open flow channels. It is assumed that half of the heat generated in the fuel rods is transported by the coolant flowing in the flow channels. In the case of blockage of some flow channels around the fuel rods, fuel temperature starts to increase due the lack of forced cooling heat transfer. If this condition prevails, the local temperature could exceed the maximum permissible limit 1600°C and could contaminate the coolant gas by fission product release due to the local failure of coated particles. This is a situation which can't be addressed by assuming the reactor cylindrically symmetric.

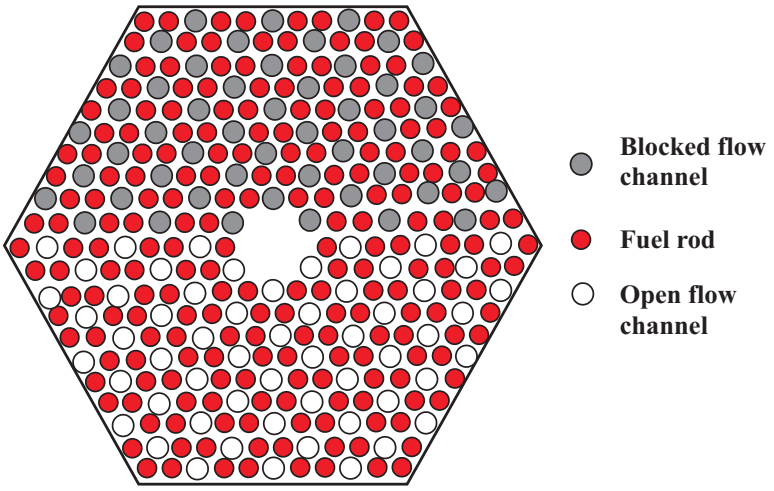

Figure 2.5: HTGR fuel assembly (FA1 type) showing fuel rod, flow channels.

Chapter 3

Factors Influence the Thermal Hydraulics of HTRs

Nuclear heat is produced inside the reactor core and this produced heat must be transported out of the reactor for avoiding any severe consequences. In nominal operation case, coolant gas flowing through the core heats up by receiving the heat produced in the fuel. The main mechanism of this heat transfer is forced convection. Almost all generated heat is transported out in the axial direction by forced convection along with very small heat loss at the radial boundaries. The heat loss at the radial boundaries is the results of radial heat conduction and radiation. But during accidents, when coolant flow is absent, the radial heat transport governs over axial heat transport. The main mechanisms of heat transport during accidents are natural convection, solid conduction and radiation. Depending on the reactor configuration, operating condition, the contribution of each heat transport mechanism varies. In the following sections, the factors that influence those heat transport mechanisms and thus the thermal hydraulics behavior of the reactor are discussed.

3.1 Coolant Flow

The amount of heat which is transferred from solid phase to gas phase depends on flow conditions, geometrical conditions, material properties, etc. and is calculated by using Newton's law of heat transfer. According to Newton's law of heat transfer, the amount of heat transferred is proportional to the heat transfer coefficient, the temperature gradient between two phases and solid surface area. Heat transfer coefficient is different for different reactor structures and will be described in details in the mathematical modeling sections. Generally, the heat transfer coefficient is directly proportional to the dimensionless Nusselt number Nu and increases with increasing value of Nusselt number if other parameters remain constant. The Nusselt number is a function of Reynolds number and Prandtl number and consequently a function of flow condition. If other parameters remain constant, the Reynolds number increases with increasing mass flow. For a pebble type fuel re-

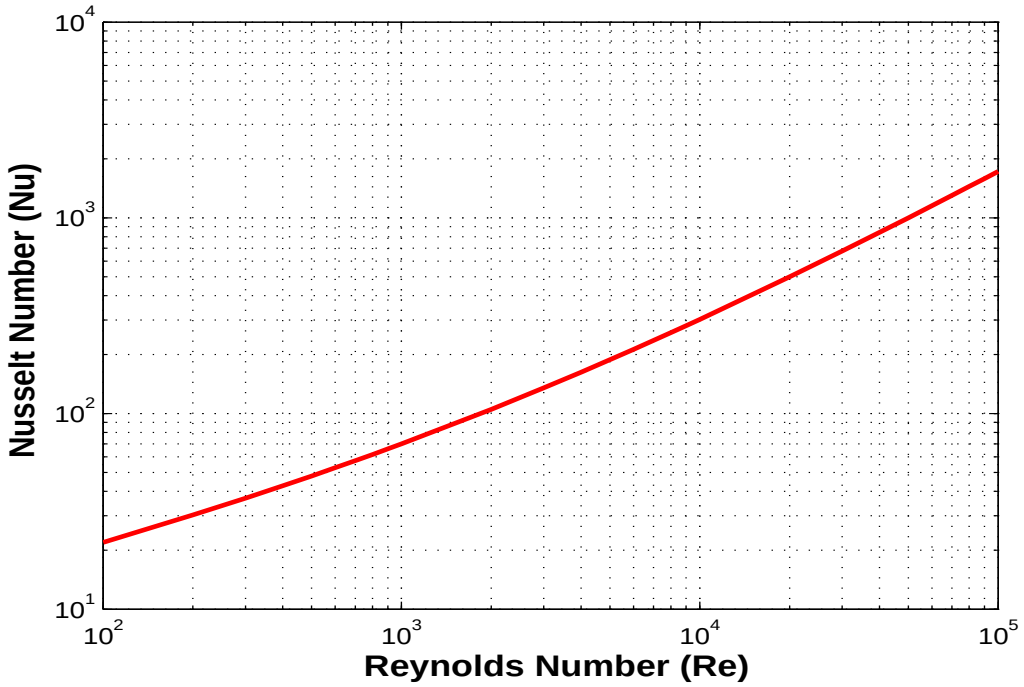

Figure 3.1: Nusselt number versus Reynolds number according to KTA norm. (Pr = 0.7, ε = 0.39).

actor (PBMR-400, HTR Module, etc) in nominal operation, the forced convective heat and mass transfer from solid phase to gas phase takes place in the range of Reynolds numbers $5 * 10^2 < Re < 10^4$ [18]. The dependency of heat transfer on Reynolds number was examined in numerous experiments by varying Schmidt number, Prandtl number and porosity. Figure 3.1 shows the dependency of Nusselt number on Reynolds number according to the KTA norm [27]. With the increasing Reynolds number, the Nusselt number and the heat transfer coefficient and thus the convective heat transfer increases.

3.2 Porosity

Porosity is the measure of the void fraction in a material volume. In other words, it is the fractional part of the volume which is not filled with the material. When the value of the porosity is expressed as fraction, mathematically its value lies in between 0-1 and when expressed in percentage, it lies in between 0%-100%. Typically porosity lies from 0.01 (for solid granite) to 0.90 (for some membranes). The porosity of a packed bed can be expressed as:

$$\varepsilon = \frac{V_{void}}{V} \tag{3.1}$$

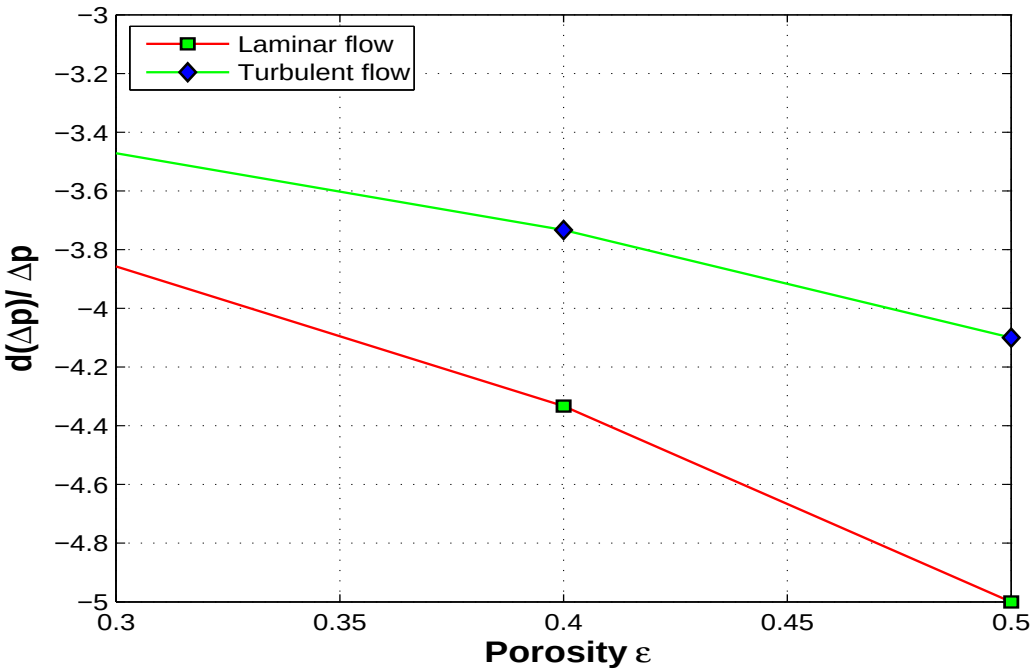

Figure 3.2: The influence of porosity on pressure drop.

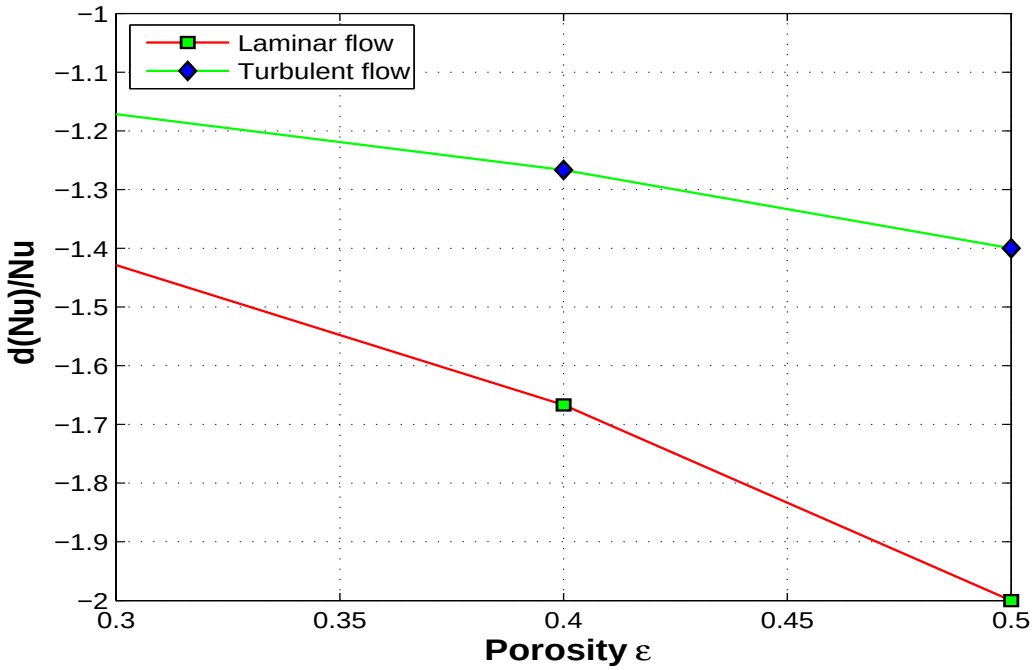

Figure 3.3: The influence of porosity on convective heat transfer.

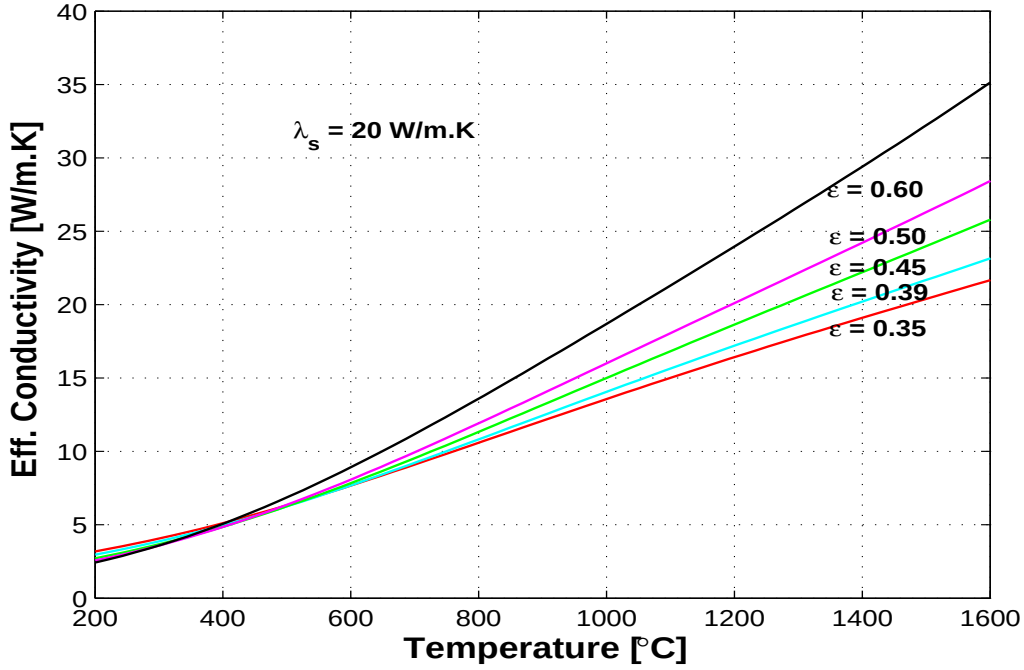

Figure 3.4: Influence of porosity on effective heat transfer,(p=1 bar, ϵ_{rad}=0.8).

where, ε is the porosity of the packed bed, V_{void}, V_{solid} and V are the volume of the void fraction, volume of the solid fraction and total or bulk volume, respectively. In the pebble bed reactor, the core consists of randomly packed same size spherical pebbles with a homogeneous porosity except at the wall region. Near the wall, the porosity is higher due to the presence of the wall. The bulk porosity of the pebble bed depends on the ratio of the core diameter D to the fuel pebble diameter d. When the ratio D/d $>$ 2, the average porosity of the pebble bed can be calculated as [9]:

$$\varepsilon_{avg} = \frac{0.78}{(D/d)^2} + 0.375 \tag{3.2}$$

where ε_{avg} is the average porosity. It can be seen from the above equation that the average porosity of the pebble bed decreases with increasing value of D/d ratio and becomes 0.375 when D/d$\rightarrow \infty$. Since the D/d ratio in the nuclear reactor is very large, the wall effects on the overall flow through the pebble bed are small. According to Kugeler/Schulten, the porosity of a pebble bed high temperature reactor lies in between 0.37 to 0.42 and a value of 0.39 is suggested for calculation purposes [28]. In the early sixties, Benenati and Brosilow have measured the void fraction as function of core radius for different D/d ratios and also showed that the void fraction is maximum (100%) at the wall and falls to a minimum (25%) at

a distance of approximately the radius of the ball away from the wall [6].

The coolant gas flowing in the reactor bed encounters a friction force. This is an additional force added in the momentum conservation equation of the gas along with pressure force, body force and shear force. Since the value of this friction force is higher than some terms in the momentum equation (e.g. viscous term, diffusion term, etc), it dominates the flow patterns significantly. The friction force relates with the bed porosity and decreases with increasing bed porosity. Henri Fenech [18] showed analytically the influence of porosity on pressure drop for a uniformly packed bed spheres. The variation of pressure drop with porosity can be written as:

$$\frac{d(\Delta p)}{\Delta p} = -\frac{3-\varepsilon(2-n)}{1-\varepsilon}\frac{d\varepsilon}{\varepsilon} \tag{3.3}$$

It can be shown from the above equation that a positive relative variation of the porosity $d\varepsilon/\varepsilon$ causes a negative variation of $d(\Delta p)/\Delta p$ by a factor of $[3-\varepsilon(2-n)]/(1-\varepsilon)$. Here n=1 for laminar flow and n=0.1 for turbulent flow which comes from the correlation used for determining friction force coefficient. Figure 3.2 shows the effect of void fraction on pressure drop.

Porosity also influences the heat transfer process. Porosity plays a role on both convective (forced and natural) as well as on conductive heat transfer. The influence of porosity on convective heat transfer can be written as:

$$\frac{d(Nu)}{Nu} = -\frac{1-n\varepsilon}{1-\varepsilon}\frac{d\varepsilon}{\varepsilon} \tag{3.4}$$

A positive relative variation of the porosity $d\varepsilon/\varepsilon$ causes a negative variation of $d(Nu)/Nu$ by a factor of $(1-n\varepsilon)/(1-\varepsilon)$. Here n = 0.6 for turbulent flow and n = 0 is used for laminar flow. Figure 3.3 shows the influences of porosity on heat transfer.

The influences of porosity on the conductive heat transfer show a quite different picture compared to the convective heat transfer. Figure 3.4 shows the variation of effective heat conductivity versus temperature depending on porosity for a packed pebble bed of uniform sphere calculated by Zehner and Schlünder model [54]. At low temperature, the solid-solid and fluid-solid conductive heat transfer dominate over the radiation heat transfer in the pores and the effective heat transfer decreases slightly with increasing porosity. But with increasing temperature, the radiation starts to dominate and the effective heat transfer increases with increasing bed porosity.

3.3 Emissivity

The radiative heat transfer is one of the most important modes of heat transfer in HTRs due to the occurrence of very high temperature during nominal operation and especially during the case of accidents. For a perfect black body, which absorbs and emits all incident radiation, the radiation heat transfer is calculated by using Stefan-Boltzmann equation and is proportional to the fourth power of the absolute temperature of the body [21]. But the reactor core, reflectors, structures, etc are made of graphite, steel, iron, which do not have the theoretical black body properties, are treated as gray bodies. For calculating radiation heat transfer for gray bodies, a term emissivity is introduced. Emissivity is a material surface property which relates the radiation of a gray surface to that of an ideal black surface. This is the ratio of radiation heat transfer of a material to the radiation heat transfer of a black body. For a pure black body, the emissivity co-efficient $\epsilon = 1$ and less than one for others.

Emissivity influences the heat transfer not only in the reactor core but also the heat transfer across the reactor cavities. Due to the complicated geometrical configuration it's very difficult to calculate the detailed radiation heat transfer in the reactor core. In the reactor core, the conductive and radiative heat transfer are coupled and calculated by using effective heat conductivity correlations which are verified by experimental values. In TH3D, several correlations were implemented but the verification calculations were made by using the well recognized Zehner and Schlünder model [53] for pebble bed reactors. Figure 3.5 shows the influence of emissivity on effective heat conductivity of the reactor core calculated by Zehner-Schlünder model. With increasing emissivity, the radiative heat transfer contribution increases and thus the total effective conductivity but the contribution of solid-solid conduction and fluid conduction remain unchanged. The influence of emissivity is more important during accident cases since this influence is more pronounced in the higher temperature region.

3.4 System Temperature and Pressure

During nominal operation, the high temperature reactor is highly pressurized and the heat produced inside the reactor core is transported by forced convective flow. But, during accident cases, the reactor could be depressurized due to the break of a pipe followed by loss of forced cooling. The thermal hydraulic behavior of HTR is significantly influenced by the system pressure during accident conditions. The influence comes from the properties of the coolant helium which varies significantly with pressure. Figure 3.6 shows the variation of helium properties with pressures [25]. With increasing pressure, the conductivity of the helium increases which enhances the conductive heat transfer inside the core. But this influence on total heat transfer process is not significant since the value is still small at high pressure. The main influence comes from the role of increased helium density with increas-

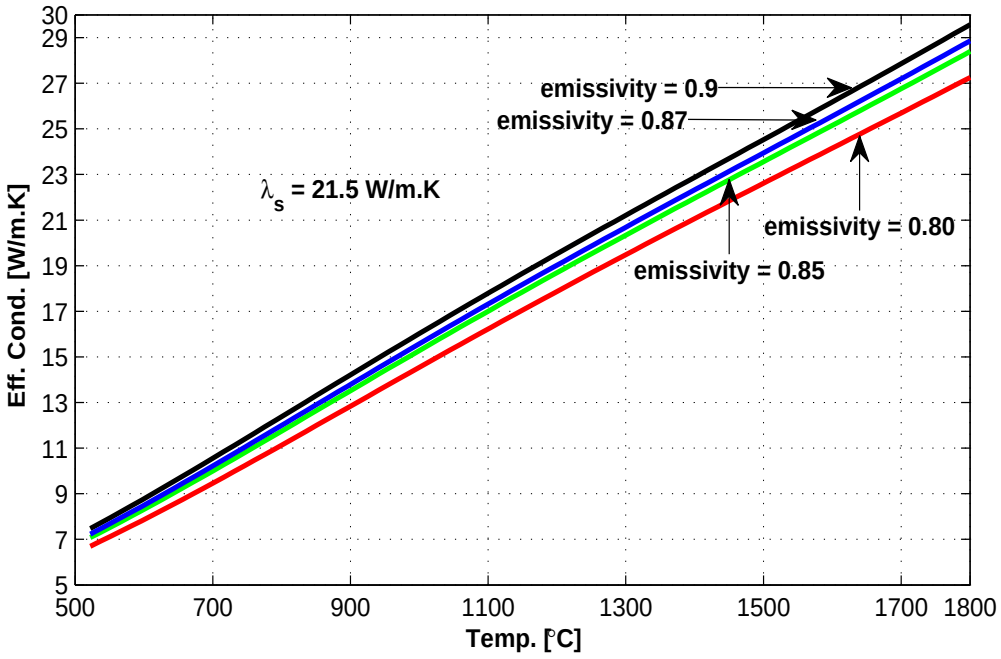

Figure 3.5: Influence of emissivity with temperature on effective conductive of the core,(p=1 bar, λ_s = 21.5 W/m.K).

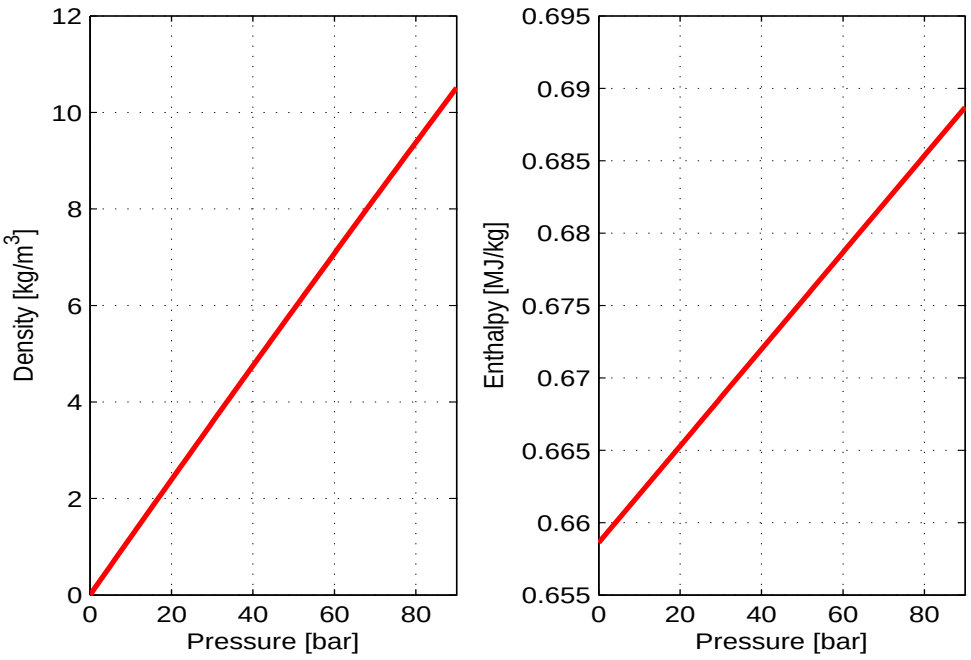

Figure 3.6: The influence of pressure on properties of Helium,(T=400K).

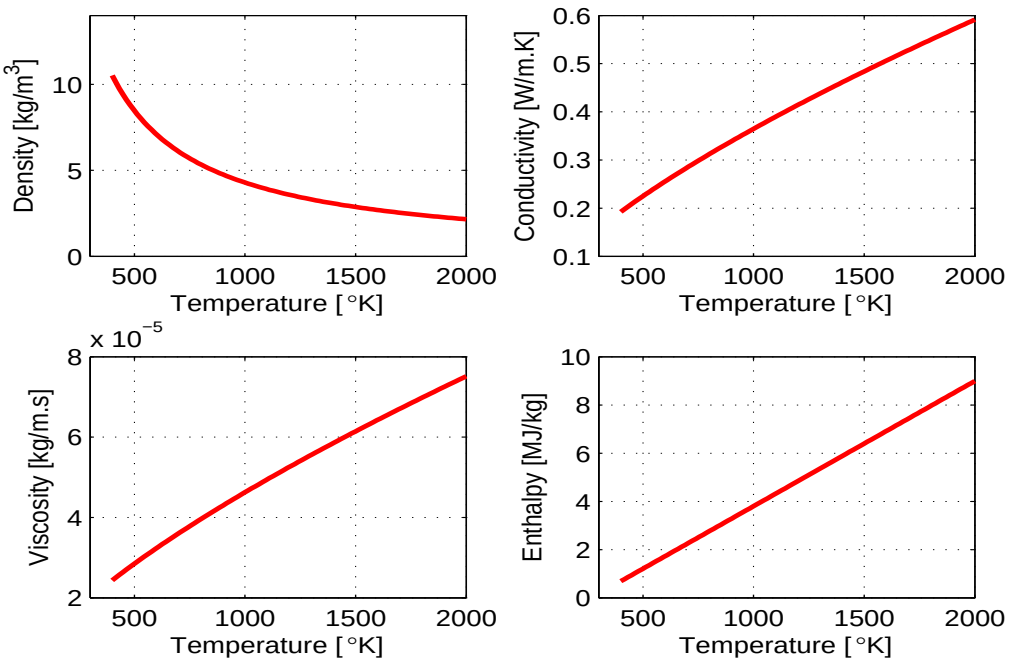

Figure 3.7: The influence of temperature on properties of Helium,(p=90 bar).

ing pressure. During accident case, the decay heat produced inside the reactor is transported by natural convection, conduction and radiation to top, bottom and side reflectors and further conducted and radiated and ultimately released to the reactor cavity cooling system or to the environment. At ambient pressure, natural convection is very small but with increasing system pressure, helium density increases which consequently increases the buoyant force and the natural convective heat transfer starts to play a significant role.

Like the system pressure, the system temperature also influences the total heat transfer process. With increasing temperature, the helium properties as well as the properties of other structure materials vary. Figure 3.7 shows the variation of helium properties with temperature [25]. With increasing temperature, the conductivity of the helium increases but the density decreases. The thermal properties of the structures materials (e.g. thermal conductivity, heat capacity, etc) also vary with temperature and most of the cases the value increases with increasing temperature and influences the thermal behavior of the reactor. Since a huge amount of graphite is used in the reactor (core fuel, central and side reflectors, top and bottom reflectors, etc), the thermal properties of the graphite play a significant role in the thermal behavior of the reactor. The thermal conductivity of graphite varies with temperature and neutron dose and will be discussed in the next section. The heat capacity of graphite increases with increasing temperature which dampens the quick temperature excursion during accidents.

3.5 Fast Fluence/Neutron Doses

The thermal conductivity of the graphite varies with exposed fast neutron fluence, temperature during exposure and its own temperature. Depending on the fabrication technique, this value varies from graphite to graphite. Figure 3.8(a) shows the experimental data performed by L. Binkele [8] for the $NUKEMA3-3$ graphite which is used for pebble type fuel elements (e.g. for PBMR fuel [34]). In this case, the graphite was radiated at 750°C. Binkele performed his experiments for different neutron exposure temperatures and it covers up to a fast doses of approximately 2.38 $\times 10^{21} n.cm^{-2}$ EDN and the temperature up to 1000°C. This experiment covers the nominal operational condition of HTRs since the expected maximum fast neutron doses and the temperature are less than the maximum doses and temperature covered by these experimental data.

Due to the crystal defect, reduction of phonon mean free paths, graphite conductivity decreases sharply with neutron dose at the beginning and becomes less likely to change with further neutron dose exposure. Due to the continuous exposures to higher neutron doses, the dimensions of the graphite are changed and internal pores are created due to the breakdown of graphitic structures which consequently decreases the conductivity [36]. Temperature at which graphite is radiated or exposure to neutron flux is also a very important parameter. Graphite which is radiated at low temperature shows lower conductivity than the graphite radiated at higher temperature [8]. Since the conductivity varies significantly with temperature and doses, consideration of both temperature and dose for calculating conductivity is very important. During nominal operation case, variation of conductivity with doses and temperature is not very important for calculating the maximum solid and gas temperature but it is very important for calculating the fuel temperature of different fuel passes, and for accident cases.

The reactor core is composed of fuel from different passes. For the PBMR-400 reactor, the core is composed of fuel from 6 passes. On the one hand, fuel from the first pass produces more power than the fuel from last pass which makes first pass fuel hotter than the last pass fuel, but on the other hand, fuel from first pass is exposed to less neutron doses than the last pass fuel and offers higher heat conductivity. In order to get the accurate temperature difference between different passes and average fuel and moderator temperature, the variation of heat conductivity with temperature and doses must be considered.

For the nominal operation, we implemented in our program the experimental data from figure 3.8(a). In this case, graphite was radiated at 750°C which most likely is the case during nominal operation of the PBMR-400 reactor. The experimental points obtained from figure 3.8(a) are plotted and fitted in a 2D surface by using a 2D polynomial interpolation function in MATLAB and the following polynomial equation is obtained. This equation calculates the heat conductivity of graphite depending on temperature and neutron doses.

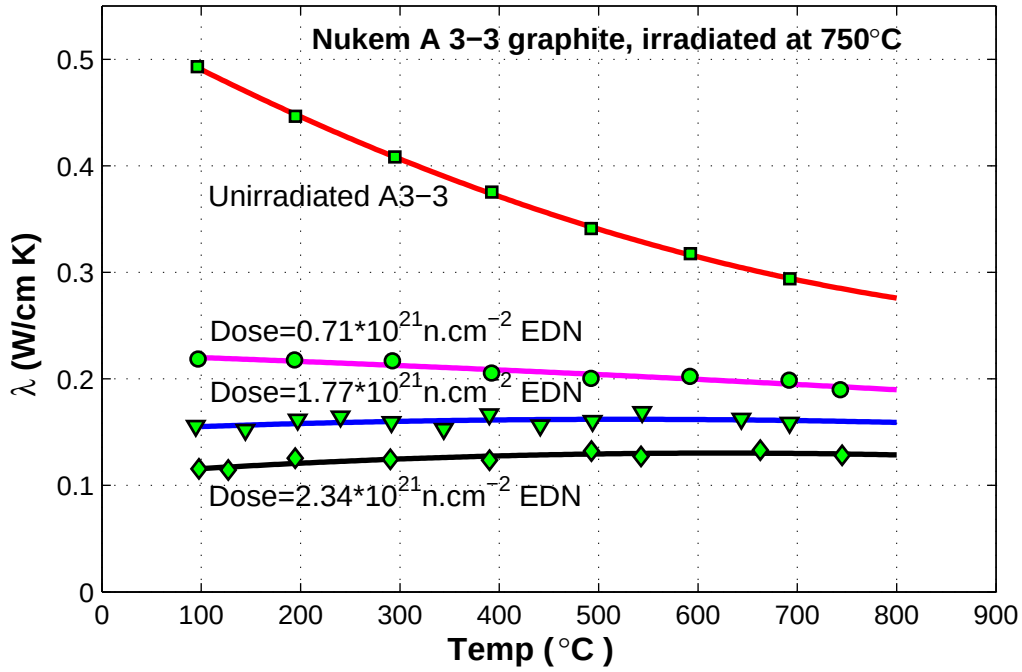

(a)

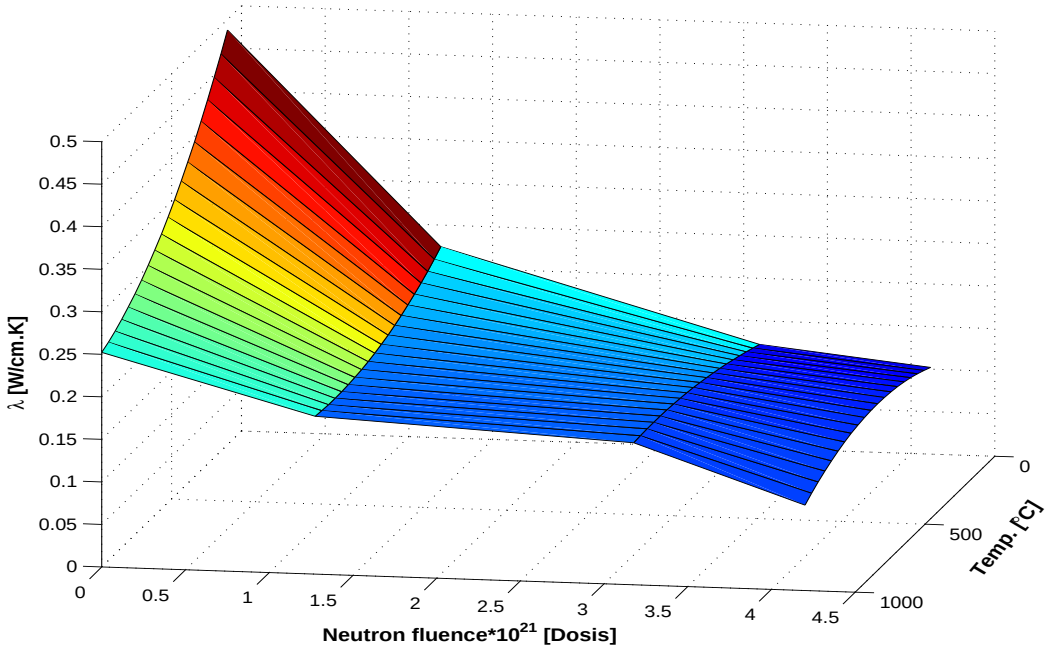

(b)

Figure 3.8: (a) Thermal conductivity versus temperature of A3-3 graphite irradiated at 750°C, (b)2D polynomial interpolation of experimental data obtained from figure 3.8(a)

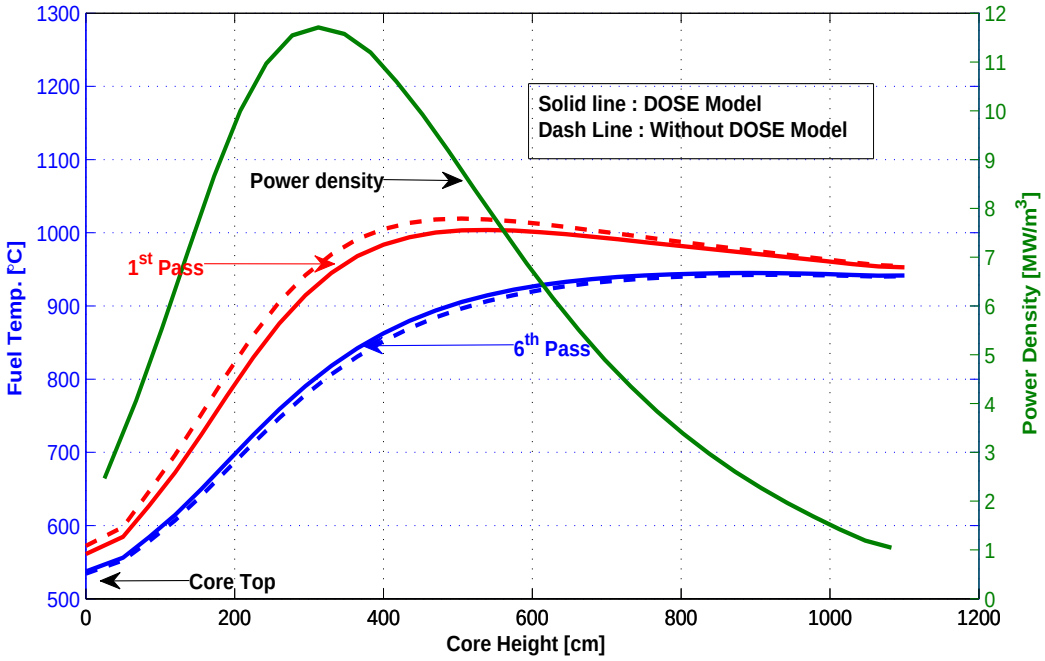

(a)

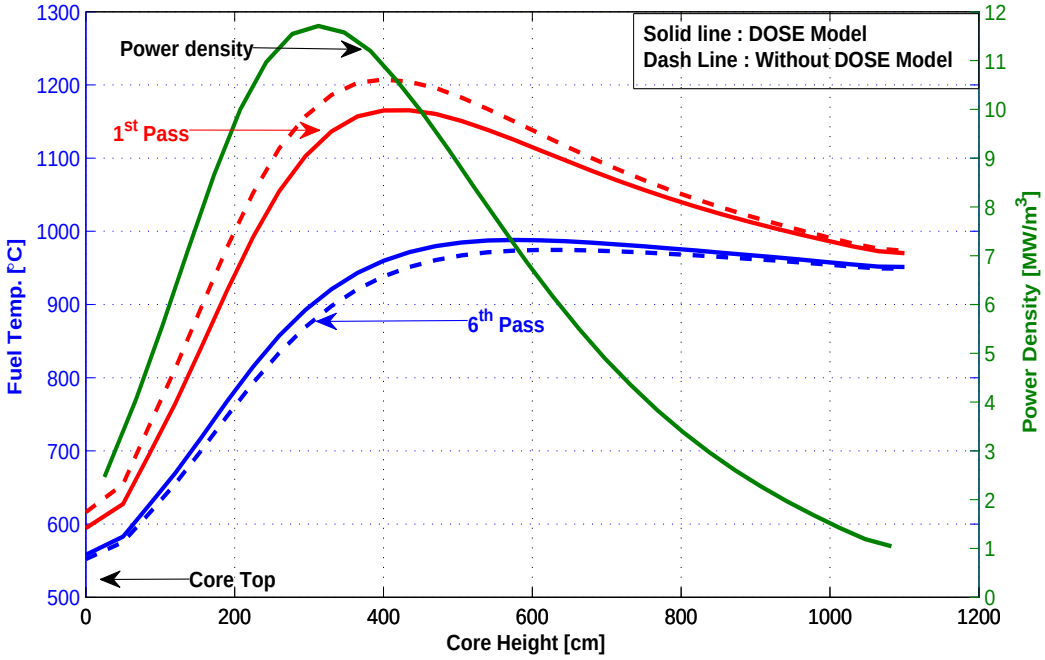

(b)

Figure 3.9: (a) Axial profile of average fuel kernel temperature, (b) Axial profile of maximum fuel kernel temperature at core and central reflector interface (r=1m) of PBMR-400 during nominal operation.

$$\begin{aligned}\lambda\left(T(^{\circ}C), D(dosis)\right) &= 0.534493982969409 - 0.000491856585285643 * T \\ &-3.08254690578566E^{-22} * D + 2.22562654064667E^{-07} * T^{2} \\ &+2.86638335739467E^{-25} * T * D + 8.15397473784508E^{-44} * D^{2} \\ &-1.29437835440441E^{-11} * T^{3} - 7.89232939178662E^{-29} * T^{2} * D \\ &-3.39004268357871E^{-47} * T * D^{2} - 7.69421581493917E^{-66} * D^{3} \quad \left[\frac{W}{cm.K}\right]\end{aligned} \tag{3.5}$$

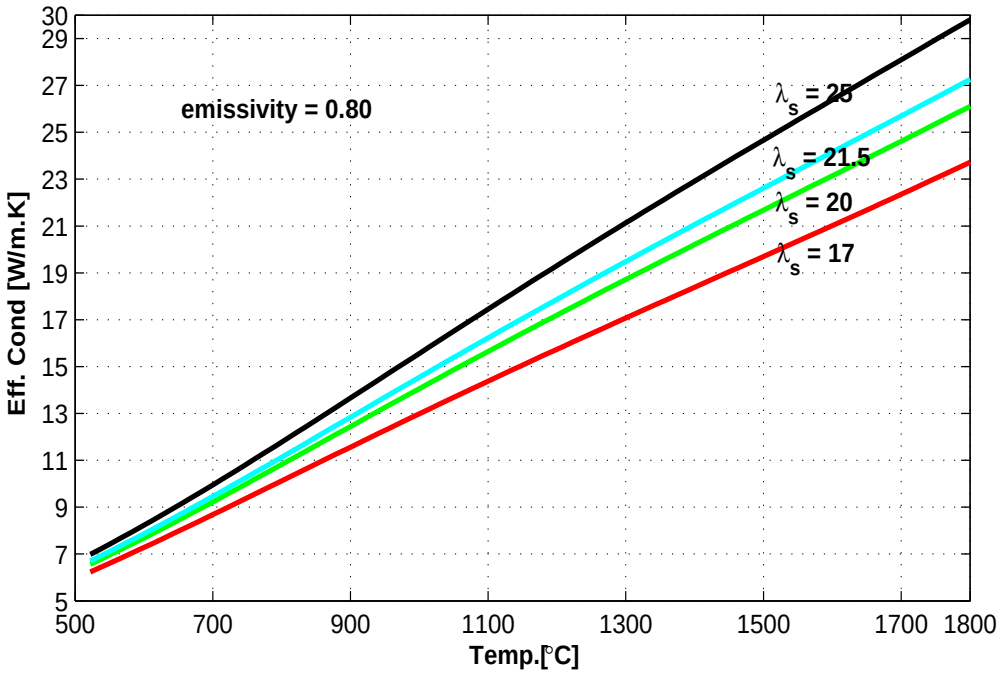

Figure 3.10: Variation of effective conductivity with solid conductivity

Here, λ, T, D are heat conductivity, temperature and neutron dose respectively. Figure 3.8(b) shows the fitted surface for graphite heat conductivity calculated from provided polynomial equation which is a result of a 2D polynomial interpolation of the experimental data. The obtained polynomial equation which is a function of neutron fluence and temperature is implemented in our program for calculating the heat conductivity. During calculation, conductivity of graphite at each cell in the core is calculated from this implemented equation depending on cell temperature and cell doses value. Figure 3.9 shows the axial power and temperature profile for the PBMR-400 reactor for average and maximum fuel kernel

temperature during nominal operation. With implementation of the dose model, the temperature difference of maximum and average fuel kernel between the first pass fuel and the last pass fuel are 215°C and 126°C respectively. These differences become higher if the dependency of graphite conductivity on doses is not considered (288°C and 163°C respectively). Graphite conductivity was taken as constant (20 W/m.K) when dose model was not considered.

Due to the dose model, the difference of temperature between fuel passes decreases during nominal operation. During accident cases, its advantages are twofold. On the one hand, the temperature reduction during nominal operation will decrease the maximum temperature during accident cases. On the other hand, higher heat conductivity offered by relatively fresh fuel will produce higher effective conductivity. Figure 3.10 shows the variation of effective conductivity in the pebble bed core depending on the solid conductivity calculated by Zehner and Schlünder model.

Chapter 4

Mathematical models of TH3D

The newly developed TH3D code is a 3D thermal hydraulic tool for the design and safety analysis of High Temperature Gas Cooled Reactors. It can be used for 3D Cartesian ($x-y-z$ geometry) or 3D cylindrical ($r-\theta-z$ geometry) geometry. Since the flow inside the gas cooled High Temperature Reactor is essentially single-phase, compressible, and non-isothermal, at least one gas phase has to be considered beside the solid phase. Each phase (e.g. solid, gas) is considered as a continuum which occupies only its respective fraction of the control volume. Instead of describing each fuel element, gaps, voids, etc explicitly (microscopic level), all physical phenomenon were examined from a distant perspective (macroscopic level) where all properties are defined by averaging over the control volume. These averaging values are defined by some functions which satisfy certain smoothness conditions consistent with fundamental continuum mechanics. Thermal non-equilibrium is assumed between phases and the model is based on a set of conservation equations (conservation of mass, momentum and energy) along with a set of constitutive equations. All conservation and constitutive equations will be described in the coming sections.

4.1 Conservation Equations

The solid phase inside the reactor (e.g. fuel, reflector, flow channels, etc) is considered as fixed and coolant gas flows around the solids. The time dependent, compressible mass conservation equation for gas is solved only in the part of the reactor where flow exists. This equation is also known as the continuity equation and the flow field must satisfy this constraint.

$$\frac{\partial\left(\varepsilon\rho c_i\right)}{\partial t}+\nabla\cdot\left(\varepsilon\rho\overrightarrow{u}c_i\right)=0; when \quad i=1,...,n \tag{4.1}$$

Where ε is the porosity or the volume fraction of gas phase in the control volume, ρ is the density of the gas, $\overrightarrow{u}$ is the velocity, and c_i is the volume fraction of the i^{th} gas component in the gas phase. The value of n is unity for high temperature gas cooled reactors during nominal operation but provision is made for simulating

more than one gas component for some especial situations (e.g. water ingress by pipes break) where more than one gas component must be taken into account.

Like the mass conservation equation, a momentum conservation equation is also solved in the part of the reactor where flow exists. When u is the x directional velocity vector, the general form of the momentum equation for a Newtonian fluid in the corresponding direction can be written as:

$$\frac{\partial}{\partial t}(\rho u) + \nabla \cdot (\rho u \overrightarrow{u}) = \nabla \cdot (\mu \nabla u) - \frac{\partial p}{\partial x} + V_x - R_x - \gamma \rho g \tag{4.2}$$

This equation is also known as the Navier-Stokes equation, an application of the Newton's second law. Two terms on the left hand side of the equation are unsteady term and convection term respectively while the terms on the right hand side represent diffusion of momentum, pressure gradient, viscous term that are in addition to the diffusion term, the pressure loss due to solid-fluid friction, and the body force due to gravity in the corresponding direction per unit volume, respectively. The quantity g is the gravitational constant and γ is a constant for direction of flow which is +1 for upward flow and -1 for downward flow. For flow in a porous media, main resistance to flow is the solid-fluid friction. In our case, a porous media approach is taken which simplifies momentum equation considerably by dropping the terms with less significance compared to the gravitational and the friction forces. So, a quasi steady, simplified, momentum conservation equation can be written as:

$$\varepsilon \nabla \cdot (p) = -\overrightarrow{R} - \gamma \varepsilon \rho \overrightarrow{g} \tag{4.3}$$

where p is the system pressure, g is the constant of the gravity and $\overrightarrow{R}$ represents the friction force between solid and gas phases. The value of the friction force is calculated by using norms/empirical equations which are generally deduced from experiments.

Since thermal non equilibrium is considered between phases, the energy conservation equation for each phase has to be solved. For getting the solid temperature inside the reactor, the energy conservation equation for solid is solved for the whole reactor. The time dependent energy conservation equation for solid can be written as:

$$(1-\varepsilon)\frac{\partial \rho_s h_s}{\partial t} = (1-\varepsilon)\nabla \cdot \left(\lambda_{s_{eff}} \nabla (T_s)\right) - \dot{q}_{conv} + \dot{q} \tag{4.4}$$

where h_s is the specific enthalpy, $\lambda_{s_{eff}}$ is the effective thermal conductivity, h_s is the enthalpy, $\dot{q}$ is the volumetric rate of nuclear heat generation, $\dot{q}_{conv}$ is the heat addition in the gas phase from the solid phase. The left hand side of the equation represents the unsteady term and the first term of the right hand side represents the

conductive heat transfer within solid (according to the Fourier law of conduction). For calculating the thermodynamic property such as temperature, the change of enthalpy with respect to temperature and pressure must be known. These changes can be written as:

$$dh = c_p dT + \frac{1}{\rho}\left[1 + \frac{T}{\rho}\left(\frac{d\rho}{dT}\right)\right] dp \tag{4.5}$$

where c_p is the specific heat at constant pressure. For most of the case the second term of the equation can be dropped. For example, for the case of material in a solid thermodynamic state and gases which follow the ideal gas equation, the second term of the equation is zero. Since c_p is considered as a constant, the relation between h, T can be written as:

$$dh = c_p dT \tag{4.6}$$

By using the relationship between h and T from equation 4.6, the energy equation for the solid phase can be written as:

$$(1-\varepsilon)\,\rho_s c_{p_s} \frac{\partial T_s}{\partial t} = (1-\varepsilon)\,\nabla \cdot \left(\lambda_{s_{eff}} \nabla\,(T_s)\right) - \dot{q}_{conv} + \dot{q} \tag{4.7}$$

In this manner, either temperature or enthalpy can be used as a dependent variable. For getting the gas/coolant temperature, the energy conservation equation for the gas is solved in the flow field part of the reactor. The time dependent energy conservation equation for the gas can be written as:

$$\frac{\partial \varepsilon \rho_g h_g}{\partial t} + \nabla \cdot (\varepsilon \rho_g \overrightarrow{u} h_g) = \nabla \cdot \left(\varepsilon \lambda_{g_{eff}} \nabla\,(T_g)\right) + \dot{q}_{conv} \tag{4.8}$$

here, h_g denotes the specific enthalpy of the gas, $\lambda_{g_{eff}}$ denotes the effective heat conductivity of the gas, T_g is the gas temperature, and q_{conv} is the heat addition in the gas phase from the solid phase. The energy conservation equation for the gas phase can also be written in terms of the gas temperature by using the relationship between enthalpy and gas temperature.

4.2 Constitutive Equations

For solving the set of equations described in the conservation equations section, several additional algebraic equations are required. These constitutive equations are macroscopic level and rely on semi-empirical correlations obtained from different experiments. The constitutive equations implemented in TH3D will be described in the following sections.

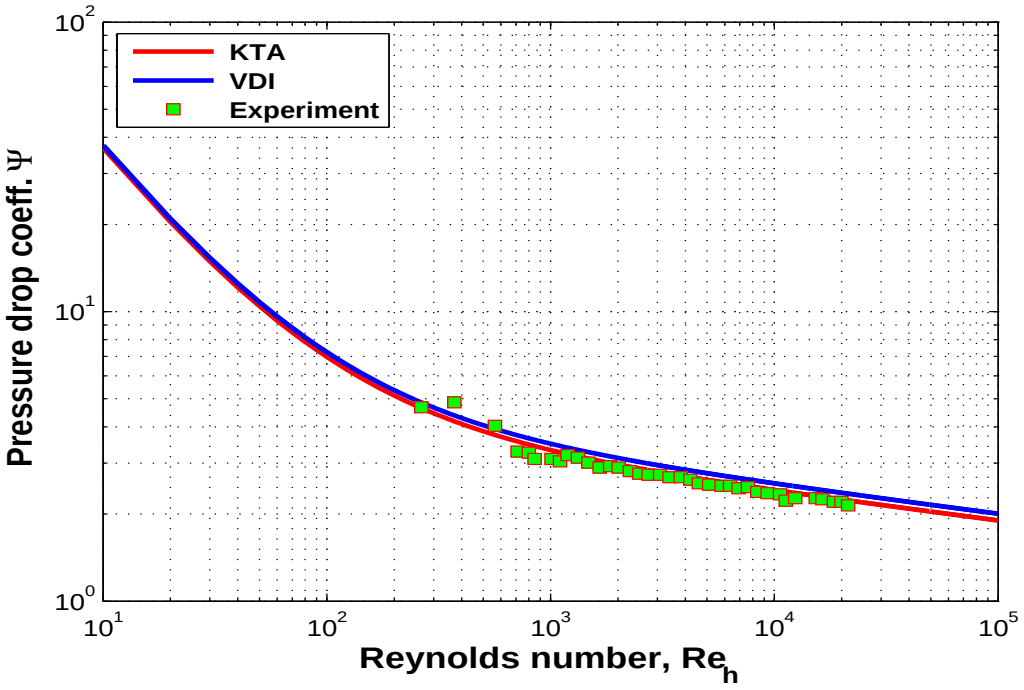

Figure 4.1: Comparison of pressure drop coefficient in a pebble bed with porosity ε = 0.387.

4.2.1 Pressure Drop Coefficient

Due to the assumption of the porous media, the momentum equation is simplified by dropping some small terms (e.g. viscous term, diffusion term, etc.) but an extra friction term is added to the equations (equation 4.2 and equation 4.3). This is the solid-fluid friction that a gas encounters when flowing inside the reactor components. These friction terms are calculated by using correlations and are different for different reactor components.

Pebble Type Fuel

For pebble bed fuel core, the pressure loss due to friction between phases (R) in the core can be expressed as:

$$R = \psi \cdot \frac{1}{d_h} \cdot \frac{\rho}{2} \cdot u_p^2 \tag{4.9}$$

where ψ is the pressure drop coefficient, d_h is the hydraulic diameter of the pebble, u_p is the mean velocity of gas in the gaps between pebbles, and ρ is the gas density. The value of the pressure drop coefficient depends on Reynolds number which can be defined as:

$$Re_h = \frac{d_h u_p \rho}{\mu} \tag{4.10}$$

The variables d_h, u_p can be expressed by variables which can be measured directly. For a packed bed consisting spheres with equal diameter d, the hydraulic diameter d_h can be expressed as:

$$d_h = \frac{4(V - V_s)}{A_s} \qquad with \qquad A_s = \frac{6V_s}{d} \tag{4.11}$$

where V_s is the volume of spheres, V is the total volume of the packed bed, and A_s is the surface area of the pebble sphere. The void fraction/porosity ε of the packed bed can be expressed as:

$$\varepsilon = 1 - \frac{V_s}{V} \tag{4.12}$$

by using the equations 4.11, 4.12 and after some simplification, the hydraulic diameter of the packed bed can be expressed as a function of the pebble's diameter as:

$$d_h \cong d\frac{\varepsilon}{1 - \varepsilon} \tag{4.13}$$

the mean velocity in the gaps between the pebbles can be expressed as a function of the mean free cross section velocity of the pebble bed as:

$$u_p = \frac{u}{\varepsilon} \tag{4.14}$$

By using the equations 4.13 and 4.14, pressure loss term (R) and Reynolds number (Re_h) can be expressed by the directly measurable variables as:

$$R = \psi \cdot \frac{1}{d} \cdot \frac{(1 - \varepsilon)}{\varepsilon^3} \cdot \frac{\rho}{2} \cdot u^2 \tag{4.15}$$

and

$$Re_h = \frac{1}{1 - \varepsilon} \cdot \frac{du\rho}{\mu} = \frac{Re}{1 - \varepsilon} \qquad where \qquad Re = \frac{du\rho}{\mu} \tag{4.16}$$

For calculating the pressure drop coefficient, which is a function of Reynolds number ($\psi = f(Re_h)$), several correlations were developed and verified against experiments. According to KTA norm [26], the pressure drop coefficient is expressed as:

$$\psi = \frac{320}{\frac{Re}{1-\varepsilon}} + \frac{6}{\left(\frac{Re}{1-\varepsilon}\right)^{0.1}} \tag{4.17}$$

The results obtained from the KTA norm are examined with experimental results and illustrated very good agreement up to $Re_h < 10^5$ and provides lower values when $Re_h > 10^5$ [2]. In pebble bed high temperature reactor core, Reynolds number (Re_h) varies from 10 to 300 for the case of natural convection during accident case and from 2×10^4 to 5×10^4 for the case of nominal operational case [42]. In our validation calculations, we have used KTA norm for pressure drop calculations since it produces satisfactory results in the range of our desired flow conditions. Beside KTA norm, several correlations (e.g. VDI norm, Ergun, Darcy) are implemented in TH3D. Figure 4.1 illustrates the results obtained from different correlations and comparison with experimental values for the case of a unique size spherical packed bed with a void fraction of 0.387.

Block Type Fuel

For block type fuel core, the pressure loss term R used in momentum equation, which comes from friction between solid and gas phases, can be expressed as:

$$R = \frac{4\psi}{d_h} \cdot \frac{\rho}{2} \cdot u^2 \tag{4.18}$$

where d_h, u are the hydraulic diameter and the mean cross section velocity, respectively. The friction factor of the coolant holes in the graphite blocks depends on the smoothness of the holes which in turn depends on the drilling techniques employed. At present it is assumed that the drilling techniques are sophisticated and smooth tube friction factor correlations are used for design calculation. The friction factor correlation used for the present calculation can be expressed as:

$$\psi = C_1 \left(Re_h\right)^{C_2} \tag{4.19}$$

where Re_h is the Reynolds number based on hydraulic diameter described in the previous section and C_1, C_2 are constants measured by experiments. The following values are applicable for the case of smooth coolant channels [18]:

- Laminar flow $Re_h < 2000, C_1 = 16.0, C_2 = -1.0$ for circular cross section.
- Transitional flow $2000 \leq Re_h \leq 4000, C_1 = 0.0007316, C_2 = 0.3147$
- Turbulent flow $Re_h > 4000, C_1 = 0.0791, C_2 = -0.25$

4.2.2 Heat Transfer Coefficient

As it is mentioned in the previous section (section 4.1) thermal non-equilibrium is considered between solid and gas phases. For getting the temperature profile, the energy conservation equations for both solid and gas need to be solved. In the reactor core, heat produced in the solid phase is transferred to the gas. The heat flux

term q_{conv} used in the previously described energy conservation equations (equation 4.7, 4.8) is calculated by using Newton's law of cooling as:

$$q_{conv} = \alpha(T_s - T_g) \tag{4.20}$$

where T_s, T_g are the solid surface and gas temperatures and α is the convection heat-transfer coefficient. An analytical calculation of α is possible for some simple cases, but for a complicated case it is generally calculated by using correlations verified by experiments. The correlations for the heat transfer coefficient varies with varying geometries, arrangements, flow conditions. The correlations used for the different parts of the reactor are discussed in the following sections.

Pebble Type Fuel

For calculating the heat transfer coefficient in the pebble bed reactor core, KTA [27] and VDI [50] norms are implemented in TH3D and an option to switch between these norms is made. According to the KTA norm, the heat transfer coefficient in the pebble bed can be written as:

$$\alpha = \frac{Nu \cdot \lambda}{d} \tag{4.21}$$

$$Nu = 1.27 \cdot \frac{Pr^{0.33}}{\varepsilon^{1.18}} \cdot Re^{0.36} + 0.033 \cdot \frac{Pr^{0.5}}{\varepsilon^{1.07}} \cdot Re^{0.86} \tag{4.22}$$

where Pr, Re, ε are the Prandtl number, the Reynolds number and porosity of the packed bed, respectively. This correlation can be used for a Reynolds number in the range of $100 \leq Re \leq 10^5$ and for a porosity in the range of $0.36 \leq \varepsilon \leq 0.42$.

In VDI norm [50], the heat transfer of spheres in a packed pebble bed is linked to a scenario of heat transfer from a single pebble by introducing an arrangement factor.

$$Nu = f_\varepsilon Nu_s \tag{4.23}$$

$$f_\varepsilon = 1 + 1.5(1 - \varepsilon) \tag{4.24}$$

where Nu, Nu_s, f_ε are the Nusselt number of the packed bed, Nusselt number of the single sphere and arrangement factor, respectively. The arrangement factor depends on the porosity of the packed bed. The Nusselt number of a single sphere can be calculated from the following equation:

$$Nu_s = 2 + \sqrt{Nu_l^2 + Nu_t^2} \tag{4.25}$$

where Nu_l and Nu_t are Nusselt number of the single sphere for laminar and turbulent flow respectively. The Nusselt number for laminar and turbulent flow can

be calculated from the following equations:

$$Nu_l = 0.664 \left(\frac{Re}{\varepsilon}\right)^{1/2} \cdot Pr^{1/3} \tag{4.26}$$

and

$$Nu_t = \frac{0.037 \left(\frac{Re}{\varepsilon}\right)^{0.8} \cdot Pr}{1 + 2.443 \left(\frac{Re}{\varepsilon}\right)^{-0.1} (Pr^{2/3} - 1)} \tag{4.27}$$

where Re, Pr and ε are the Reynolds number, Prandtl number and porosity of the packed bed, respectively. This norm can be used in the range of Reynolds number $5 \times 10^2 < Re < 5 \times 10^5$, of Prandtl number and Schmidt number $0.6 < Pr, Sc < 10^4$ and of porosity $0.26 < \varepsilon < 0.935$ [18].

Block Type Fuel

The heat transfer correlations generally used for block type fuel core are derived from the correlations developed for smooth pipe-flow heat transfer. For the case of flow in block fuel channels, these values would be slightly higher than values for smooth pipe-flow due to the surface roughness in the coolant channels. In nominal operational case or from 25% to 100% power level operation, the flow in the block channels is turbulent and the minimum Reynolds number at 25% power operation is about 7000 [18]. But during shutdown, refueling, or accident conditions the flow can be laminar or transitional. In turbulent flow region, where Reynolds number is over 6000, the heat transfer coefficient can be calculated from the following equation as:

$$\alpha = 0.02 \cdot \left(\frac{\lambda}{b}\right) \cdot Re^{0.8} \cdot Pr^{0.4} \tag{4.28}$$

where Re and Pr are the local Reynolds and Prandtl number and λ and b are the thermal conductivity of the coolant and diameter of the coolant hole. In laminar flow region, where Reynolds number is less than 3000, the heat transfer coefficient can be estimated from the following equation as:

$$\alpha = \left(\frac{\lambda}{b}\right) \left\{3.65 + \frac{0.0668 \cdot (b/L) \cdot Re \cdot Pr}{1 + 0.04 \left[(b/L) \cdot Re \cdot Pr\right]^{0.66}}\right\} \tag{4.29}$$

where L is the heated length of the coolant channel. When the Reynolds number is in the range of $3000 < Re < 6000$, the heat transfer coefficient is calculated by interpolating the coefficient values obtained at upper value of laminar flow $(Re = 3000)$ and the lower value of the turbulent value $(Re = 6000)$.

4.2.3 Effective Heat Conductivity

The heat produced inside the reactor core must be transported out to get the desired outlet temperature and to keep the temperature with in a certain permissible limit. In nominal operation, the main mechanism of this transport is forced convection. Heat transfer in axial and radial direction by conduction and radiation is very small. But for the case when the reactor is scrammed due to accidents, conduction, radiation and natural convection are the main heat transport mechanisms. Due to the complicated configuration of the reactor core, it is difficult to calculate the exact convective, conductive and radiative heat flux. In high temperature reactors, the core is generally composed of spherical pebble fuels or of block fuels containing fuel and coolant holes. For both cases, the core of the reactor is modeled as a porous media in TH3D. The heat transfer in a porous media is calculated by regarding the effective thermal conductivity of the packed bed. During past years, several models/correlations were developed for calculating the effective heat conductivity by considering the main mechanisms of the heat transport in the porous media. The correlations used for calculating the effective heat conductivity for pebble bed reactors and for block type reactors will be discussed in the coming sections.

Pebble Type Fuel

The main mechanisms of heat transfer inside a packed pebble bed core can be listed as:

- Heat conduction through the pebble.
- Heat conduction through the contact area of two pebbles.
- Heat conduction through the gas in the gap.
- Radiation between two neighboring pebble surfaces.
- Radiation through gap which comes from a distant pebble surface.
- Convective heat through the gas.

The contribution of any of the above mentioned mechanisms depends on temperature, pressure and flow condition inside the reactor core. In all of the following described models, all contributions except the convective heat flux through the gas are combined and modeled as an effective heat conduction by introducing a term called effective heat conductivity λ_{eff}. Scientists are trying for last 100 years with different approach for calculating the effective heat conductivity in the porous media. Tsotsan and Martin made a review over more than 50 models and according to their study, all models can be differentiated into four different categories as [48]:

- Detailed analytical or numerical models.
- Simple model with circuit of heat resistance.

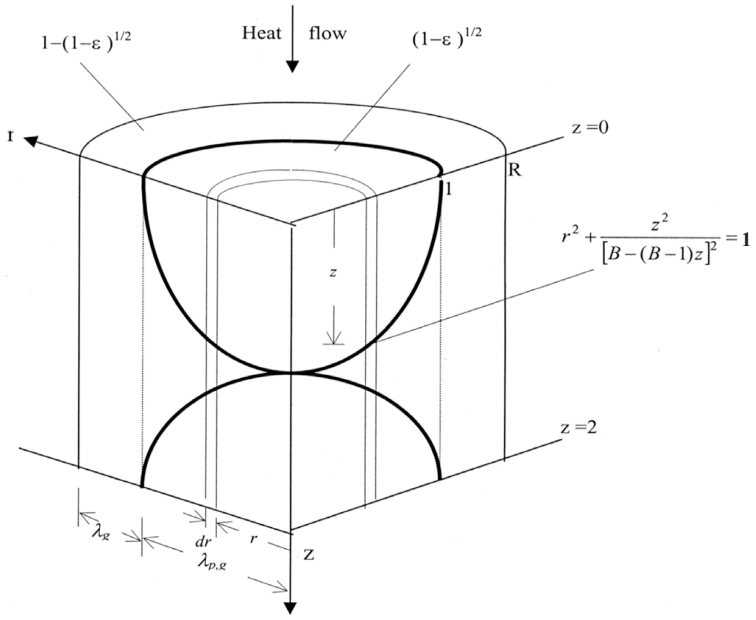

Figure 4.2: Unit cell model.

- Unit cell model.
- Quasi homogeneous model.

Zehner and Schlünder Model

This is the most widely used model for calculating the effective thermal conductivity of a porous packed bed. This model is suitable for a packed bed composed with pebbles of any size and shape but with same thermal conductivity [1]. This is a unit cell model where heat flow in a cell is considered. The unit cell contains two connecting pebbles which occupy the solid volume fraction of the cell while the rest is filled with the coolant gas. It is assumed that the heat flows through several parallel paths. Figure 4.2 shows the schematic diagram of the unit cell model. The total heat flow mechanism in this model is subdivided into three parallel paths.

- Path1 - In the outer ring zone with relative area of $1-(1-\varepsilon)^{1/2}$, which represents the voidage filled with coolant gas, heat is transported through molecular conduction and radiation in the gas phase.

The inner ring zone with relative area of $(1-\varepsilon)^{1/2}$, which is composed of solid and gas phase, can be further subdivided into two parts depending on the direct contact area between two neighboring pebbles.

- Path2 - In the direct contact area with relative area of s, the innermost area, heat is transported through solid-solid conduction.

- Path3 - The remaining area of $(1-\varepsilon)^{1/2}$, which represents the gap between two pebbles with relative area of $(1-s)$, heat flow path can be written as solid conduction in the pebble - conduction in the gas and radiation in between the pebble surfaces - solid conduction in the pebble.

By considering the above mentioned flow path resistances as a circuit of three parallel heat resistances, the effective heat conductivity of the total system can be written as:

$$k_{eff} = \frac{\lambda_{eff}}{\lambda_g} = \underbrace{(1-\sqrt{1-\varepsilon})\frac{\lambda_H}{\lambda_g}}_{Path1} + \underbrace{\sqrt{1-\varepsilon}\left[s\frac{\lambda_p}{\lambda_g}\right]}_{Path2} + \underbrace{\sqrt{1-\varepsilon}\left[(1-s)\frac{\lambda_C}{\lambda_g}\right]}_{Path3} \tag{4.30}$$

where λ_H and λ_C are used to designate the heat conductivity of the outer and inner ring zone of the unit cell. λ_p and λ_g are the heat conductivity of pebble and coolant gas respectively. By considering also the secondary influential parameters, the detailed model can be written as:

$$\begin{aligned} k_{eff} = \frac{\lambda_{eff}}{\lambda_g} = & \underbrace{(1-\sqrt{1-\varepsilon})\cdot\varepsilon\cdot\left[\left(\varepsilon-1+k_G^{-1}\right)^{-1}+k_{rad}\right]}_{Path1} \\ & + \underbrace{\sqrt{1-\varepsilon}\,[sk_p]}_{Path2} + \underbrace{\sqrt{1-\varepsilon}\,[(1-\varepsilon)k_C]}_{Path3} \end{aligned} \tag{4.31}$$

with

$$\begin{aligned} k_C = \frac{\lambda_C}{\lambda_g} = & \frac{2}{N}\left\{\frac{B(k_p+k_{rad}-1)}{N^2k_Gk_p}ln\frac{k_p+k_{rad}}{B[k_G+(1-k_G)(k_p+k_{rad})]}\right\} \\ & +\frac{2(B+1)}{2BN}\left\{\left[\frac{k_{rad}}{k_G}-B\left(1+\frac{1-k_G}{k_G}k_{rad}\right)\right]-\frac{B-1}{Nk_G}\right\}\Big\} \end{aligned} \tag{4.32}$$

and

$$N = \frac{1}{k_g}\left(1+\frac{k_{rad}-Bk_G}{k_p}\right) - B\left(\frac{1}{k_G}-1\right)\left(1+\frac{k_{rad}}{k_p}\right) \tag{4.33}$$

Here, B is a shape factor and its value depends on the shape of the particle and the porosity of the packed bed. For a packed bed filled with spherical pebble, the shape factor can be written as:

$$B = 1.25\cdot\left[\frac{1-\varepsilon}{\varepsilon}\right]^{10/9} \tag{4.34}$$

The radiation heat transport which is dependent on temperature can be calculated as:

$$k_{rad} = \frac{\lambda_{rad}}{\lambda_g} = \frac{4\sigma}{(2/\epsilon)-1}T^3\frac{x_R}{\lambda_g} \tag{4.35}$$

where σ is the Boltzmann constant for black body, ϵ is the emissivity coefficient of the surface of the particles and x_R is the effective radiation length. The dependency

of the heat transfer mechanisms on pressure which is know as Schmoluchowski effect can be written as:

$$k_G = \frac{\lambda_G}{\lambda_g} = \left[1 + \frac{2\Lambda}{x_D}\left(\frac{2}{\gamma} - 1\right)\right]^{-1} \tag{4.36}$$

where Λ, x_D, and γ are mean free path of the gas molecule, effective gas length, and accommodation coefficient respectively. The values of the effective radiation length and effective gas length are taken as the diameter of the pebble particle and determined from experiments. The influence of each part of the heat transport to the total heat transport mechanism is examined to get an idea about the contribution of any individual part (figure 4.3). Another reason for this examination was to simplify the model by eliminating part of the model which produces hardly any influence on the total mechanism. It has been seen that the heat conduction through direct contact of the pebble and the dependency on pressure is very small. In this case the contact area value $s = 0$ and the pressure dependency term $k_G = 1$ can be taken.

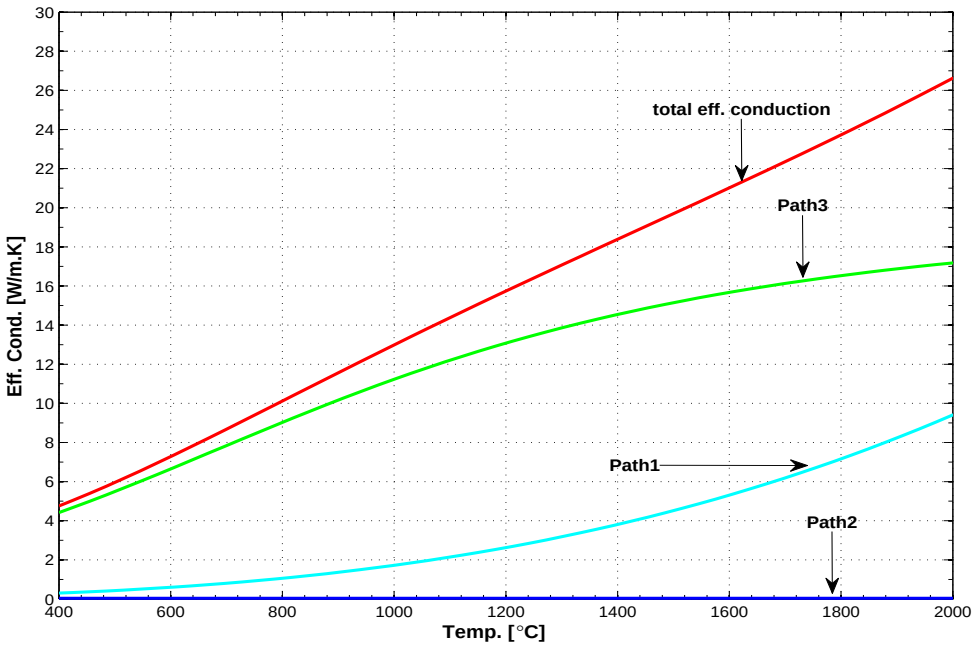

Figure 4.3: Contribution of different heat transport mechanism on effective conductivity

Quasi-homogeneous model of Vortmeyer and Robold

In the cell model (Zehner and Schlünder Model) described earlier, the radiative heat transport in between two connecting pebbles is considered along with molecular conduction but the radiative heat transport through the gaps between pebbles which goes beyond the connected pebbles is not considered. Since radiation heat transfer increases with increasing temperature, this fraction of heat plays a role at higher temperature. In order to capture this effect, Kasperek and Vortmeyer [51] arranged the spherical particles in layers and analyzed the heat transfer phenomenon. He assumed that the conductivity of the particles is high and all particles in a layer observe the same temperature. So, the radiative heat transfer occurs only from layer to layer and one-dimensional radiative heat transfer is considered.

The limitation of the Kasperek and Vortmeyer model is consideration of only the radiative heat transfer phenomenon and ignorance of the conductive heat transfer. Robold [40] modified this model by considering the molecular heat transfer in the fluid between the particles. For a small temperature difference, the effective heat conductivity of the particle bed can be written as:

$$\lambda_{eff}^{R} = \left[1 - \frac{\chi\Delta_0}{1+\frac{\frac{\lambda_s}{d_s^\varepsilon}}{4\psi_0\sigma T^3+\frac{\lambda_g}{d_g^\varepsilon}}}\right] 4\psi\sigma T^3 d^\varepsilon + \left[1 - \frac{\Delta_0}{1+\frac{\frac{\lambda_s}{d_s^\varepsilon}}{4\psi_0\sigma T^3+\frac{\lambda_g}{d_g^\varepsilon}}}\right] \lambda_g \frac{d^\varepsilon}{d_g^\varepsilon} \tag{4.37}$$

with global heat transfer coefficient

$$\psi = \frac{2B + \epsilon(1-B)}{(1-B)(2-\epsilon)} \tag{4.38}$$

local heat transfer coefficient

$$\psi_0 = \psi(B=0) = \frac{\epsilon}{2-\epsilon} \tag{4.39}$$

width of the model plate, the distance from the center of one layer to the center of neighboring layer

$$d^\varepsilon = \frac{\pi}{6} \cdot \frac{d_k}{1-\varepsilon} \tag{4.40}$$

the width of the solid part and fluid part of the model plate can be written as:

$$d_s^\varepsilon = d^\varepsilon \cdot \frac{\pi}{1+\pi} \tag{4.41}$$

$$d_g^{\varepsilon} = d^{\varepsilon} \cdot \frac{1}{1+\pi} \tag{4.42}$$

the ratio χ and weight factor Δ_0 are

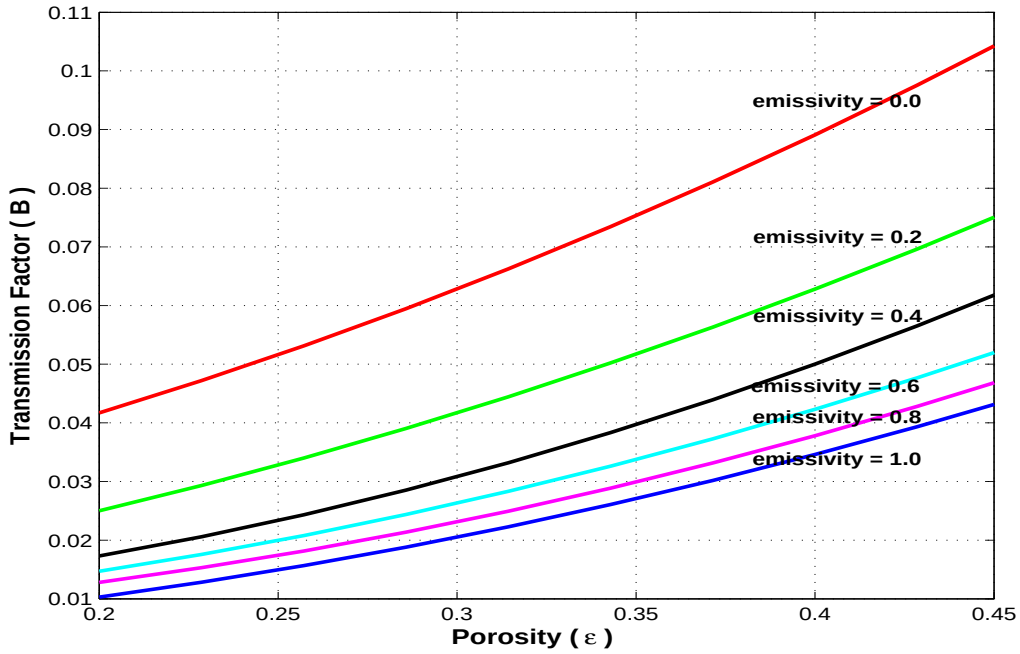

Figure 4.4: Radiative transmission factor B [40].

$$\chi = \frac{\psi_0}{\psi} \tag{4.43}$$

$$\Delta_0 = \frac{\psi\left[1 - B(\epsilon = 0, \varepsilon)\right] - B(\epsilon = 0, \varepsilon)}{\psi_0\left[1 - B(\epsilon = 0, \varepsilon)\right]} \tag{4.44}$$

Here, ϵ is the emissivity coefficient, ε is the porosity of the packed bed and B is the radiative transmission factor which depends on emissivity (ϵ) and porosity (ε). The result of the radiative transmission factor calculated by Robold [40] is shown in figure 4.4.

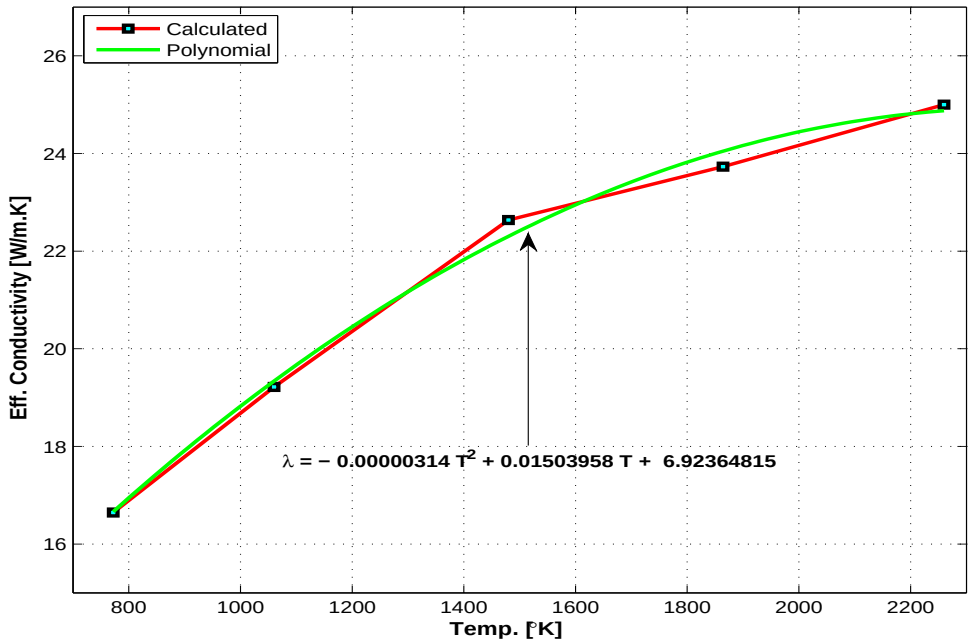

Figure 4.5: Effective heat conductivity of block fuel core calculated by Haque [20].

Block type Fuel and Reflector

For calculating the effective heat conductivity of block type fuels and reflectors, two polynomial equations are implemented in TH3D. The polynomial equation used for calculating the effective heat conductivity of the block fuel core is developed by Haque et al. and published in nuclear engineering and design journal [20]. The equation was developed by considering all the possible heat flow paths and representing the flow paths as heat resistors. Figure 4.5 shows the effective heat conductivity of block type fuel core developed by Haque. For calculating the effective heat conductivity of the block type reflector, a simple model based on the heat resistance is developed and implemented in TH3D. Also in this case, all possible heat flow paths were presented as heat resistors and the total system is represented as a circuit of some parallel and series heat resistors and the total heat resistance was calculated at different temperature. The results obtained from calculation were plotted and was represented by a polynomial equation. Figure 4.6 shows the calculated results as well as the polynomial equation.

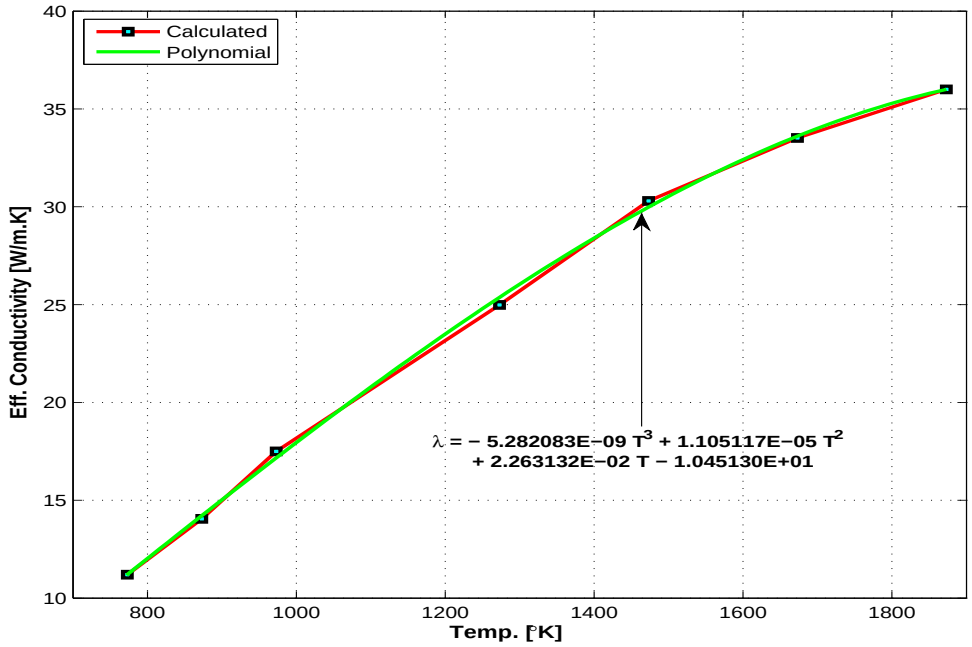

Figure 4.6: Effective heat conductivity of block reflectors calculated by simple model.

Coolant Helium

Due to a big gas temperature gradient in radial and axial direction, the diffusive heat transport in the gas phase plays also a role in the total heat transport mechanisms along with convective heat transport. The contribution of this diffusive heat transport which is also known as dispersive heat transport is calculated by replacing the diffusion coefficient with an effective heat transfer coefficient in the diffusion term of the energy equation of the gas. The effective heat conductivity of the gas can be calculated from the following equation as:

$$\lambda_{eff_g} = \lambda_g \frac{Pe}{K} \tag{4.45}$$

The contribution of the dispersive heat transport varies in axial and radial direction and so does the value of K. According to Schlünder [44], the value of K in the radial direction depends on the ratio of the sphere-to-core diameter d/D and can be written as:

$$K_r = 8\left[2 - \left(1 - 2\frac{d}{D}\right)^2\right] \tag{4.46}$$

For a very small d/D value, the $K_r = 8$ can be used. The value of K in axial

direction is smaller than the value in the radial direction and according to Yagi [52], the value can be taken as: $K_z = 1.3$.

4.3 Fuel Model

Pebble Fuel Model

In order to get the solid temperature profile, the total reactor geometry is subdivided into a number of control volumes and the energy conservation equation of solid is resolved for each control volume. It is assumed that the heat source is homogeneously distributed inside the solid fraction of each control volume. The solution of the energy equation with a homogeneous heat source assumption is the average temperature of the solid. But the reality is different where thousands of Triso coated particles (around 12000 for PBMR-400) are embedded in the inner 2.5 cm radius graphite matrix and are surrounded by a 0.5 cm graphite layer. The heat source is concentrated inside the 0.5 mm fuel kernel sphere which is surrounded by four different types of coatings (shown in figure 4.7). The thermal properties (e.g. heat conductivity, heat capacity, etc.) of the fuel kernel are different than the properties of graphite and the surrounding layers. During a steady state operation or for a slow transient, the time of changing the power with changing reactivity is higher than the relaxation time for the temperature adjustment between fuel kernel and its surrounding graphite. For high temperature reactors, this relaxation time varies from 10^{-2} to 10^{-1} seconds [45] and the assumption of homogeneous heat source can be justified for steady state and slow transients. But for the case of a fast transient, where the time of changing reactivity is very small compared to temperature relaxation time, large differences are observed between the results obtained from a homogeneous and a heterogeneous assumption [37].

In TH3D, a heterogeneous fuel model for pebble fuel is implemented where the temperature profile inside the pebble is calculated by considering the heterogeneous heat source distribution. In this model, a particle representing the average properties of all the Triso particles in the graphite matrix zone is defined as a representative particle and is used to calculate the temperature profile. In this representative particle, the fuel kernel and its four layers are surrounded by a part of graphite matrix. The amount of graphite matrix which surrounds one Triso particle is the volume fraction of the total graphite matrix for a single Triso particle. The temperature of the fuel kernel of this representative particle is used for the neutronic calculation to get the reactivity feedback.

To get the maximum fuel temperature, discretization of the graphite matrix zone into shells is made. It is clear that the maximum temperature occurs at the inner most shell of the matrix. Another triso particle also surrounded by volume fraction of graphite matrix, called test particle, is taken from innermost shell of matrix zone and used to get the maximum fuel temperature inside the fuel sphere. The

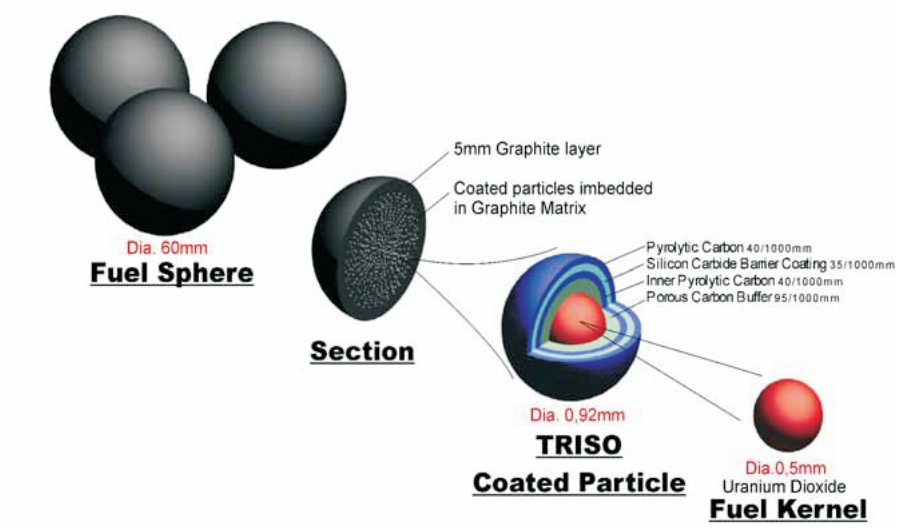

Figure 4.7: Pebble fuel specifications

average temperature of the shells is assigned as the outer boundary temperature for the representative particle and the maximum temperature at the inner most shell is assigned as the outer boundary temperature for the test particle. The heat transfer between different matrix zone, surrounding graphite surface and different layers of the Triso particle were calculated by a heat resistance model.

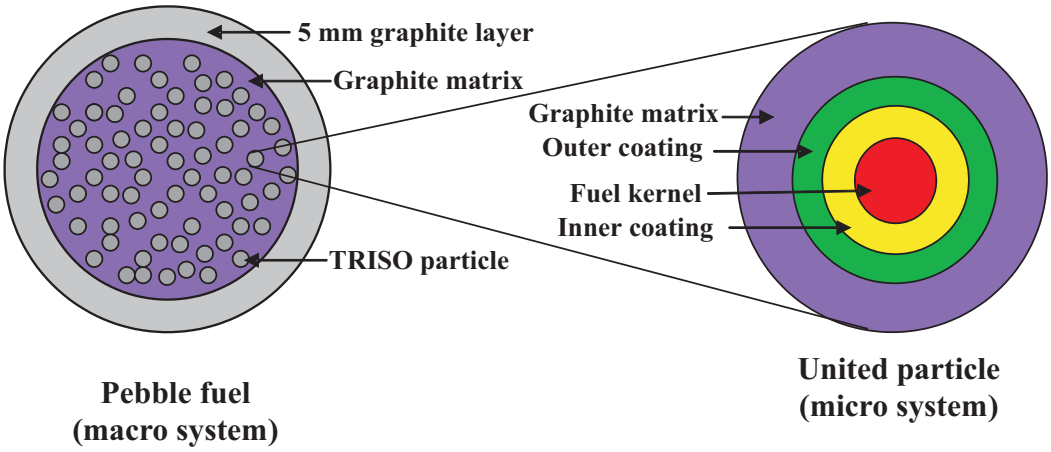

Figure 4.8: Representation of fuel model (macro system and micro system)

Each particle (representative and test particle) contains UO_2 fuel kernel surrounded by four coatings and the volumetric fraction of the graphite matrix for one Triso particle. The graphite matrix that belongs to one Triso particle is calculated from the following equation:

$$n_p \cdot \frac{4\pi}{3} \cdot r_m^3 = \frac{4\pi}{3} \cdot r_M^3 \tag{4.47}$$

Here, n_p is the number of Triso particles embedded in graphite matrix of each pebble fuel, r_M and r_m are the radius of graphite matrix zone and the radius of the united particle (Triso particle along with volume fraction of matrix graphite) respectively. For the pebble fuel generally used in high temperature reactors, the value of $r_M = 2.5cm$ and $r_m \approx 1mm$.

The temperature profile in both particles (representative and test particles) is calculated by solving the heat conduction equation. For the stationary case, the heat conduction equation for the test particle can be written as:

$$-\nabla \cdot (\lambda \nabla (T)) = \begin{cases} \dot{q_k} & \text{if } r \leq r_k \\ 0 & \text{if } r_k \leq r \leq r_m \end{cases} \tag{4.48}$$

Here, r_k is the radius of the fuel kernel, r_m is the radius of the united particle, and $\dot{q_k}$ is the average power density in the fuel kernel. The value of the average power density in the fuel kernel can be expressed as:

$$\dot{q_k} = \frac{\dot{q}}{1-\varepsilon} \frac{V_S}{V_M} \frac{V_m}{V_k} = \frac{\dot{q}}{1-\varepsilon} \frac{r_S^3}{r_M^3} \frac{r_m^3}{r_k^3} \tag{4.49}$$

Here, $\dot{q}$ is the volumetric rate of nuclear heat generation in the core, V_S, V_M, V_m and V_k are the volume of the pebble sphere, matrix graphite, united particle, and fuel kernel respectively. In this present temperature model, the inner most coating (porous carbon buffer layer) of united particle is considered as inner coating and other three coatings (inner Pyrolytic carbon, Silicon carbide barrier coating, and outer Pyrolytic carbon layer) are considered together and defined as outer coating (shown in figure 4.8). The material properties of this outer coating layer is calculated by averaging the values of three layers. The temperature profile in the united representative particle can be written as:

$$T(r) = \begin{cases} T_k(r) & \text{when } 0 \leq r \leq r_k \\ T_{ic}(r) & \text{when } r_k \leq r \leq r_{ic} \\ T_{oc}(r) & \text{when } r_{ic} \leq r \leq r_{oc} \\ T_m(r) & \text{when } r_{oc} \leq r \leq r_m \end{cases} \tag{4.50}$$

Here, T_k, T_{ic}, T_{oc}, and T_m are the temperature and r_k, r_{ic}, r_{oc}, and r_m are the radius of fuel kernel, inner coating, outer coating, and surrounded graphite matrix respectively for the united representative particle. By integrating the equation 4.48

for a spherical co-ordinate system and using the boundary condition $\frac{\partial T}{\partial r} \mid_{r=0} = 0$, the temperature profile in the fuel kernel for the representative particle can be expressed by the following equations as:

$$T_k(r) = T_{kic} + \frac{\dot{q_k}}{6\lambda_k} \cdot \left(r_k^2 - r^2\right) \tag{4.51}$$

Here, T_{kic} is the temperature at the boundary between fuel kernel and inner coating ($T_k(r = r_k) = T_{ic}(r = r_k) = T_{kic}$), and λ_k is the heat conductivity of the fuel kernel. The volumetric average temperature of the fuel kernel for the representative particle is:

$$\overline{T}_k = \frac{\int 4\pi r^2 T_k(r) dr}{\int 4\pi r^2 dr} \tag{4.52}$$

By using the equation 4.52 and 4.51, the average temperature in the fuel kernel can be expressed as:

$$\overline{T}_k = T_{kic} + \frac{r_k^2}{15\lambda_k} \cdot \dot{q_k} \tag{4.53}$$

Similarly, by integrating the equation 4.48, the average temperature in the inner coating of the united representative particle can be written as:

$$\overline{T}_{ic} = T_{kic} - \frac{r_k^3}{3\lambda_{ic}} \left(\frac{1}{r_k} - \overline{\left(\frac{1}{r}\right)}_{kic}\right) \cdot \dot{q_k} \tag{4.54}$$

Here,

$$\overline{\left(\frac{1}{r}\right)}_{kic} = \frac{3}{2} \cdot \frac{r_{ic}^2 - r_k^2}{r_{ic}^3 - r_k^3} \tag{4.55}$$

Here, $\overline{T}_{ic}$ is the average inner coating temperature and λ_{ic} is the inner coating heat conductivity. The stationary heat flow at the boundary between fuel kernel and inner coating can be written according to Ohm's law by using the thermal resistance between fuel kernel and inner coating ($RKIC$) and can be expressed as:

$$\frac{4\pi r_k^3}{3} \cdot \dot{q_k} = \frac{4\pi r_k^3}{3} \cdot \frac{\overline{T}_k - \overline{T}_{ic}}{RKIC} \tag{4.56}$$

Here,

$$RKIC = \frac{r_k^2}{15\lambda_k} + \frac{r_k^3}{3\lambda_{ic}} \left(\frac{1}{r_k} - \overline{\left(\frac{1}{r}\right)}_{kic}\right) \tag{4.57}$$

A possible xenon gas build up which could produce a gas layer in between fuel

kernel and inner buffer coating and enhances the thermal resistance is also considered. Provision is made in this model to consider the resistance from this gas layer. If the thickness of the gas layer is δ, the thermal resistance in between fuel kernel and inner buffer coating can be written as:

$$RKIC = \frac{r_k^2}{15\lambda_k} + \frac{r_k^3}{3\lambda_x}\left(\frac{1}{r_k} - \frac{1}{r_k+\delta}\right) + \frac{r_k^3}{3\lambda_{ic}}\left(\frac{1}{r_k+\delta} - \overline{\left(\frac{1}{r}\right)}_{xic}\right) \tag{4.58}$$

Here,

$$\overline{\left(\frac{1}{r}\right)}_{xic} = \frac{3}{2}\cdot\frac{r_{ic}^2 - (r_k+\delta)^2}{r_{ic}^3 - (r_k+\delta)^3} \tag{4.59}$$

Here, λ_x is the thermal conductivity of the xenon gas, and δ is the thickness of the xenon gas layer. In the similar procedure, the thermal resistance between inner coating and outer coating (RICOC) can be expressed as:

$$RICOC = \frac{r_k^3}{3\lambda_{ic}}\left(\overline{\left(\frac{1}{r}\right)}_{xic} - \frac{1}{r_{ic}}\right) + \frac{r_k^3}{3\lambda_{oc}}\left(\frac{1}{r_{ic}} - \overline{\left(\frac{1}{r}\right)}_{icoc}\right) \tag{4.60}$$

Here,

$$\overline{\left(\frac{1}{r}\right)}_{icoc} = \frac{3}{2}\cdot\frac{(r_{oc}^2 - r_{ic}^2)}{(r_{oc}^3 - r_{ic}^3)} \tag{4.61}$$

Here, λ_{oc} is the effective heat conductivity of the outer coating which is calculated from the heat conductivity and thickness of the three layers from which the outer coating is composed of and can be expressed by the following equation:

$$\lambda_{oc} = \frac{\left(\frac{1}{r_{ic}} - \frac{1}{r_{oc}}\right)}{\frac{1}{\lambda_1}\left(\frac{1}{r_{ic}} - \frac{1}{r_{c1}}\right) + \frac{1}{\lambda_2}\left(\frac{1}{r_{c1}} - \frac{1}{r_{c2}}\right) + \frac{1}{\lambda_3}\left(\frac{1}{r_{c2}} - \frac{1}{r_{oc}}\right)} \tag{4.62}$$

Here, λ_1, λ_2 and λ_3 are the thermal conductivities and r_1, r_2, and r_3 are the radius of the three layers respectively. Similarly the thermal resistance between outer coating and the surrounding matrix graphite (ROCM) can be written as:

$$ROCM = \frac{r_k^3}{3\lambda_{oc}}\left(\overline{\left(\frac{1}{r}\right)}_{oc} - \frac{1}{r_{oc}}\right) + \frac{r_k^3}{3\lambda_m}\left(\frac{1}{r_{oc}} - \overline{\left(\frac{1}{r}\right)}_{ocm}\right) \tag{4.63}$$

Here,

$$\overline{\left(\frac{1}{r}\right)}_{ocm} = \frac{3}{2}\cdot\frac{(r_m^2 - r_{oc}^2)}{(r_m^3 - r_{oc}^3)} \tag{4.64}$$

Here, λ_m is the heat conductivity of the matrix graphite. The temperature of the

surrounding graphite matrix for the representative particle is the average temperature of the total matrix zone and for the case of test particle, it is the maximum graphite matrix temperature. As it is mentioned earlier, the graphite matrix is discretized into several shells and the thermal resistance model, used for representative and test particle, is also used for calculating the heat flow between two matrix shells.

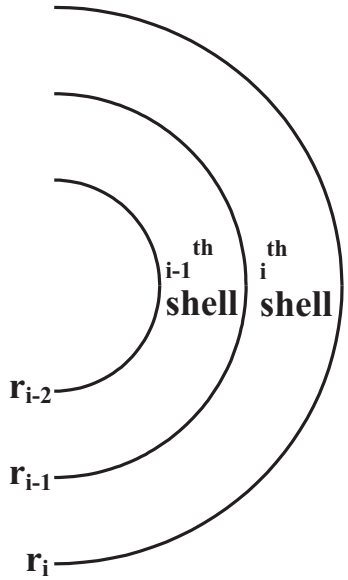

Figure 4.9: Representation of the different shells in the pebble fule

The thermal resistance for heat flow between two matrix shells (i^{th} and $(i-1)^{th}$ shells) can be expressed by the following equation as:

$$RMMZ(i) = \frac{1}{10\lambda_m}\left(\frac{r_{i-1}^5 - r_i^5}{r_{i-1}^3 - r_i^3} - \frac{r_i^5 - r_{i+1}^5}{r_i^3 - r_{i+1}^3}\right) \tag{4.65}$$

The numbering of the shells starts from outer most shell to inner most shell and r_i and r_{i-1} are the outer and inner radius of the i^{th} shell. At the boundary between outermost matrix shell and fuel free graphite hull, $r_i = r_1 = r_M$ and the thermal resistance for heat flow at the boundary (RMMS) can be written as:

$$RMMS = RMMZ(1) = \frac{1}{10\lambda_m}\left(0 - \frac{r_1^5 - r_2^5}{r_1^3 - r_2^3}\right) + \frac{r_M^2}{6\lambda_m} + \frac{r_M^2}{3\lambda_S}\left(1 - r_M\overline{\left(\frac{1}{r}\right)}_{MS}\right) \tag{4.66}$$

Here,

$$\overline{\left(\frac{1}{r}\right)}_{MS} = \frac{3}{2}\cdot\frac{(r_S^2 - r_M^2)}{(r_S^3 - r_M^3)} \tag{4.67}$$

Here, λ_S is the heat conductivity and r_S is the radius of the fuel free graphite hull/surface layer. For stationary case, the heat conduction equation for pebble fuel can be written as:

$$-\nabla \cdot (\lambda \nabla (T)) = \begin{cases} \dot{q_M} & \text{if } r \leq r_M \\ 0 & \text{if } r_M \leq r \leq r_S \end{cases} \tag{4.68}$$

where, r_M is the radius of the matrix zone, r_S is the radius of the pebble sphere, and $\dot{q_M}$ is the average nuclear power density in the matrix zone. The value of the nuclear power density in the matrix zone can be expressed as:

$$\dot{q_M} = \frac{\dot{q}}{1-\varepsilon} \frac{V_S}{V_M} = \frac{\dot{q}}{1-\varepsilon} \frac{r_S^3}{r_M^3} \tag{4.69}$$

where, $\dot{q}$ is the average volumetric rate of nuclear heat generation in each control volume, V_S, V_M are the volume of the pebble sphere and matrix graphite respectively. The temperature profile in the pebble fuel can be written as:

$$T(r) = \begin{cases} T_{MMZ}(r) & \text{when } 0 \leq r \leq r_M \\ T_S(r) & \text{when } r_M \leq r \leq r_S \end{cases} \tag{4.70}$$

where, T_{MMZ} and T_S are the temperature and r_M and r_S are the radius of matrix zone and fuel free graphite hull/surface layer respectively. By integrating the equation 4.68 for spherical co-ordinate system and using the procedures described earlier for both representative and test particle, the average pebble surface layer temperature can be written as:

$$\overline{T}_S = T_W + \dot{q_M} \cdot \frac{r_M^3}{3\lambda_S} \left(\overline{\left(\frac{1}{r}\right)}_S - \frac{1}{r_S} \right) \tag{4.71}$$

when,

$$\overline{\left(\frac{1}{r}\right)}_S = \frac{3}{2} \cdot \frac{r_S^2 - r_M^2}{r_S^3 - r_M^3} \tag{4.72}$$

where, T_W is the pebble surface/wall temperature, $\overline{T}_S$ is the average temperature of the fuel free graphite hull/surface layer and λ_S is the heat conductivity of the surface layer. Heat produced inside the pebble fuel is transported by the coolant gas flowing around the surface of the pebble fuel. The heat flow at the surface of the pebble fuel ($r = r_S$) must satisfy the following boundary condition.

$$-\lambda_S \frac{dT_S}{dr} = \alpha(T_W - T_g), \qquad at \quad r = r_S \tag{4.73}$$

where, α is the heat transfer coefficient between pebble surface and gas, T_g is the

surrounding gas temperature and T_W is the pebble surface temperature. The heat flow at the surface of the pebble W_{SG} can also be written by using thermal resistance as:

$$W_{SG} = \frac{4}{3}\pi r_M^3 \frac{\overline{T}_S - T_g}{RSG} \tag{4.74}$$

where, RSG is the thermal resistance between pebble surface and gas and W_{SG} is the heat flow from pebble surface to gas. By using equation 4.71, 4.73, and 4.74 the thermal resistance RSG can be written as:

$$RSG = \frac{r_M^3}{3\lambda_S}\left(\overline{\left(\frac{1}{r}\right)}_S - \frac{1}{r_S}\right) + \frac{r_M^3}{3\alpha r_S^2} \tag{4.75}$$

For dealing with transient problems, it is assumed that the spatial temperature profile during a power excursion remains the same and the heat flow between different layers, which are calculated analytically for stationary case by using Ohm's law, is also valid for this case. By using the thermal resistance derived earlier, the temperature in different zones (e.g. layers, shells, kernels) can be expressed by the following ordinary differential equations.
Fuel kernel:

$$c_k \rho_k \frac{dT_k}{dt} = \dot{q_k} - \frac{T_k - T_{ci}}{RKIC} \tag{4.76}$$

where, c_k, ρ_k are the specific heat capacity and density of fuel kernel respectively and $\dot{q_k}$, $RKIC$ are the average nuclear power density in fuel kernel and the thermal resistance between fuel kernel and inner coating (see equations 4.49 and 4.57).
Inner coating:

$$c_{ic} \rho_{ic} \frac{dT_{ic}}{dt} = \frac{X_k}{X_{ic}}\left(\frac{T_k - T_{ic}}{RKIC} - \frac{T_{ic} - T_{oc}}{RICOC}\right) \tag{4.77}$$

Outer coating:

$$c_{oc} \rho_{oc} \frac{dT_{oc}}{dt} = \frac{X_k}{X_{oc}}\left(\frac{T_{ic} - T_{oc}}{RICOC} - \frac{T_{oc} - T_{mm}}{ROCM}\right) \tag{4.78}$$

Graphite matrix is subdivided into several shells (see fig. 4.9) and for i^{th} shell, the equation can be written as:

$$\begin{aligned} c_M \rho_M \frac{dT_{MMZ}(i)}{dt} = \big(&\tfrac{T_{MMZ}(i+1) - T_{MMZ}(i)}{RMMZ(i+1)} \cdot \tfrac{r(i+1)^3}{r(i)^3 - r(i-1)^3} \quad + \\ &\tfrac{T_{OC} - T_{mm}}{ROCM} \cdot X_k - \tfrac{T_{MMZ}(i) - T_{MMZ}(i-1)}{RMMZ(i)} \cdot \tfrac{r(i)^3}{r(i)^3 - r(i-1)^3}\big)/X_M \end{aligned} \tag{4.79}$$

when,

$$T_{mm} = \frac{\sum_i \overline{T}_{MMZ}(i) \cdot V(i)}{\sum_i V(i)} \tag{4.80}$$

Fuel free graphite hull/surface layer:

$$c_S \rho_S \frac{d\overline{T}_S}{dt} = \left(\frac{T_{MMZ}(1) - \overline{T}_S}{RMMZ(1)} - \frac{\overline{T}_S - T_g}{RSG} \right) \tag{4.81}$$

where, X_k, X_{ic}, X_{oc}, and X_M are the volume fraction of fuel kernel, inner coating, outer coating and surrounding matrix graphite in the united particle. For getting the feedback of neutronics and thermal hydraulics, the averaged fuel kernel temperature $\overline{T}_k$ is used as fuel temperature and the moderator temperature is calculated by volumetric average of graphite matrix and graphite hull temperature and can be written as:

$$\overline{T}_{moderator} = \frac{\left(V_{matrix} \cdot T_{mm} + V_{hull} \cdot \overline{T}_S \right)}{V_{pebble}} \tag{4.82}$$

where, $\overline{T}_{moderator}$ is the average moderator temperature used for neutronics feedback calculation, T_{mm} is the average matrix graphite temperature (see equation 4.80) and $\overline{T}_S$ is the average fuel free graphite hull/surface layer temperature (see equation 4.81) and V_{matrix}, V_{hull}, V_{pebble} are the volume of graphite matrix, graphite hull, and total pebble respectively.

4.4 Numerical Methods

Spatial Discretization

The set of partial differential equations illustrated in the previous sections, which are used for getting the dependent variables of interest (temperature, pressure, velocities, etc), obeys a generalized conservation principle and can be expressed as:

$$\frac{\partial}{\partial t} (\rho\phi) + \nabla \cdot (\rho u \phi) = \nabla \cdot (\Gamma \nabla \phi) + S \tag{4.83}$$

where Γ is the diffusion coefficient, S is the source term and ϕ is the intended dependent variable. The terms in the left hand side of the equation represent the unsteady and convection terms respectively while the terms in the right hand side of the equation represent diffusion and source terms respectively. A variety of variables (e.g. mass flux, temperature/enthalpy, velocity, turbulence kinetic energy, etc) can be represented by ϕ and depending on the variable, the value of the diffusion coefficient Γ and source term S have to be supplied. The integral form of the differential equation can be written as:

$$\int_{\triangle V} \frac{\partial(\rho\phi)}{\partial t} \cdot dV + \int_{\triangle A} (\rho u \phi - \Gamma \nabla \phi) \cdot \overrightarrow{dA} = \int_{\triangle V} S \cdot dV \tag{4.84}$$

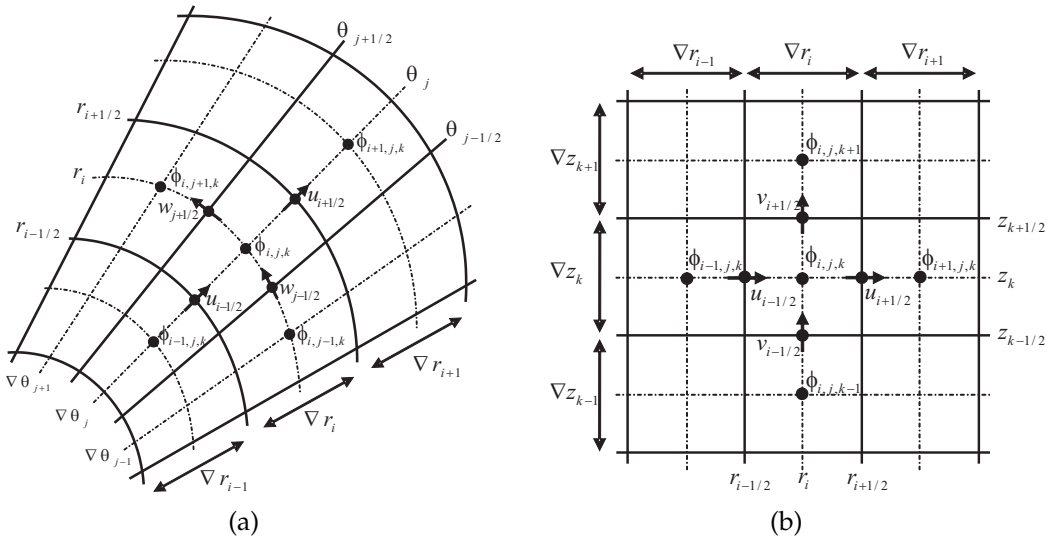

Figure 4.10: Staggered grid used in TH3D: (a) $R - \Theta$ grid (b)$R - Z$ grid

Finite volume approximation is used for spatial discretization of the integral form of the conservation equation in 3D cartesian or cylindrical co-ordinate system. Finite volume method approximates the partial differential equation (PDE) over a control volume surrounding a grid node. The discretization equations are obtained by integrating the PDE over the control volume. To overcome the discretization problem of the pressure gradient, staggered grid technique is used in TH3D program where all variables are calculated at the cell centre while velocities are calculated at the cell surfaces. Figure 4.10 shows the typical staggered grid showing the position of the variables. The values required at the control volume surface, which are not calculated at the surface, are obtained from the cell centered values by an interpolation method.

TIME INTEGRATION

A set of ordinary differential equation is obtained from spatial discretization of the partial differential equation. The obtained ordinary differential equation along with constitutive equations forms a set of differential algebraic equation which is integrated in the direction of time. The time marching integration is performed by the backward differentiation formula method [3]. Backward differentiation formula method is a fully implicit and time adaptive multistep method where time is selected automatically depending on the history of the previous steps. Due to the implementation of the fully implicit method, a non-linear system of equation is produced at each time step.

$$g(y_n) = \sum_{k=1}^{n} \alpha_i y_{n-i} - h\beta_0 f(t_n, y_n) \tag{4.85}$$

Modified Newton method is implemented in TH3D with backward differentiation formula method for solving the nonlinear system of equation at each time step.

$$y_n^{\nu+1} = y_n^{\nu} - \left(\frac{\partial g}{\partial y}(y^{\nu})\right)^{-1} \cdot g(y^{\nu}) \tag{4.86}$$

Instead of computing the matrix inverse to get the value for the next iteration directly, it is better for numerically ill conditions and never worse to solve the linear system for the difference δ,

$$\left(\frac{\partial g}{\partial y}\right)\delta = -g(y^{\nu}) \tag{4.87}$$

For solving the linear system of equations, both direct solver and iterative solver are implemented in TH3D and provision is made for choosing the desired solver. Newton's method requires the evaluation of the Jacobian matrix. For a large system of equations, it is very difficult or a cumbersome task to evaluate the Jacobian matrix analytically. In TH3D, the Jacobian matrix is evaluated by using a difference approximation technique. The Jacobian matrix is evaluated at a previous time step and new Newton iteration is obtained from,

$$y_n^{\nu+1} = y_n^{\nu} + \delta \tag{4.88}$$

Chapter 5

Application to reactor and model verification

According to the defined goals, TH3D is developed to simulate both pebble bed and block type fuel reactors. In order to show the capability of simulating pebble bed reactors, a benchmark calculation oriented to pebble bed reactor is performed. Validation of the results are done by calculating the same benchmark with an existing recognized two dimensional thermal hydraulic program and comparing the results. The capability of TH3D for simulating block fuel reactor is shown by calculating another benchmark oriented to a block fuel reactor. In this case, validation of the results is done by comparing the obtained results with the results obtained by different organizations participated in the benchmark program. The following sections describe the benchmark definition and comparison results for both types of reactor.

5.1 Pebble Bed Reactor

In order to validate the tool's capabilities for simulating pebble bed reactors, a two dimensional benchmark problem is calculated, which is oriented to PBMR-400 design and proposed for a common OECD/NEA/NSC exercise [38]. The calculations address steady state under nominal operation conditions and behavior under loss of cooling accidents with and without de-pressurization. The results of TH3D are compared to those of the well known, well-established thermal-hydraulic code THERMIX/KONVEK [4] [35]. THERMIX/KONVEK is a 2-D thermal hydraulic tool initially developed by research center Jülich, Germany and subsequently used and developed by Siemens for HTR-Module analyses. An in-house version of the code (with some improvements and extended capabilities to simulate various HTR designs, to couple with a neutronics code ZIRKUS) is routinely used at IKE, University of Stuttgart [7] [41].

In the benchmark definition, several assumptions and simplifications are made which help to simulate and analyze the reactor but care has been taken that all

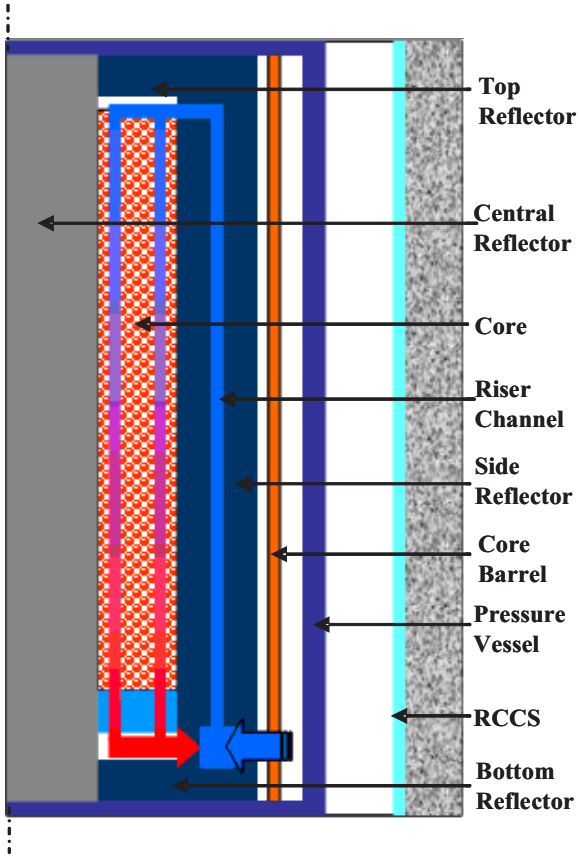

Figure 5.1: Simplified sketch showing geometrical condition used for benchmark definition.

important characteristics of the reactor design are preserved and the results of the benchmark calculation would be representative of the original design. The major assumptions made in the benchmark definition are:

- Flattening of the pebble beds upper surface and neglecting the bottom cone and the de-fuel channel that results a flat bottom reflector.
- Thermal hydraulics simplification includes the consideration of helium and air in the gaps (gaps in between side reflector, core barrel, RPV and RCCS) as stagnant which excludes the convective heat transfer. So, only the heat transfer mechanisms are conduction and radiation in these gaps.
- Reflector cooling, control rod cooling flow, core barrel leakage flow, etc, were removed assuming that these exclusion will be balanced by the assumption that no other heat sources exist outside the core.
- Input plenum, riser channel, bottom porous area and output plenum are suggested to be modeled as porous media with 20% porosity and thermal conductivity of these zones is suggested to be reduced by its porosity.

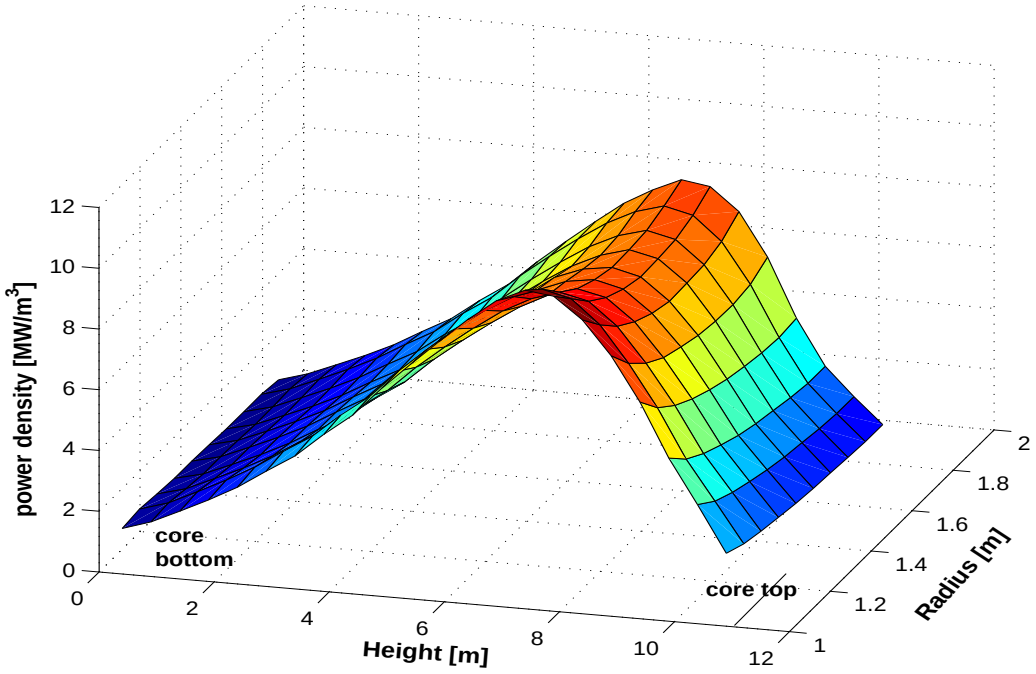

Figure 5.2: Steady-state power density profile in the annular core of the reactor calculated by ZIRKUS code system.

- Flow channels within the pebble bed have been simplified to be parallel and at equal speed.

With the above mentioned assumptions and simplifications, the reactor can be modeled as two dimensional (R, Z) and only a situation of partial control rod operation needs 3-D model. Figure 5.1 shows the simplified sketch of the benchmark geometry. The coolant enters at the bottom of the inlet plenum and flows through the riser channel to the top of the inlet plenum and flows downward through the reactor core, porous bottom reflector to outlet plenum and leaves at the bottom of the outlet plenum. The reflector cooling and leakage paths were not defined as suggested by the benchmark definition. An isothermal boundary condition of constant temperature of 20 $^{\circ}C$ is defined in radial direction and adiabatic boundary condition is defined at the top and bottom plate. The material properties are also used according to the benchmark definition. The details of the geometrical description as well as material properties are given in the official benchmark documentation [38]. The nominal operating condition and core dimensions are given in Table 5.1.

Helium enters at the bottom of the inlet plenum with a flow rate of 192.7 kg/s and with an inlet temperature of 500 $^{\circ}C$. The system pressure is kept at 90 bars. The

Table 5.1: Geometrical and operational data used for comparison calculation.

Description	**Unit**	**Value**
Core inner diameter	m	2
Core outer diameter	m	3.7
RPV outer diameter	m	6.56
Thermal Power	MW	400
Helium mass flow rate	kg/s	192.7
Helium inlet temperature	$^{\circ}C$	500
System pressure	bar	90

inlet plenum, riser channel, porous bottom area and outlet plenum are modeled as porous media with 20% porosity as suggested by the benchmark definition and modeled as one dimensional flow elements. The effective thermal conductivity, which is a key property for reactor design, depends on neutron fluence, irradiation temperatures and also the current temperature of the material (see chapter 3). In the present calculations, only the temperature dependence has been taken into account for all the graphite reflector regions, in order to facilitate the comparison between the models. The thermal conductivity of the reflector with porous area is reduced by its porosity, as suggested in benchmark definition [38]. The effective thermal conductivity inside the pebble bed considers heat transfer by several heat transfer phenomena such as radiation between pebbles, conduction through connected pebbles, convection and conduction in gap. In both models (THERMIX/KONVEK and TH3D), the effective conductivity is calculated by well known Zehner - Schlünder correlation (see chapter 4.2.3).

The nuclear power density of the equilibrium core under steady-state operation conditions is shown in figure 5.2. Power density is calculated by coupling the tool THERMIX to the ZIRKUS neutronics system [7]. The parameters for the neutronics calculations with ZIRKUS have also been taken from the benchmark definition. In the coupling process, an assumed temperature distribution is firstly supplied to the neutronics system (in our case ZIRKUS), which in turn returns the nuclear power densities. In the next step, thermal-hydraulic tool calculates the temperature by using the obtained power densities from neutronics system. Calculated temperature is again supplied to the neutronics system for getting the changed power densities. These processes are continued until a steady-state condition is reached. The decay power profile and history, which was used for the transient calculations, was also calculated by the ZIRKUS system, taking into account the steady state power distribution and the burnup.

In the following sections, the simulation results obtained for the above described problem by using our new thermal hydraulic tool TH3D is presented. The com-

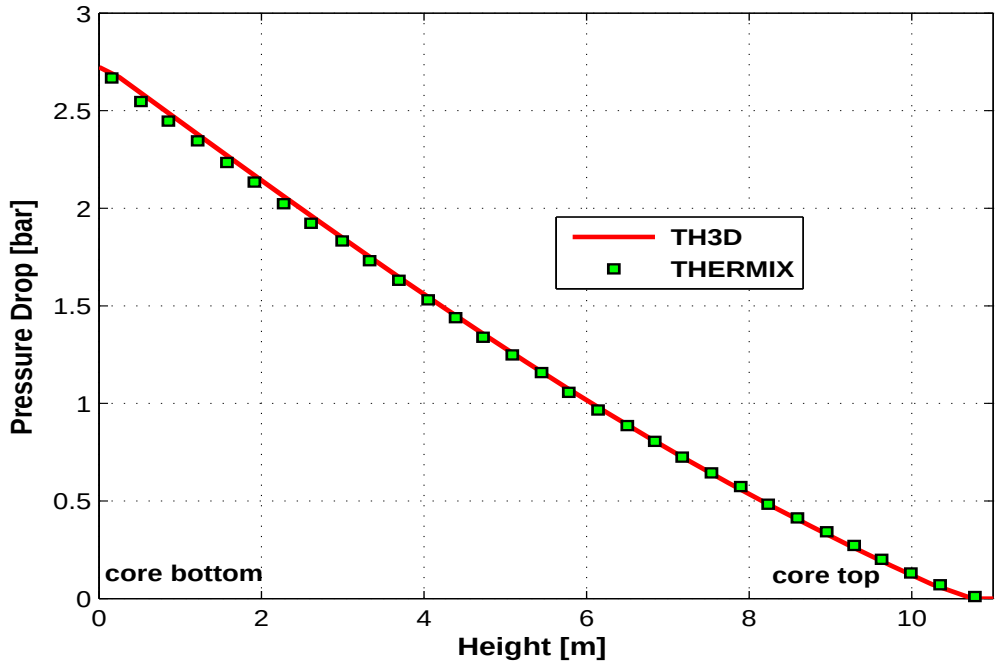

Figure 5.3: Pressure drop along the reactor core at nominal operation.

parison results for the same problem obtained by using the well established code THERMIX/KONVEK is also presented.

5.1.1 Nominal Operation (Steady State)

In normal operating condition, helium enters at the lower part of the inlet plenum with a flow rate of 192.7 kg/s and an inlet temperature of 500 $^{\circ}C$. The system pressure is kept at 90 bars. Helium goes up through the riser channel, upper part of the inlet plenum to top of the reactor core and then flows down through pebble bed, bottom porous reflector to outlet plenum. Heat produced inside the reactor core is transported by the helium gas. Helium gas leaves the outlet plenum with an outlet temperature of around 900 $^{\circ}C$. Figure 5.3 shows the pressure drop of the flow through the reactor core. For this calculation, the pressure drop coefficient was calculated by using KTA norm [26]. It shows a very good agreement with THERMIX result.

Figure 5.4 and figure 5.5 show the radial gas temperature and solid temperature profile at different heights in the reactor. Solid lines represent the profile obtained from TH3D and markers represent the profile obtained from the THERMIX calculation. These radial profiles show a very good agreement between TH3D and THERMIX. Some differences observed especially at the middle of the reactor

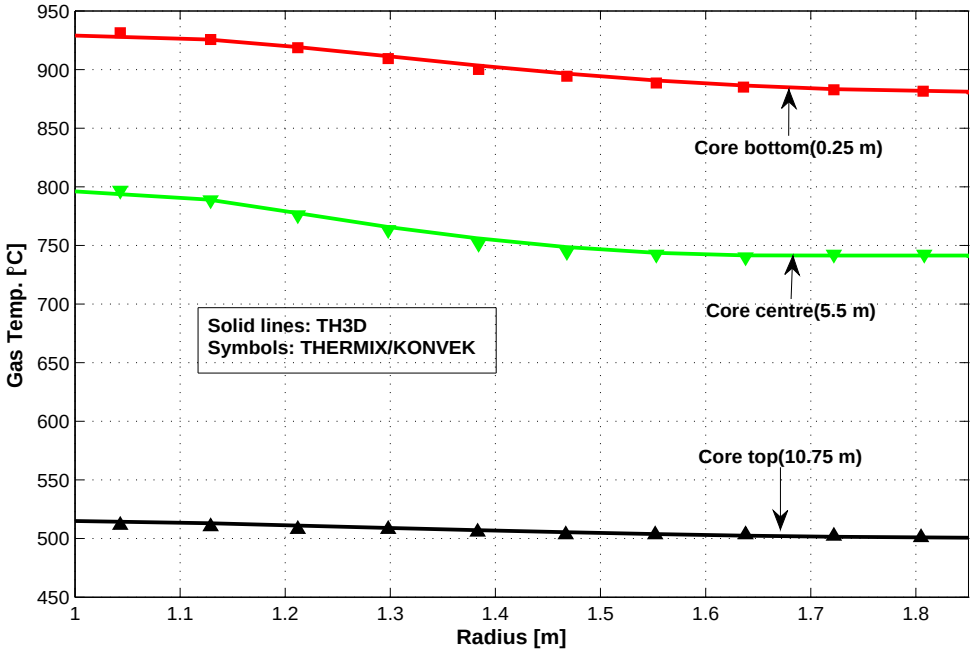

Figure 5.4: Comparison of radial gas temperature profiles at different heights of the reactor.

height could be explained by the positional difference of the plotted variable. Figure 5.6 shows the axial solid temperature profile at the center of the pebble core. It shows also a good consistency between the results, especially in regions with gas flow (core, lower reflector). At the solid structures above and below the gas flow region, some differences are obtained for solid temperature, with the largest value of around 50 $^{\circ}C$ at the lower boundary. At this point, it is difficult to pinpoint the exact reasons for the discrepancy. The assumption of adiabatic top and bottom boundaries clearly enhances differences, which could results from differences in material properties and modeling of heat transfer in the outlet plenum. Also the different discretization schemes (THERMIX uses finite differences with nodes located on material boundaries, while TH3D uses finite volumes with values located in volume centers) may play a role.

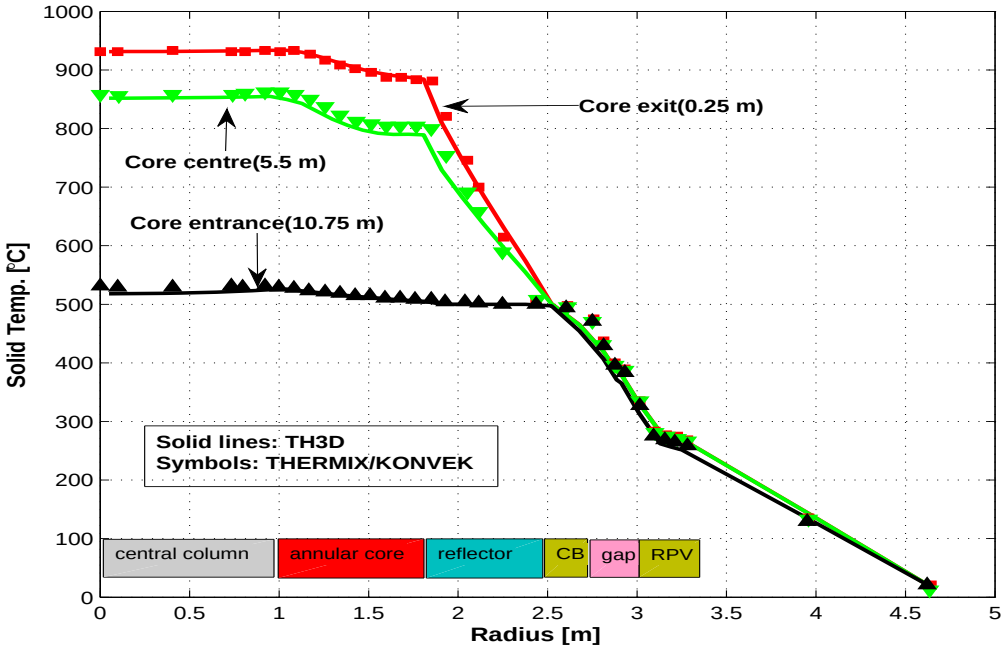

Figure 5.5: Radial solid temperature profiles at different heights of the reactor.

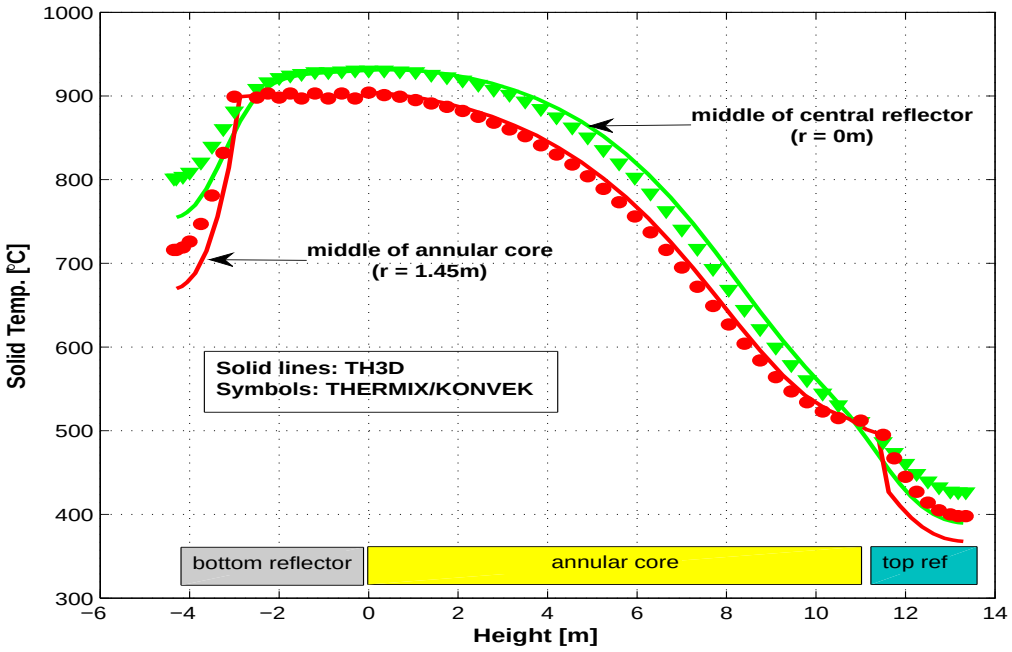

Figure 5.6: Axial solid temperature profiles at the center of the reactor $(r = 0)$ and in the middle of the annular core $(r = 1.425m)$.

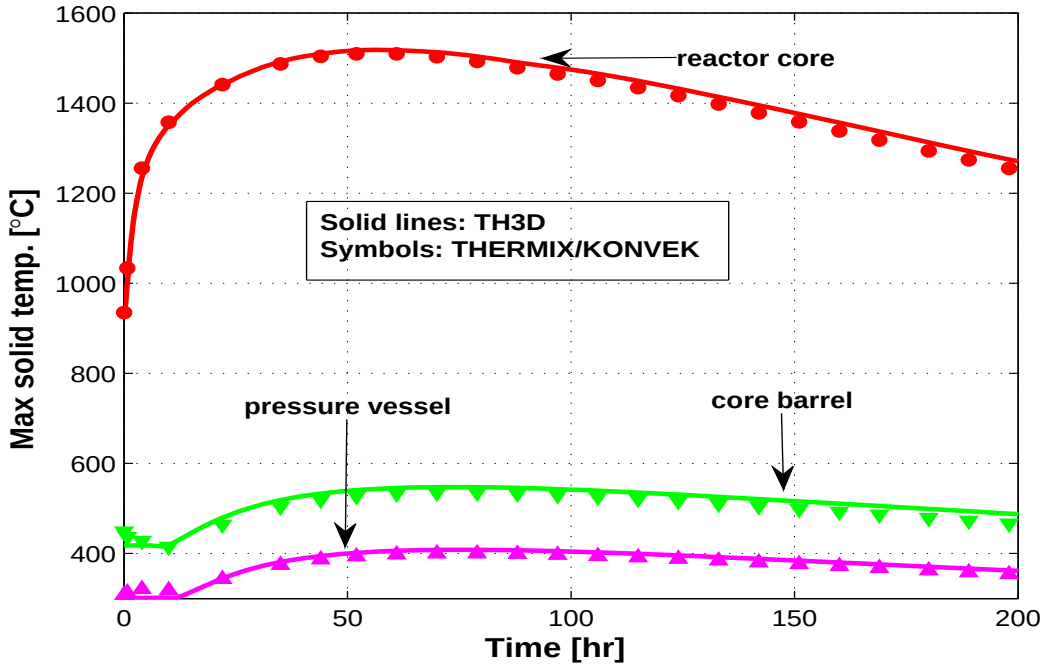

Figure 5.7: Maximum solid temperatures during depressurized loss of coolant accident case.

5.1.2 Depressurized Cooldown

In this section, calculations are presented for an accident scenario with loss of forced coolant and depressurization to ambient pressure, e.g. due to a break of a coolant pipe. This is one of the worst case scenarios where the maximum fuel temperatures are reached, since the only effective mechanisms of transporting decay heat produced in the reactor core are conduction and radiation. Heat transfer by natural convection is negligible due to the low density of helium at atmospheric pressure. Therefore, helium flow has not to be calculated with THERMIX/KONVEK and TH3D for this case. After initiation of the accident the reactor is shut down and the reactor core starts to heat up due to decay heat production. The calculations start with the steady-state solid temperatures and simulate the transient behavior determined by the decay power history, the thermal inertia of materials used in the reactor and the heat removal at the cooled cavity walls (the RCCS is assumed to be working).

Figure 5.7 shows the maximum solid temperatures development during the depressurized loss of coolant accident case for different reactor components. The temperature inside the reactor increases gradually since the produced decay heat is larger than the heat removal by conduction and radiation initially. The temperature inside the core reaches its maximum value 1518 $^{\circ}C$ at around 2.33 days

after the reactor is shut down. At maximum temperature, it shows a quasi-steady behavior for a while and the temperature starts to decrease gradually with decreasing decay heat production and increasing heat removal at RCCS from reactor. For the case of the core barrel and pressure vessel, temperature decreases initially few hours after initiation of the accident instead of increasing. The reason is the very high heat capacity of the reactor internals (fuel, inner, side, top and bottom reflectors). Initially after accident, the produced decay heat starts to heat up the core, inner and side graphite reflectors through radiation and conduction. It takes a few hours to heat up these components and during this time the temperature of the side components (e.g. core barrel, pressure vessel, etc) decreases and heat removal rate at RCCS is low. But once the core, inner and side reflectors are heated up, heat starts to flow in the radial direction and the temperature of the core barrel and pressure vessel starts to increase and so does the heat removal rate at RCCS. With time, the temperature of the core barrel and pressure vessel reach some maximum value and decrease again with decreasing decay heat production. The comparison of the THERMIX and TH3D results shows a very close agreement and small discrepancies can be the result of different discretisation used, material properties, etc.

Figure 5.8 shows the temperature profile at steady state conditions/prior to shut down of the reactor and at different time, during the transient. In Figure 5.8, it can be seen that the hottest region (region of maximum solid temperature) which occurs at the exit of the reactor core at initial normal operation condition is shifted axially upwards during the depressurized loss of coolant accident (DLOCA) transient and finally shows an axially symmetric temperature profile due to decay heat source distribution.

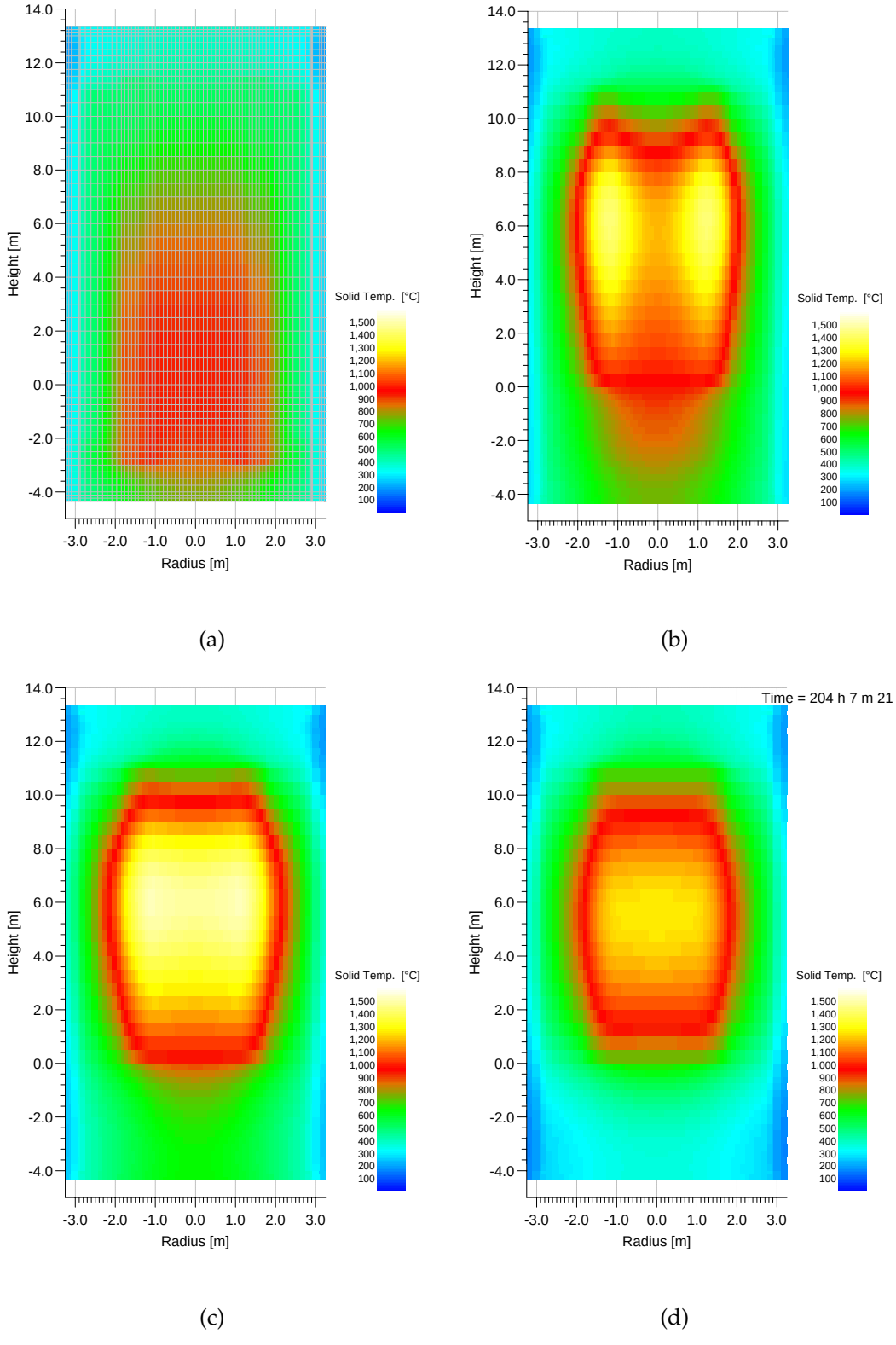

Figure 5.8: Solid temperature profiles at different times during the DLOCA transient: (a) initial steady state, (b)during heat-up at 20hrs, (c) at 56hrs when maximum temperatures are reached and (d) during cool-down at 200hrs

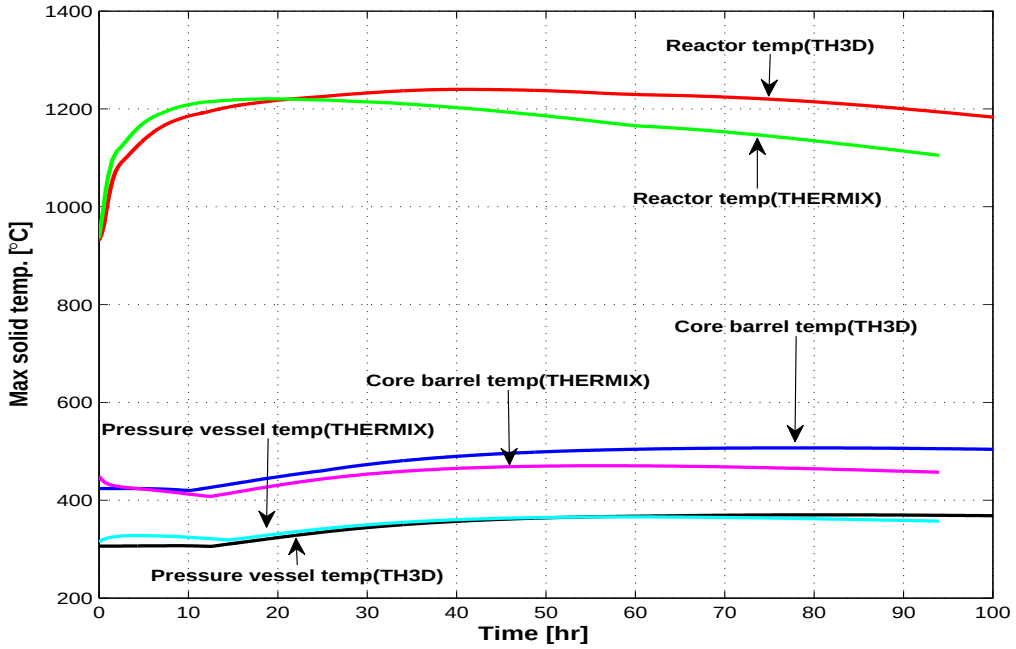

Figure 5.9: Maximum solid temperatures during pressurized cooldown accident.

5.1.3 Pressurized Cooldown

In this section, calculations are presented for an accident scenario where forced convection cooling fails, but the reactor is not depressurized. In this case, natural convection flow is an important mechanism for decay heat removal in addition to conduction and radiation. As in the DLOCA case it was also assumed that after initiation of the accident the reactor is shut down and the RCCS is assumed to be working.

Figure 5.10 shows the temperature distribution and the natural convection flow field at different times. It can be seen that shortly after initiation of the accident a natural convection loop establishes in the core, where helium flows upwards along the inner boundary next to the central column and downwards along the colder boundary to the side reflector. This natural convection loop transports heat towards the upper core regions, so the hottest spot in the reactor moves from the core outlet, where it was during normal operation, to about 8m above the lower core end. The natural convection provides an effective mechanism to enhance the heat removal from the core.

Figure 5.9 shows the maximum temperature development during a pressurized loss of coolant accident (PLOCA) in the core, core barrel and in the pressure vessel. Compared with the results for the DLOCA case in figure 5.7, the maximum

temperature reached is about $300°C$ lower; the time to reach the temperature maximum is significantly shorter. This difference stems from natural convection in overall heat transport mechanism. Since the natural convection is one of the most important heat transport mechanism during PLOCA, heat disperses quickly inside the reactor and the heat removal of the reactor cavity cooling system is consequently enhanced.

Since the maximum temperature during PLOCA is much less than in a DLOCA case, this case does not play a role for defining the permissible maximum reactor's power. But in this case, temperature changes very rapidly compared to the DLOCA case due to the role of natural convection. This rapid temperature change is very important for stress, strain calculation of some reactor components like top, side and bottom reflectors, absorber systems and control rod systems, etc. Beside the rapid temperature change, the top reflector and the upper part of the side reflectors experienced higher temperature during PLOCA case than DLOCA case which is important for designing the upper part of the reactor.

Looking at the results in figure 5.9, it can be seen that the agreement between the results with TH3D and THERMIX/KONVEK is not as close as it was for the DLOCA case. The maximum temperatures in the core is almost the same (differs by less than $20°C$) but the temperature development profile (the time to reach the maximum temperature, cooldown process, etc) differs strongly. These differences could come from the difference in convective heat transport modeling and deserve further inspection and benchmark calculation.

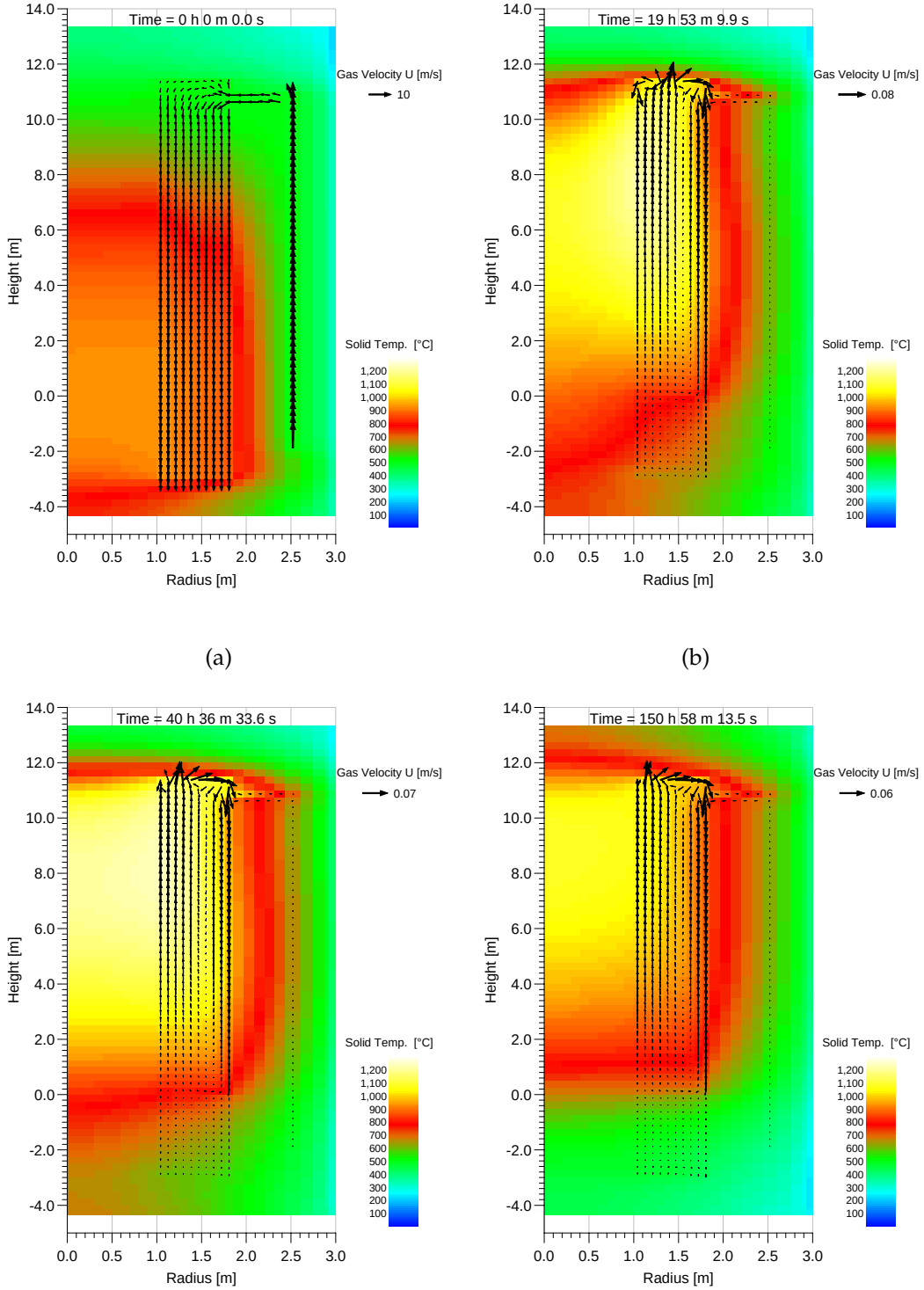

Figure 5.10: Solid Temperature profiles (color scale) and gas velocities (arrows) at different times during the PLOCA transient: (a) initial steady state, (b) during heat-up at 20hrs, (c) at 40.5hrs when maximum temperatures are reached and (d) during cool-down at 151hrs

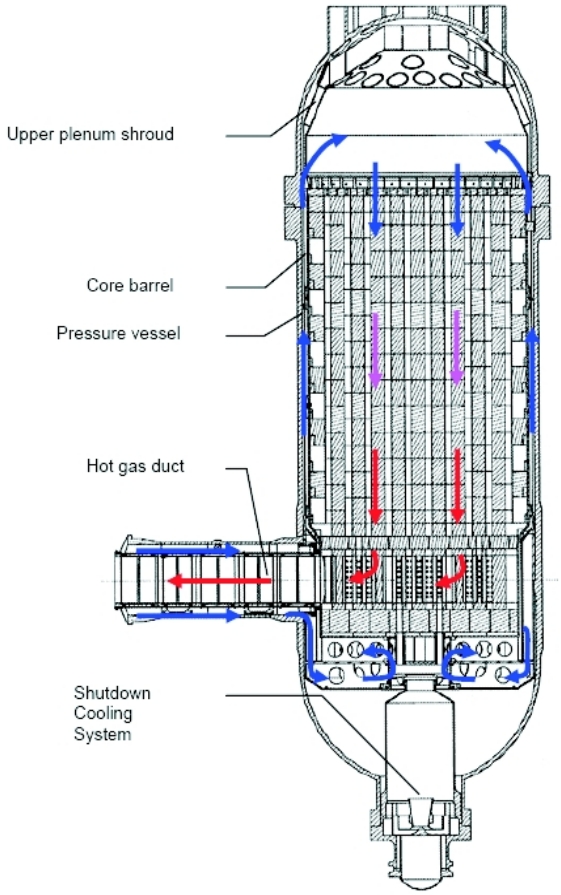

Figure 5.11: GT-MHR reactor layout.

5.2 Block Fuel Reactor

For validating the tool's capabilities for simulating block type fuel reactors, an IAEA CRP-3 benchmark problem which is related to the Gas Turbine Modular Helium Reactor (GT-MHR) [46] [47] [32] was calculated and own results were compared with the results obtained from different code systems used by different countries participants in the CRP-3 program. It is a 2D benchmark problem and several simplifications were made in the benchmark layout. Figure 5.11 illustrates the GT-MHR core layout.

The GT-MHR is a passively safe, helium cooled, graphite moderated modular reactor which uses weapon grade plutonium as fuel. The reference plant consists of four 600 MWt (286 MWe) module reactors and a total electricity generation capacity is 1144 MWe. The core consists of 1020 hexagonal prismatic fuel elements stacked in a ten element high annular array with 120 columns. The height of each fuel element is 0.8m and it is 0.35m wide across the flat. Each prismatic block contains 108 coolant passage channels with 16mm diameter and in-between these

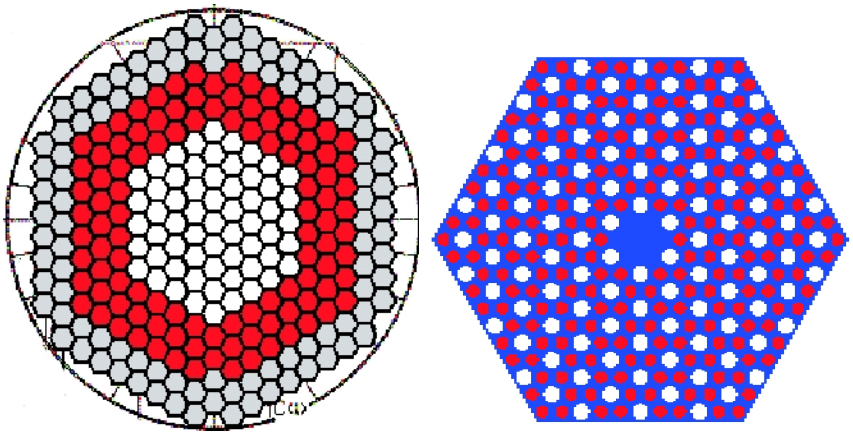

Figure 5.12: Arrangements of fuel and reflector blocks in the core (left) and arrangements of the coolant passage channels and fuel compact channels in the fuel blocks (red circles are fuel rods and white circles are coolant channels).

Table 5.2: Key design parameters for GT-MHR PU burner reactor.

Core thermal power	600 MWt
Average power density	6.5 MW/m^3
Helium pressure at inlet	70.7 bar
Helium flow rate	320 kg/s
Inlet/Outlet temperature	490 / 850 $^\circ C$
Core inner/outer diameter	2.96 / 4.48 m
Core height	8 m
Pressure vessel outer diameter	7.7 m
Total number of fuel blocks	1020
Block type	Hexagonal
No of helium channel per block	108 (dia 16mm)
No of fuel compacts per block	216 (dia 12.5mm)
Gap between blocks	2 mm
Power conversion system	Brayton cycle
Core electric power	286 MWe

coolant passage channels there are 216 channels for fuel compacts. Figure 5.12 illustrates the arrangements of the fuel and reflector blocks in the core as well as the arrangements of the coolant and fuel channels in the prismatic fuel blocks.

Coolant helium enters into the core with a flow rate of 320 kg/s and the entrance temperature and pressure are 490$^{\circ}C$ and 7.07 MPa respectively. The thermal power (600MWt) produced in the core is transported by the coolant helium and leaves the core exit at 850$^{\circ}C$ and 7.01MPa. Since the direct Brayton power cycle is used for power conversion, the helium coolant leaving the core flows through centre hot duct within the cross vessel and expands through the turbine in the power conversion vessel. All technical data for calculating this benchmark problem were taken from the CRP-3 benchmark description for GT-MHR plutonium burner accidents [23] and from thermal response of high temperature reactor during passive cooldown under pressurized and depressurized conditions [20]. The major design parameters are listed in Table 5.2.

The nuclear power of the equilibrium core under steady state operation condition and decay heat source during accident conditions are illustrated in figure 5.13 and figure 5.14. The power distribution and decay heat sources were taken from Haque [20] and were calculated for THERMIX mesh points. Parameters used for this neutronics calculation were also taken from CRP-3 benchmark description [23]. Calculations were performed for steady state condition as well as for loss of forced cooling (LOFC) with and without depressurization conditions. Obtained results were compared with results obtained for the same benchmark calculation performed by other countries/organizations, which participated in the CRP-3 program. Participated countries and codes used for this benchmark calculation are listed in Table 5.3.

The decay heat produced during accident condition must be removed through boundaries to keep the temperature of the reactor components (e.g. fuel compacts, core barrel, reactor vessel, cavity, concrete, etc.) within required limits. The GT-MHR Pu-burner reactor offers two Reactor Cavity Cooling Systems (RCCS) at the radial and lower directions which remove the heat from the reactor cavity. And small portion of the heat is removed from the reactor vessel to the top iron-concrete closure and further to the surrounding air. For this benchmark calculation, boundary conditions for heat removal in the radial and lower boundaries (which represents RCCS) are set to 65$^{\circ}C$ and 40$^{\circ}C$, respectively, according to the benchmark definition. In the upper direction, the air temperature above the iron-concrete closure is set to 30$^{\circ}C$.

Table 5.3: Perticipated organizations in the CPR-3 benchmark program.

Organizations	**Used Code**
CEA, France	CASTEM, a 2D finite element code
ECN, Netherlands	CFX-F3D, a computational fluid dynamics code
OKBM, Russia	GTAS, a 2D code
INET, China	THERMIX/KONVEK, a 2D code
ORNL, USA	MORECA, a 3D code

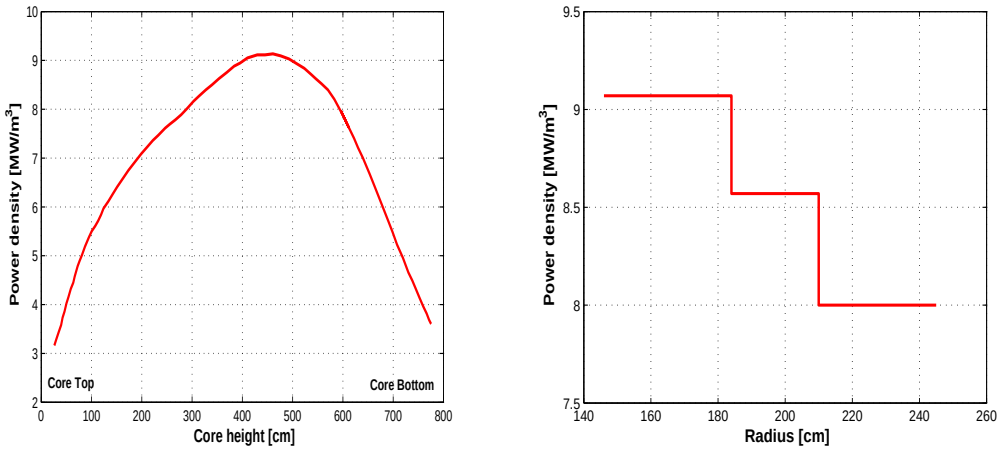

(a) (b)

Figure 5.13: Power profile in GT-MHR reactor core: (a) Axial power distribution (b)Radial power distribution

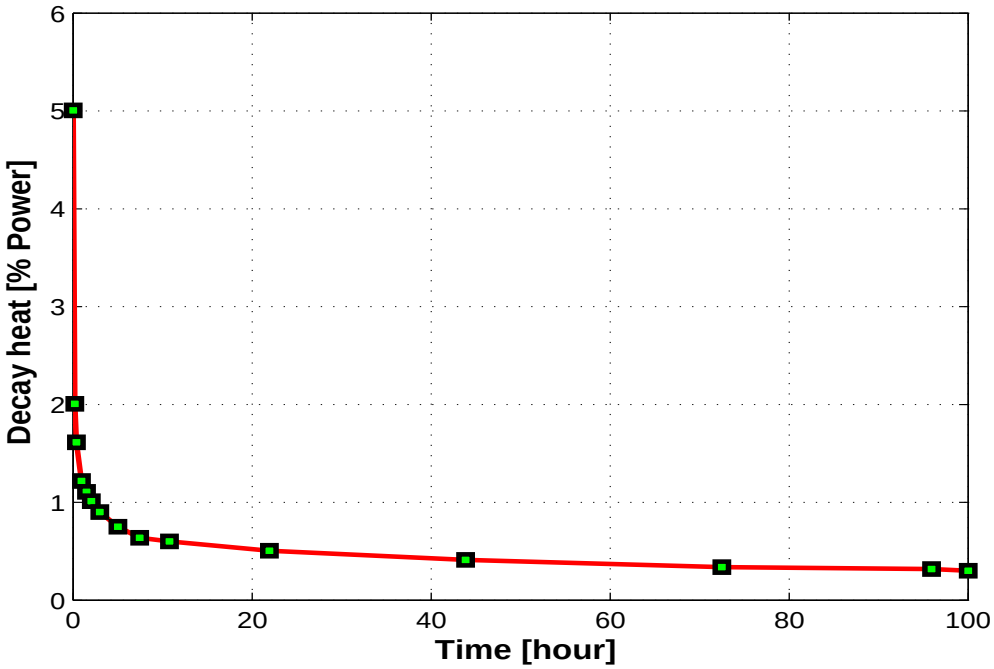

Figure 5.14: Decay heat vs. time.

5.2.1 Nominal Operation (Steady State)

In the case of nominal operation condition, helium gas enters into the inlet plenum with a flow rate of 320 kg/s, temperature 490°C and pressure 7.07 MPa. Helium flows through the raiser channel to the top cold plenum. From the top cold plenum, the main fraction of the gas (90%) flows through the coolant channels inside the fuel blocks and gaps between the fuel blocks and small fraction of the gas (10%), know as bypass flow, flows through the gaps between the reflector blocks to the hot bottom plenum. The amount of this bypass flow is taken according to the benchmark definition. Almost all thermal heat produced inside the reactor core is transported by the helium gas and it exits the reactor core with 850°C outlet temperature. Figure 5.15 and figure 5.16 illustrate the radial and axial solid temperature profile inside the reactor.

For the radial temperature profile (figure 5.15), relatively good agreement is observed between TH3D and GTAS in the core region. In the central and side reflector region as well as at the interface between core and central and side reflectors, it shows good agreement also with THERMIX. A sharp temperature gradient is observed at the interface between core and reflectors due to the dominance of forced convective heat transport inside the core and quite flat temperature profile in observed in the side and central reflector regions. The discrepancies observed in the results could come from different modeling procedures, different correlation used,

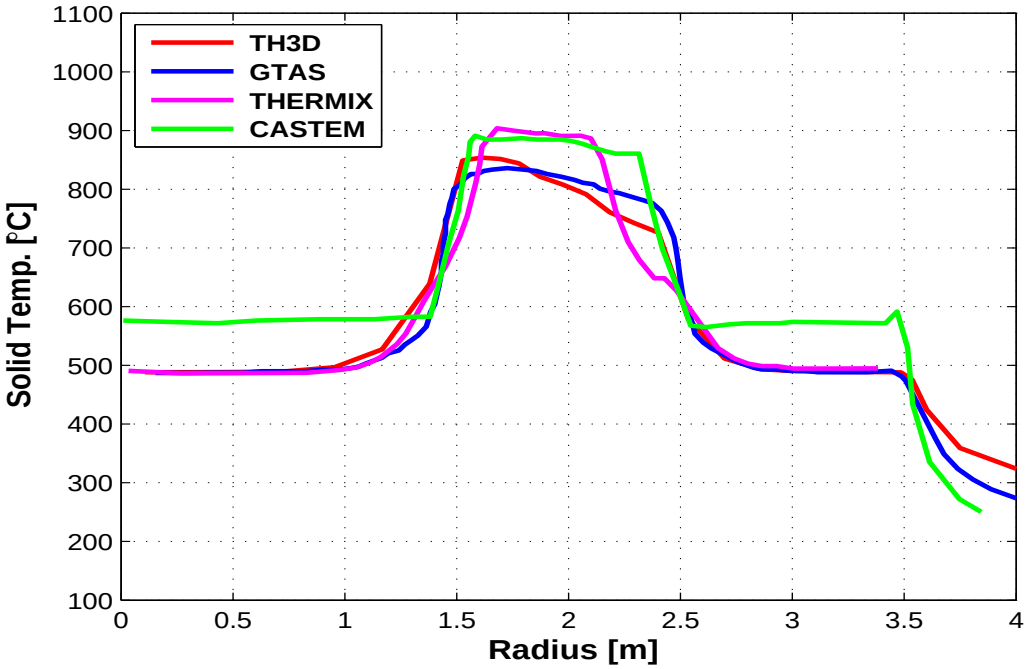

Figure 5.15: Radial solid temperature profile at core outlet.

difference in power distribution.

In the axial temperature profile (figure 5.16), close agreement is observed between TH3D, GTAS, and CFX. In this figure all except CASTEM results were taken at radius = 1.7m but CASTEM result was taken at radius = 1.96m. Since results for other code systems were extracted from IAEA documentation [23], it was not possible to plot all data exactly at the same plane.

5.2.2 Depressurized Cooldown

This is the case where loss of forced cooling (LOFC) is accompanied by rapid depressurization of the reactor to ambient pressure (1bar). This is one of the worst case scenarios where convective heat transfer inside the reactor is negligible due to the low gas density at ambient pressure and the reactor is cooled down only by conduction and radiation. This is a case to study the pure conduction cool down behavior of the reactor. Since convection plays no significant role in the heat transfer mechanism during depressurized cooldown, calculation for the helium flow was not performed in this calculation. Both RCCS, which are responsible for removing the decay heat produced inside the reactor, are assumed to be functioning as designed. After initiation of the accident the reactor starts to heat up due to decay heat production. The calculation starts with the steady state solid temperature

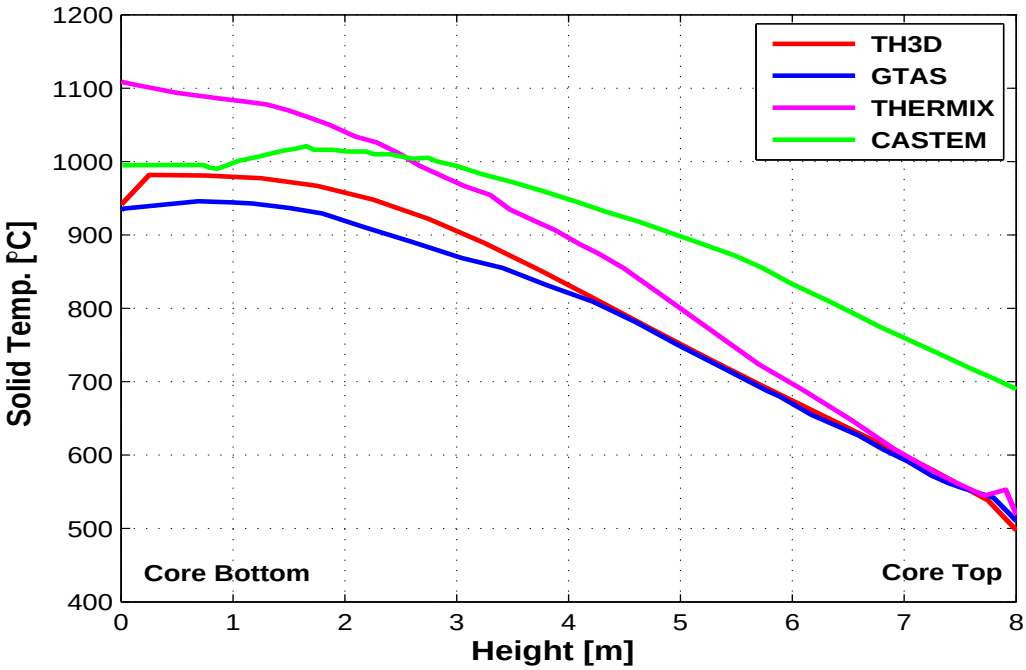

Figure 5.16: Axial temperature profile inside the reactor at radius = 1.7m.

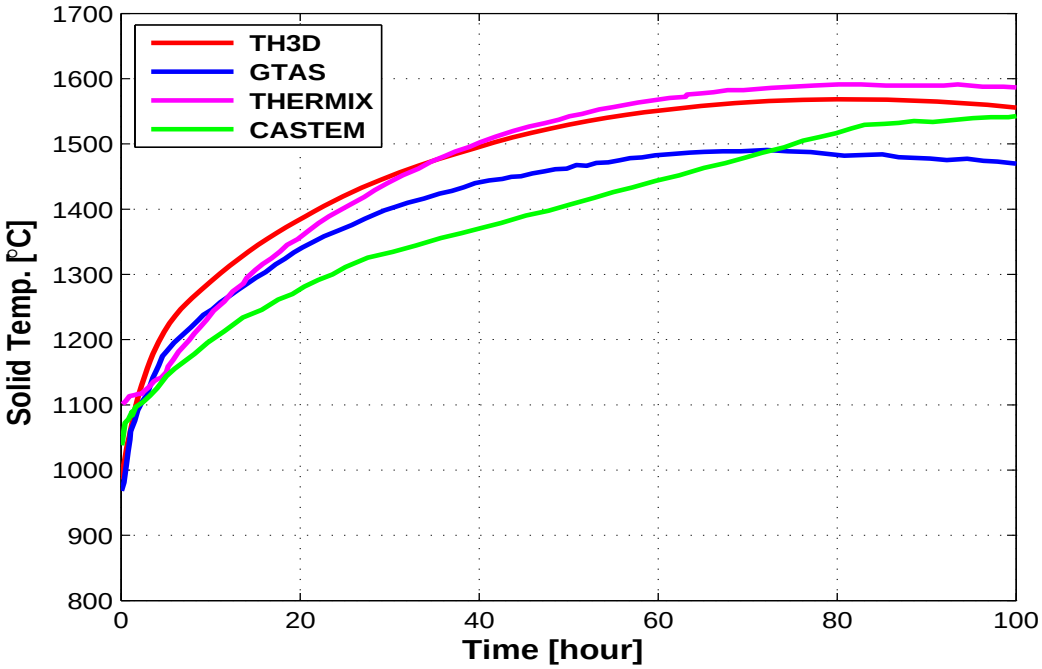

Figure 5.17: Peak fuel temperature profile during depressurized cooldown.

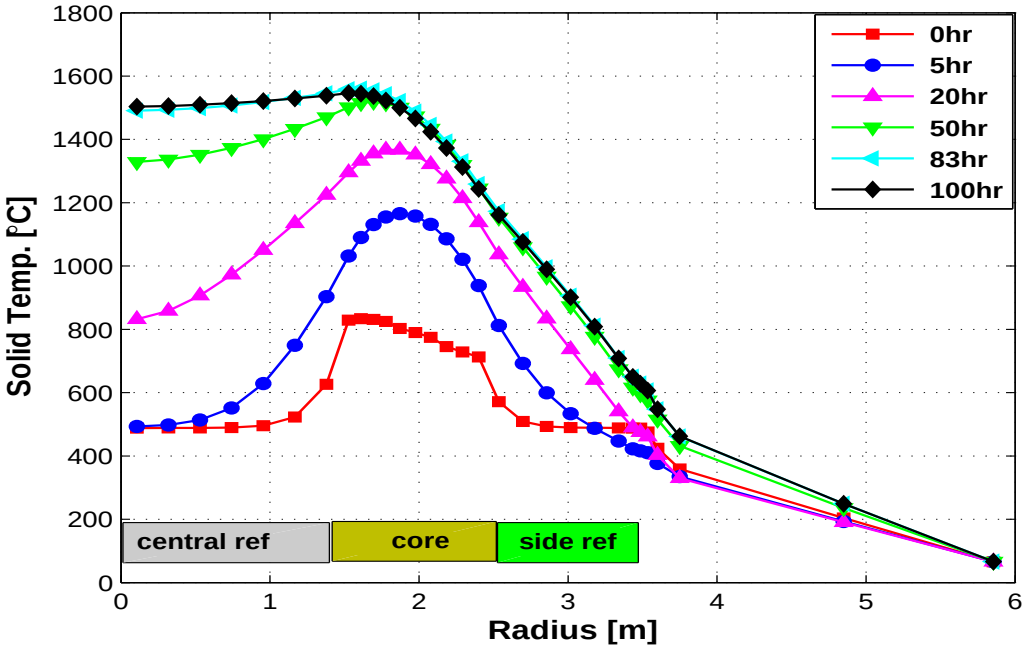

Figure 5.18: Radial temp. profile during depressurized cooldown at height = 4.0m (TH3D is used for calculation).

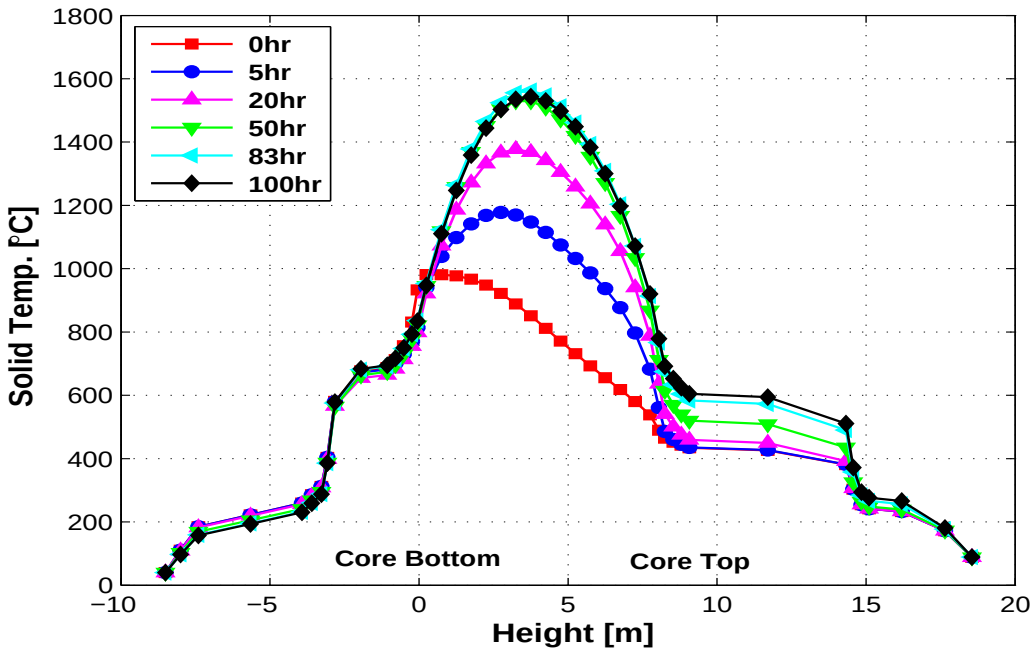

Figure 5.19: Axial temp. profile during depressurized cooldown at radius = 1.7m (TH3D is used for calculation).

profile as initial condition and simulates the transient behavior of the reactor. The transient behavior of the reactor depends on several factors like decay heat source, thermal conductivity, specific heat capacity of the materials used, heat removal rate of RCCS, etc.

Figure 5.17 illustrates the comparison of maximum fuel temperature during depressurized cooldown obtained from TH3D with other tools used by several countries. After initiation of the accident, the reactor core start to heat up adiabatically since the heat removal at reactor cavity cooling system is very small and the temperature inside the reactor core starts to increase. The gradient of temperature increase, which is stiff at the initial hours, decrease gradually and the maximum fuel temperature is reached at around 80 hours after the accident took place. It shows quasi-steady behavior for a while at maximum temperature level and starts to decrease since the decay heat sources diminish gradually and the heat removal at boundaries increases. The maximum temperature observed during this depressurized cooldown is $1568^{\circ}C$ which is just below the limiting temperature ($1600^{\circ}C$) and does not offer any margin for uncertainties. The result for maximum temperature during this case obtained from TH3D shows good agreement especially with THERMIX results.

Figure 5.18 and figure 5.19 illustrate the radial and axial solid temperature profile calculated by TH3D at steady state condition and at different time periods during the transient. During the nominal operation, the central reflector blocks and side reflectors are colder than the hot fuel blocks and radial temperature gradients are very high. Heat released by fuel blocks starts to heat up the side and central reflectors. As time progresses, the central and side reflectors heat up and the radial temperature gradient diminishes. The maximum solid temperature during nominal operation which is observed at the core exit starts to shift gradually upwards with time and finally shows axially symmetric profile due to symmetric decay heat source distribution (figure 5.20).

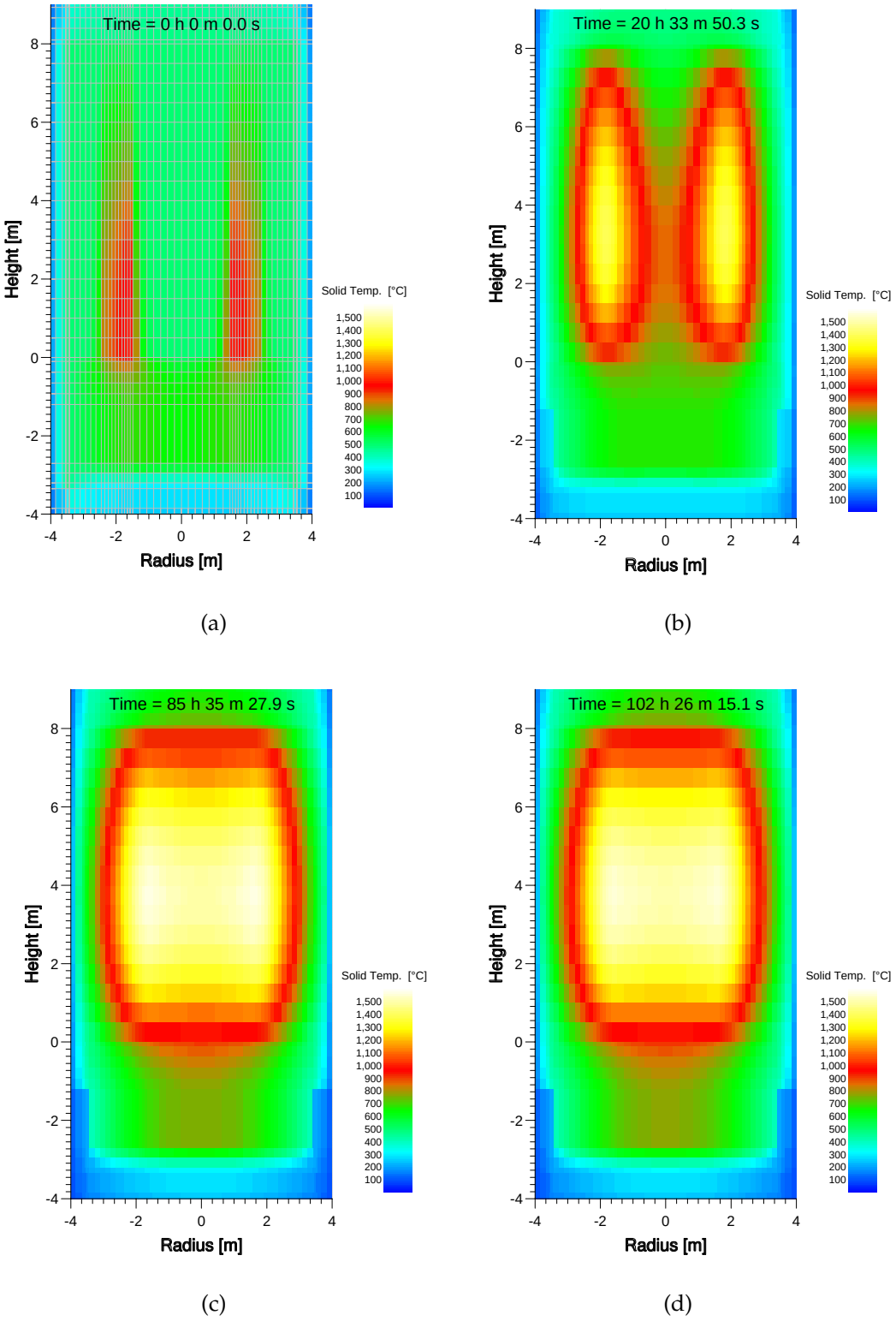

Figure 5.20: Solid temperature profiles at different time during the DLOCA transient calculated by TH3D, (a) initial steady state, (b) during heat-up at 20.55hrs, (c) at 85.58hrs when maximum temperatures are reached and (d) during cool-down at 102.5hrs

5.2.3 Pressurized Cooldown

In this case the reactor is scrammed from nominal operation after the loss of forced cooling but the primary system remains pressurized. It is assumed that both RCCS are functioning properly and that the boundary conditions remain the same as it is described for the nominal operation case.

The peak solid temperature calculated by TH3D for this case (figure 5.21) shows good agreement with the results obtained from GTAS and THERMIX calculation. Like the depressurized cooldown case, the calculation for this case also starts with a steady state solid temperature profile as initial condition and simulates the transient behaviors. At high system pressure, natural convection plays the most important role for heat transport beside radiation and conduction due to the higher gas density. Due to the significant role of natural convection, the peak fuel temperature and the time to reach this peak is lower than for the case with depressurized cooldown (figure 5.17).

Figure 5.23 shows the solid temperature and gas velocity profile during pressurized cool down accident. Due to large radial temperature difference between central reflector blocks and side reflector to annular fuel blocks during nominal operation, two natural convection loops develop after initiation of the accident. Due to the presence of the hottest region at the bottom of the reactor core during the early phase of the accident, helium gas at the bottom of the core becomes hotter and lighter and goes up through the middle of the hot annular fuel blocks, heats up the upper part of the reactor, flows downward through the gaps in central and side reflectors blocks, releasing heat to the central and side reflectors. As the central reflectors blocks become hotter and radial temperature gradient becomes smaller, the first convective loop disappears after few hours. Since the side reflector blocks and solid side reflectors are still colder, the second convective loop continues to heat up the side reflectors and the side reflectors are cooled down by conduction and radiation in the radial direction. Due to these convective loops, the hottest region (maximum temperature region) which was initially at the bottom of the core is shifted to the upper part of the reactor core.

It shows significant difference especially in the case of axial temperature profile during pressurized and depressurized calculation case (figure 5.19 and figure 5.22). The difference is created again due to the role of natural convection in the total heat transfer process. During pressurized cool down accident, upper part of the core and upper reflector zones become very hot compared to depressurize cool down. Though the maximum fuel temperature is much lower in the pressurized case than in the depressurized case, the top reflector temperature in the pressurized case is significantly higher (around $1100^{\circ}C$) than in the depressurized case (around $900^{\circ}C$).

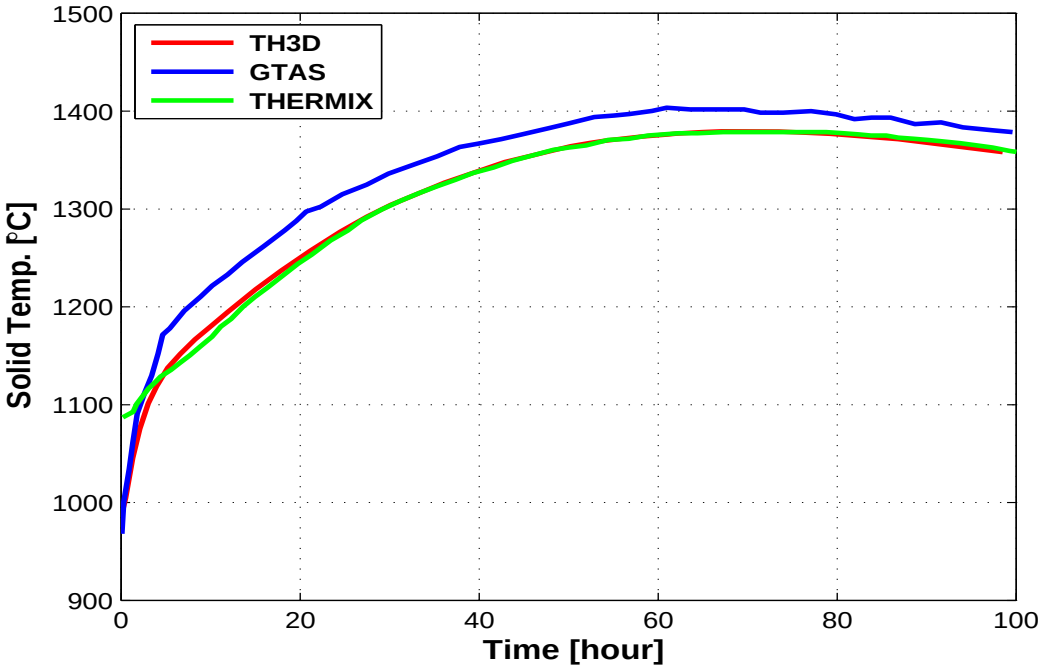

Figure 5.21: Peak solid temperature profile during pressurized cooldown.

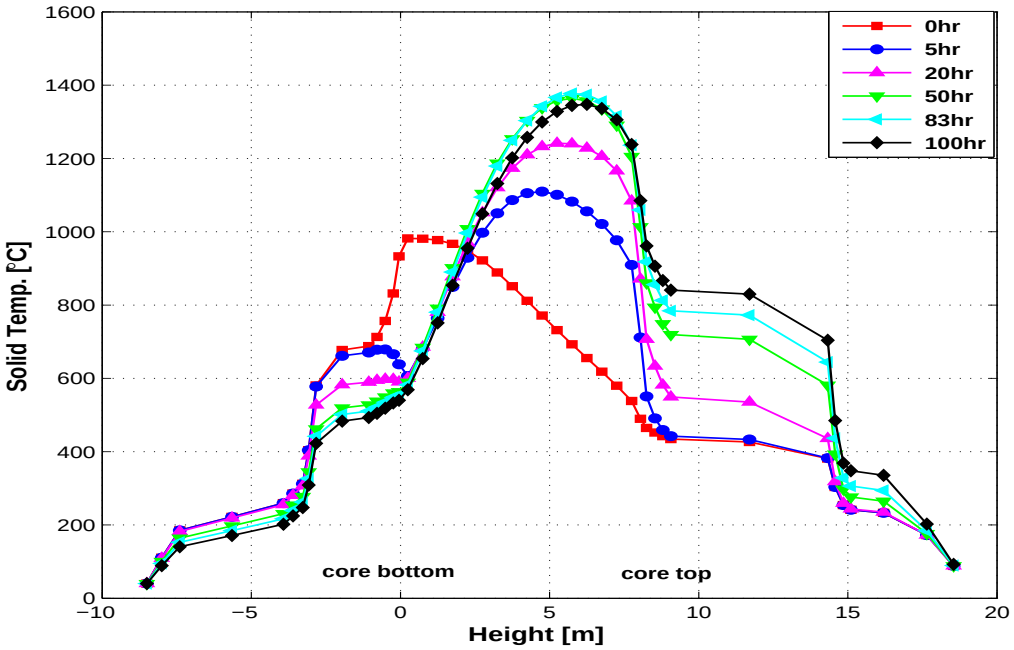

Figure 5.22: Axial temperature profile calculated by TH3D during depressurized cooldown at radius = 1.69m.

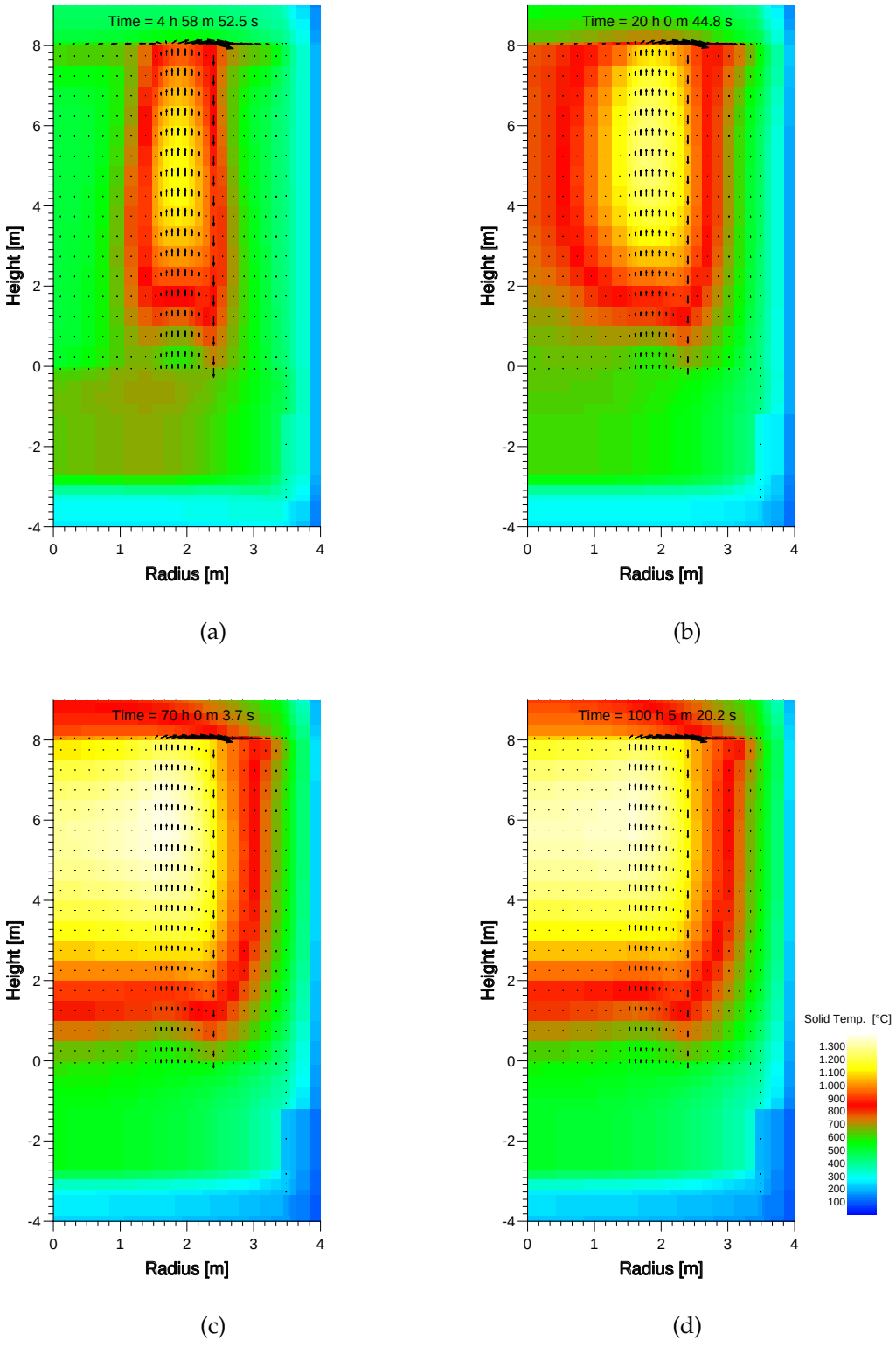

Figure 5.23: Temperature profiles (color scale) and gas velocities (arrows) at different times during the PLOCA transient.

5.3 Sample 3D calculation

A sample 3D steady state calculation is presented here to show the basic capabilities of our new tool. Here, the nuclear power profile was calculated with the Monte-Carlo-Code MCNPX. MCNPX is a general purpose, continuous energy, generalized geometry, time dependent, coupled neutron/photon/electron transport code based on Monte Carlo methods [11]. Monte Carlo methods are very different from the most commonly used deterministic methods. Deterministic method is a discrete ordinates method which solves the transport or diffusion equation for the average particles behavior while the Monte Carlo methods obtain the particle behavior by simulating individual particles. A neutron movement is followed through the different material regions of the geometry from the initial emission to the final absorption or escape. The basis of this simulation process is the sampling of the free path length between two neutron collisions. The probability that a neutron will travel a distance x within an infinite homogeneous material without any collision and will collide while moving the distance dx from x is:

$$p(x)dx = \Sigma_T e^{-x\Sigma_T} dx \tag{5.1}$$

Here, Σ_T is the macroscopic total cross section. The probability distribution function of the free path can be written as:

$$f(x) = \Sigma_T e^{-x\Sigma_T} \tag{5.2}$$

and the cumulative distribution function:

$$F(x) = \int_0^x \Sigma_T e^{-x\Sigma_T} dx = 1 - e^{-x\Sigma_T} \tag{5.3}$$

Now, the free path of a neutron (path between two collisions) can be sampled with the help of the inversion method as:

$$x = -\frac{1}{\Sigma_T} ln(1 - \xi) \tag{5.4}$$

Here, ξ is a uniformly distributed random number and its value lies in the range $0 < \xi \leq 1$. The types of the collisions depend on the macroscopic cross section. The direction of the neutron after the collision can also be calculated with the help of isotropic scattering and a uniformly distributed random number.

MCNPX can be used for modeling neutron transport in critical or sub-critical reactors. Neutron histories are tracked from the point of production to the end of its life cycle by the use of evaluated cross sections libraries (elastic scattering, inelastic scattering and absorption). The resulting collection of neutron tracks represents the neutron flux. The fission spectrum is calculated by a mesh tally and the power

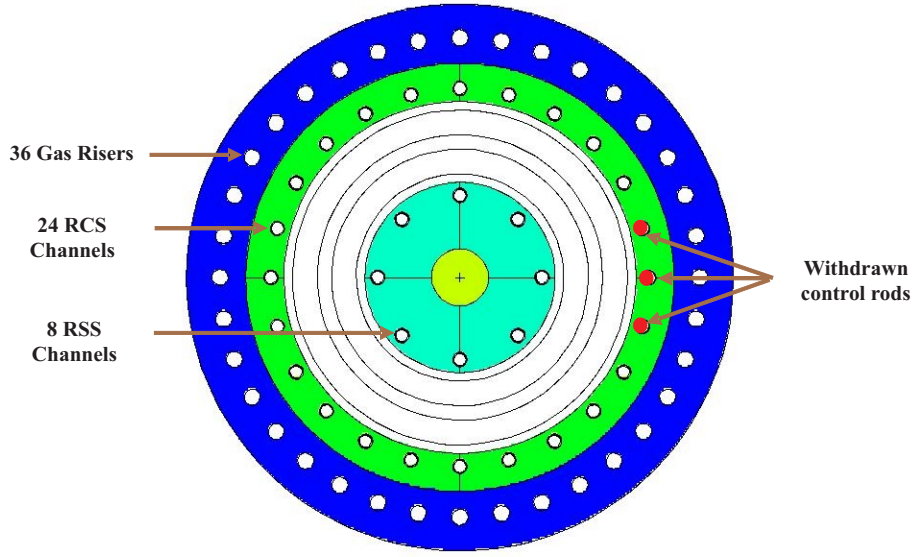

Figure 5.24: Reactor section showing the position of the withdrawn control rods(red circles).

density of a zone can be written as:

$$P_Z^* = \int_{V_Z} \sigma_N(x,y,z) \cdot N_N(x,y,z) \cdot p_N \cdot \phi(x,y,z) dV \tag{5.5}$$

Here, P_Z^* is the power fraction of the zone Z, σ_N is the microscopic cross section of nuclide N, N_N is the particle density of the nuclide N, ϕ is the neutron flux, and p_N is the heat production from each fission. The obtained power fraction of the zone needs to be normalized to the real reactor power.

Figure 5.24 illustrates a section of the PBMR-400 reactor showing the positions of control rods as well as the positions of withdrawn control rods (red circles).It was assumed that three control rods at 0°, -15°, and 15° angular positions were fully withdrawn while the rest of the control rods were inserted 3.5m below the bottom of the top reflector to get a symmetric power distribution for every 180° sector and one sector was used for the 3D calculation case. Figure 5.25 shows the asymmetric power density profile at the top cell of the reactor core. It shows peak values for the power density at the position where control rods were withdrawn and shows periodicity with 180° symmetry over the whole reactor. The simulation geometry was discretised by 33, 18, and 36 radial, angular and axial meshes. This relatively coarse discretisation was chosen for first tests and will be refined in subsequent calculations.

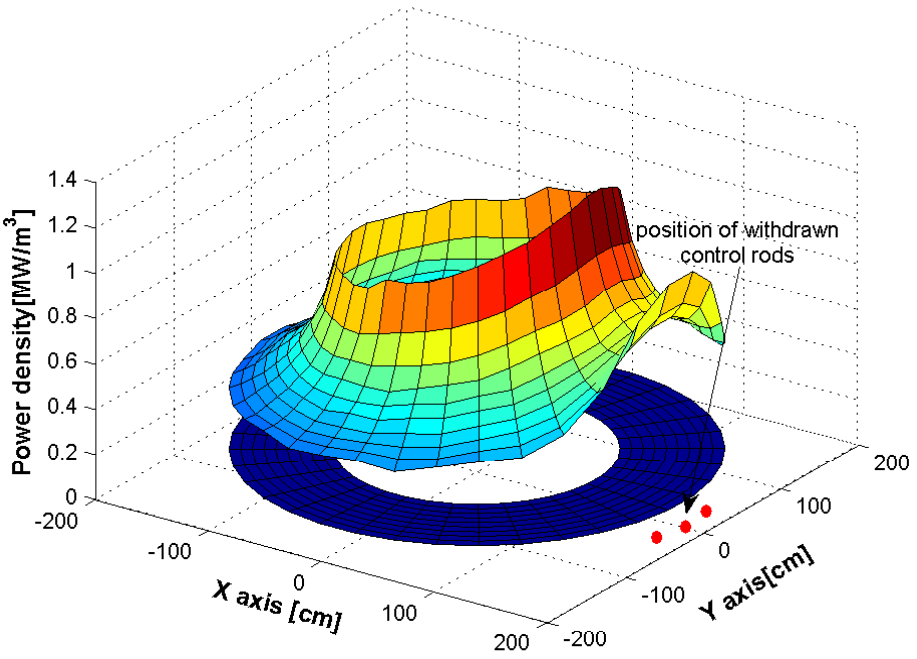

Figure 5.25: Power density profile at the top of the reactor core.

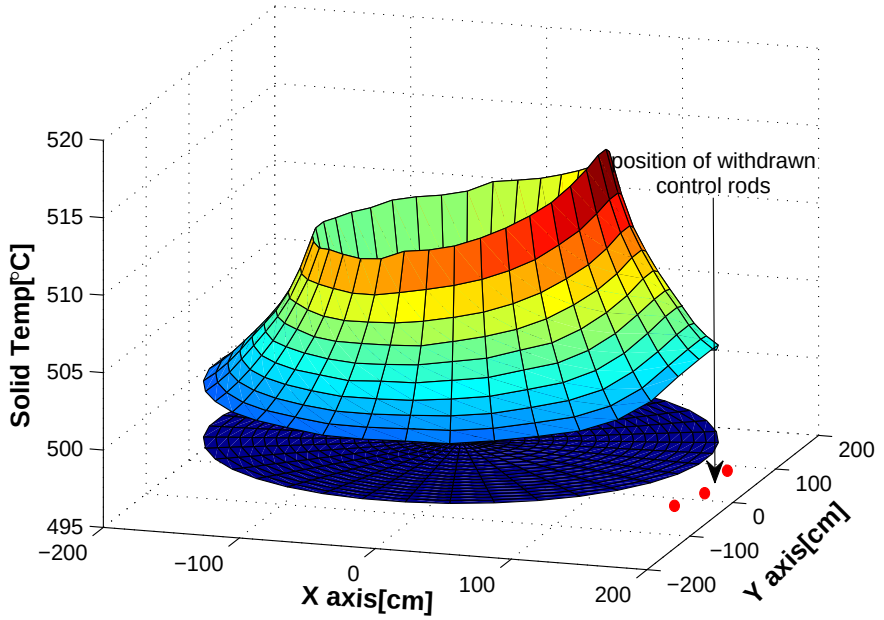

Figure 5.26: Solid temperature profile at the top of the reactor core.

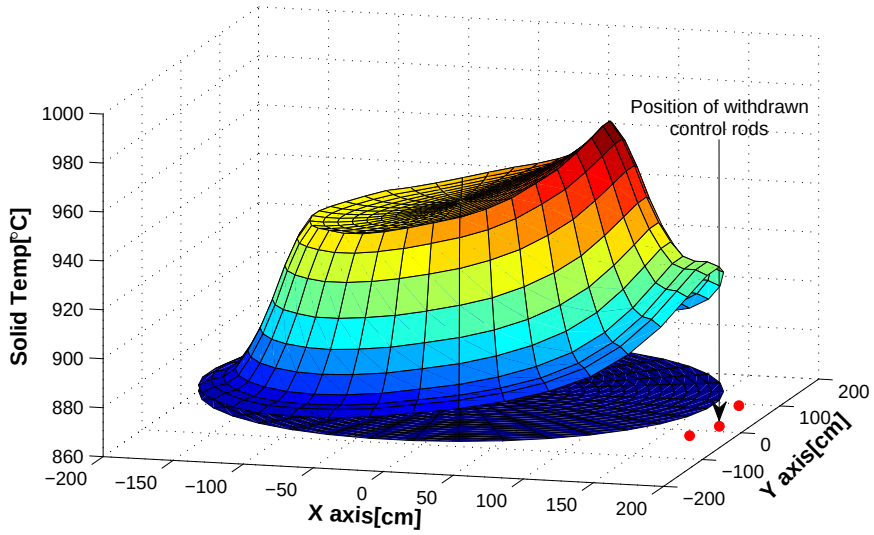

Figure 5.27: Solid temperature profile at the core's exit.

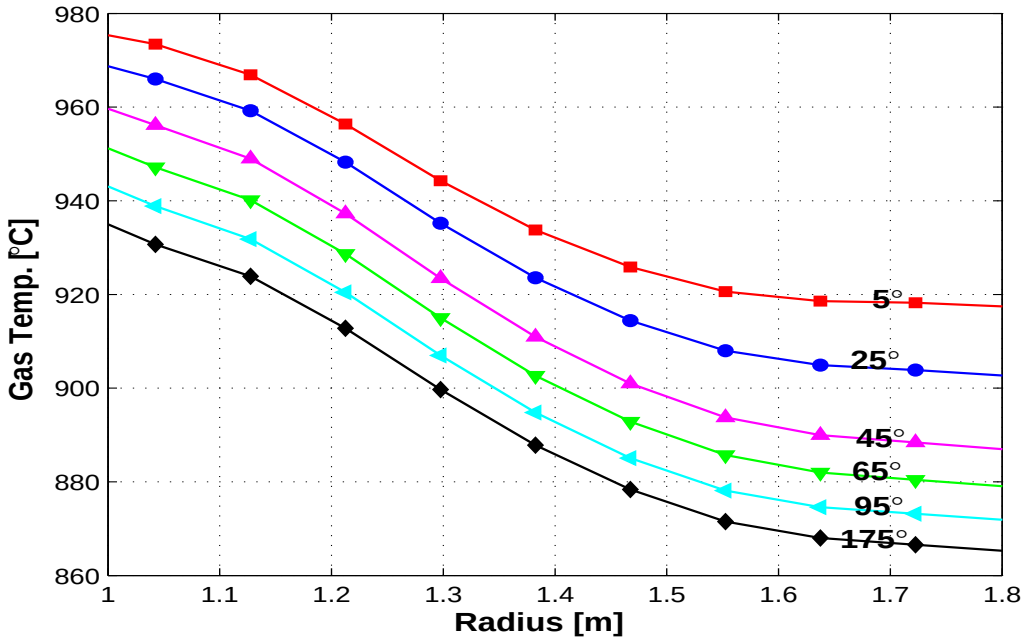

Figure 5.28: Gas temperature profile at core exit for different angular position.

Figure 5.26 and figure 5.27 also show an angular variation for solid temperature; the maximum value is observed at the position where the power profile peak exists due to the withdrawn control rods. It shows around $50^{\circ}C$ difference for the solid temperature as well as $40^{\circ}C$ difference for gas temperature at the core exit due to the asymmetric power distribution in angular direction which is better visible from figure 5.28. In figure 5.28, 5° and 175° curves represent the gas temperatures at core exit position.

Chapter 6

Coupling with Neutronics

In a nuclear reactor, heat is produced by nuclear fission, a process in which neutrons react with the target nuclei, creates an unstable compound nucleus, splits into smaller nuclei by releasing two or more neutrons and energy [24]. Not all produced neutrons take part in the next fission process since some part of the produced neutrons are absorbed by non-fissile material and some are absorbed parasitically in fissile material. The infinite multiplication factor k_∞ measures the increase or decrease of the neutron flux in an infinite reactor and is written as:

$$k_\infty = \frac{neutron\ production\ rate}{neutron\ absorption\ rate} \tag{6.1}$$

In thermal reactors, the infinite multiplication factor can be calculated by the following four factor equation with a fair degree of accuracy as:

$$k_\infty = \varepsilon \cdot p \cdot f \cdot \eta \tag{6.2}$$

where, ε, p, f, and η are the fast fission factor, the resonance escape probability, the thermal utilization factor and the reproduction factor, respectively [24]. In thermal reactor, some fast neutrons (energies above 1 MeV) cause fission in ^{235}U and ^{238}U fuel before slowing down. This effect is described by fast fission factor and its value is always more than one since each fission produces more than one neutron.

After production, neutrons start to diffuse through the reactor and collide with nuclei of fuel, non-fuel and moderator and lose energy. During this slowing down process, some neutrons can be captured by ^{238}U nuclei because of the presence of several resonance peaks in the absorption cross-section of ^{238}U nuclei in the energy range of 1000 to 6 eV. The probability that the neutron will not be captured by the resonance peaks is known as resonance escape probability and the value of the factor is always less than 1 (normally 0.95 to 0.99 [33]). The value of the resonance escape probability does not significantly depend on pressure or poison concentration but depends on temperature. With increasing temperature, the resonance absorption in ^{238}U nuclei increase due to the Doppler effect, a broadening

of narrow resonance peaks due to thermal motion of the nuclei.

Once thermalized, neutrons continue to diffuse and to be absorbed by fuel, moderator as well as by other materials like control rods, chemical shim, poisons. The thermal utilization factor is defined as the ratio of thermal neutrons absorbed in fuel to the thermal neutrons absorbed in the entire core. The value of the thermal utilization factor is less than 1 and generally it does not depend on temperature. But for water moderated reactor, thermal utilization factor increase with increasing temperature due to the decrease of moderator density as moderator expands with temperature. The reproduction factor represents the number of neutron released/produced in thermal fission per number of thermal neutrons absorbed by fissile fuel. The value of the reproduction factor is always more than unity and for thermal reactor fuel, the value is ~ 2.

The neutron life cycle in an infinite reactor can be explained by infinite multiplication factor but in a real, finite reactor some neutrons leak out of the reactor and must be considered for getting exact neutron balance. The term effective multiplication factor k_{eff} measures the increase or decrease of neutron flux in a finite reactor and can be expressed as:

$$k_{eff} = k_{\infty} \cdot P^{th}_{non-leak} \cdot P^{fast}_{non-leak} \tag{6.3}$$

where, $P^{th}_{non-leak}$ and $P^{fast}_{non-leak}$ are the thermal and fast non-leakage probability respectively. For ensuring the safety and optimizing the performance, it is very important to maintain the reactor at critical/steady state during operation. In critical state, the k_{eff} must be equal unity. So, at critical state, number of neutrons is constant in each generation and so is the fission rate. Since nuclear power is proportional to neutron flux, reactor power also remains constant. The reactor power increases exponentially with a value of k_{eff} greater than unity, a state of the reactor known as supercritical. Similarly, the power decreases with a k_{eff} less than unity, a state known as subcritical.

During transient state, a state apart from critical/steady state, the neutron flux as well as the reactor power varies with time. Transient behavior of a reactor is a function of its reactivity. Reactivity is the percent change in effective multiplication factor in a reactor which describes the departure of neutron population and thus the reactor power from steady state and can be expressed as:

$$\rho = 1 - \frac{1}{k_{eff}} = \begin{cases} k_{eff} = 1 \rightarrow \rho = 0 & \text{critical} \\ k_{eff} > 1 \rightarrow \rho > 0 & \text{supercritical} \\ k_{eff} < 1 \rightarrow \rho < 0 & \text{subcritical} \end{cases} \tag{6.4}$$

where, k_{eff} is the effective multiplication factor and ρ is the reactivity. The following factors could change the reactivity in the reactor core and consequently leads to a reactor transient:

- Fuel depletion - fuel depletes with time due to the burn up/consumption of fissionable nuclei so does the neutron flux.
- Poisons - during the operation of the reactor fission products accumulate and among the accumulated fission products, non fissile fission products especially Xenon (^{135}Xe) and Samarium (^{149}Sm) with large thermal neutron absorption cross sections tend to reduce neutron multiplication factor.
- Control rod operation - control rods are used to regulate the reactor criticality. Insertion of control rods make more neutrons to be absorbed and make the reactor subcritical while withdrawing cause multiplication factor to increase.
- Temperature - among the six factors used for calculating effective multiplication factor (equation 6.2, 6.3), resonance escape probability (p) and thermal utilization factor (f) depends on fuel and moderator temperature. So, increase or decrease of temperature change effective multiplication factor and that the reactivity, and thus the reactor power.

6.1 Neutron Kinetics

In order to harness the reactor safely and make the nuclear energy cost-effective, the variation of the neutron population and that the power with time and space must be analyzed. In a transient reactor neutron balance can be written as:

$$Change\,rate = Production - Leakage - Absorption \tag{6.5}$$

The exact interpretation of neutron transport in a reactor core which is composed of several materials is very difficult and several simplifications and assumptions are made for estimating the average characteristics of the neutron population. The following sections describe briefly some methods for calculating neutron flux in a transient reactor.

6.1.1 Point Kinetics Equations

In this model, it is assumed that the shape of the neutron flux profile during transient remains unchanged, only its value changes with time. The total reactor is considered as a whole/point and time dependent neutron balance is made. If $n(t)$ is the total of all type of neutrons in the reactor and l is the average life time of one neutron, at every second $n(t)/l$ neutrons are lost from the reactor by absorption and leakage. In a multiplying medium with an effective multiplication factor k, at every second $k \cdot n(t)/l$ new neutrons are released for the cost of the $n(t)/l$ lost neutrons. Not all the neutrons produced from fission are released at the same time. Nearly 99% of all neutrons are released almost instantaneously (within about 10^{-13} seconds) [24] which are known as prompt neutrons and referred as $(1-\beta)$ where β

is the fraction of the neutrons which are released after the decay of fission products and know as delayed neutrons. Delayed neutrons are emitted due to the β-decay of a fission fragment, know as delayed neutron precursor. The emission time of the delayed neutron depends on decay constant and varies from a fraction of a second to few seconds [24]. The total delayed neutrons come from six different precursor classes and are subdivided in six groups.

$$\beta = \sum_{i=1}^{6} \beta_i \tag{6.6}$$

where, β_i is the delayed neutron fraction of the i^{th} group. If c_i is the precursor concentration and λ_i is the β-decay constant of i^{th} group, at every second $\lambda_i c_i$ i^{th} group delayed neutrons are released. By balancing the production and loss of neutrons, the change of the neutron flux $n(t)$ can be written as:

$$\frac{d}{dt}n(t) = \frac{(1-\beta)k-1}{l}n(t) + \sum_{i=1}^{6} \lambda_i c_i(t) \tag{6.7}$$

The time dependent precursor concentration $c_i(t)$ can be written as:

$$\frac{d}{dt}c_i(t) = \frac{\beta_i k}{l}n(t) - \lambda_i c_i(t) \qquad where\ i = 1, 2, ..., 6 \tag{6.8}$$

In equation 6.8, the first term of the right hand side represents the build-up of precursor concentration from nuclear fission and second term represents the degradation of the precursor concentration by radioactive decay. By introducing the term generation time $\Lambda = l/k$ and reactivity ρ (equation 6.4), equation 6.7, 6.8 can be rearranged as:

$$\frac{d}{dt}n(t) = \frac{\rho-\beta}{\Lambda}n(t) + \sum_{i=1}^{6} \lambda_i c_i(t) \tag{6.9}$$

$$\frac{d}{dt}c_i(t) = \frac{\beta_i}{\Lambda}n(t) - \lambda_i c_i(t) \qquad where\ i = 1, 2, ..., 6 \tag{6.10}$$

This is a system of seven ordinary differential equations and known as point kinetics equations.

6.1.2 Diffusion Equation

Instead of balancing neutron globally, which is the case for point kinetics model, neutron balance is made locally in diffusion equations. In this case, neutron density $n(\overrightarrow{r}, E, t)$ is a function of space, time and energy. The time dependent energy dependent neutron diffusion equation can be written as:

$$\frac{\partial}{\partial t}n = \nabla \cdot D\nabla\phi - \Sigma_T\phi + Q + \int_{E'} \Sigma_S(E' \rightarrow E)\phi(E')dE' \tag{6.11}$$

Here, the left hand side represents the change term. The first term of the right hand side represents the leakage rate, second term represents the lose of neutron due to absorption and scattering from present energy group to lower energy group, third term represents the source term and the last term represents the part of scattered neutron coming from higher energy group [15][16]. Due to the importance of the delayed neutron, the source term Q in equation 6.11 must be calculated by considering both prompt and delayed neutron and can be written as:

$$Q = \chi_0(E) \int_{E'} \left[1 - \beta(E')\right] \nu(E')\Sigma_f(E')\phi(E')dE' + \sum_{i=1}^{6} \chi_i(E)\lambda_i c_i \tag{6.12}$$

Here, the first term of the right hand side represents the prompt neutrons source and second term is the contribution from delayed neutrons from $\beta-$decay of precursors. The precursor concentration $c_i(\overrightarrow{r}, t)$ which is a function of space and time can be written as:

$$\frac{\partial}{\partial t} c_i = \int_{E'} \beta_i(E')\nu(E')\Sigma_f(E')\phi(E')dE' - \lambda_i c_i \qquad where\ i = 1, 2, ..., 6 \tag{6.13}$$

Here, the first of the right hand side is the production of precursors from nuclear fission and the second term is the decay of the precursors while left hand side represents the change rate.

6.2 Neutronics/Thermal-hydraulics Feedback

We have seen in the previous sections that thermal hydraulic parameters of the reactor (e.g. temperature) influences the effective multiplication factor of the reactor and that the reactivity, and thus the reactor power. Temperature is a function of power densities and thus neutron densities and comes from neutronics analysis. In one hand, the reactor temperature profile depends on the reactor power and on the other hand, reactor power profile can be changed by the change of temperature. So, a coupled neutronics/thermal-hydraulics calculation is required for getting a actual power/temperature profile.

6.2.1 Thermal-hydraulics Parameters

Reactivity coefficients (α) are used to quantify the effect of change of a parameter on reactivity in the core. The change in reactivity with temperature is quantified by the temperature coefficient of reactivity. Since the reactor is composed of several materials, the temperature changes in different materials influence differently. With increasing power, the fuel temperature changes instantly but it takes seconds

to increase the moderator temperature and even longer to change the reflector temperature. The temperature coefficient of reactivity can be written as:

$$\alpha_T = \frac{\partial \rho}{\partial T} = \frac{\partial}{\partial T}\left(\frac{k_{eff}-1}{k_{eff}}\right) = \frac{1}{k_{eff}^2}\frac{dk_{eff}}{dT} \cong \frac{1}{k_{eff}}\frac{dk_{eff}}{dT} \quad since \quad k_{eff} \approx 1 \tag{6.14}$$

Since, k_{eff} is always a positive value, dk_{eff}/dT is positive if α is positive which consequently increase the neutron population and thus the reactor power. So, with increasing temperature, reactor power will increase and it will further increase the temperature and so on and vice versa. If alpha is negative, an increase in temperature will drop the reactor power and consequently drop the temperature and return the reactor to its original condition. For this reasons, it is always necessary to have a negative temperature co-efficient. In HTRs, two main temperature coefficients are the fuel temperature coefficient and the moderator temperature coefficient and will be described in the coming sections.

Fuel Temperature Coefficient

Since fuel temperature increases almost instantly with power, fuel temperature coefficient reacts immediately with temperature change. This is also known as prompt temperature coefficient or nuclear Doppler coefficient. Due to its prompt reaction, a negative fuel temperature coefficient is important and absolutely necessary than moderator or reflector temperature coefficient. The fuel temperature coefficient describes the effect of increasing absorptions in non-fissile material with increasing temperature. Prominent resonance absorbers are ^{238}U and ^{240}Pu.

For interaction of neutrons with nuclei in a certain volume, it is convenient to start the observation of reactions of monoenergetic neutrons with nuclei at 0°K. At 0°K the atoms do not show any thermal motion, it is completely at rest and only the velocity of the neutron is taken into account. The probability of interaction is described in the cross section σ. In reality, the nuclei certainly do have a temperature above 0°K, they are in thermal motion. Now, not only the neutron's velocity, but also the relative velocity v_{rel} between neutron and nucleus is determining the reaction. The motion of the nuclei in a certain volume follows a certain velocity distribution, namely the Maxwell distribution $M(v_A, T)$.

In order to correctly understand the nuclear Doppler Effect one first has to introduce the effective cross section σ_{eff} that takes into account the above mentioned relative velocity between nucleus and neutron.

The reaction rate of the neutrons with the nuclei in thermal motion is given by,

$$F = \int_{v_A} v_{rel} n N \sigma(v_{rel}) M(v_A, T) dv_A \tag{6.15}$$

Here, v_{rel} is the relative velocity between nucleus and neutron, n is the neutron

density, N is the atomic density, $\sigma(v_{rel})$ is the microscopic cross section and $M(v_A, T)$ is the Maxwell distribution. It is convenient to describe the reaction rate F in terms of neutron velocity instead of relative velocity. This is done by introducing an effective cross section that accounts for deviation of velocities.

$$F = vnN\sigma_{eff}(v, T) \tag{6.16}$$

If one compares equation 6.15 with equation 6.16, $\sigma_{eff}(v, T)$ can be defined by,

$$\sigma_{eff}(v, T) = \int_{v_A} \frac{v_{rel}}{v} \sigma(v_{rel}) M(v_A, T) dv_A \tag{6.17}$$

With convolution and Fourier-Transformation of equation 6.17 one finds,

$$\sigma_{eff}(v, T') = \int_{v_A} \frac{v_{rel}}{v} \sigma(v_{rel}) M(v_A, T' - T) dv_A \tag{6.18}$$

This enables the calculation of an effective cross section at a temperature T' that differs from T, because the averaging over the Maxwell -Boltzmann distribution of the temperature difference T'-T yields the temperature transformation of interest.

Now the temperature broadening (Doppler Broadening) can be calculated. However, the integral value of σ_{eff} remains constant. It is only due to a weighting function, namely the flux $\phi(E)$, that the absolute reaction rate F undergoes change.

At 0°K, the cross section exhibit very narrow resonances. The corresponding energy-dependent flux experiences a strong depression at the resonance energy. When the average temperature is increased the resonances broaden and the flux depression decreases. Since the reaction rates are,

$$F = \int_E \Sigma_{eff}(E, T) \phi_{eff} dE \tag{6.19}$$

One can see that the absorption rate increases if temperature increases.

Moderator Temperature Coefficient

In a high temperature reactor, the moderator coefficient describes the effect of hardening of the neutron spectrum with increasing temperature. This shifts the maximum of the thermal neutrons to higher energies where absorption resonances are present (a strong resonance absorber is e.g. ^{238}U). The neutrons are absorbed before they reach lower energies needed for thermal fissions in the fissile material and, subsequently, the number of fissions decreases.

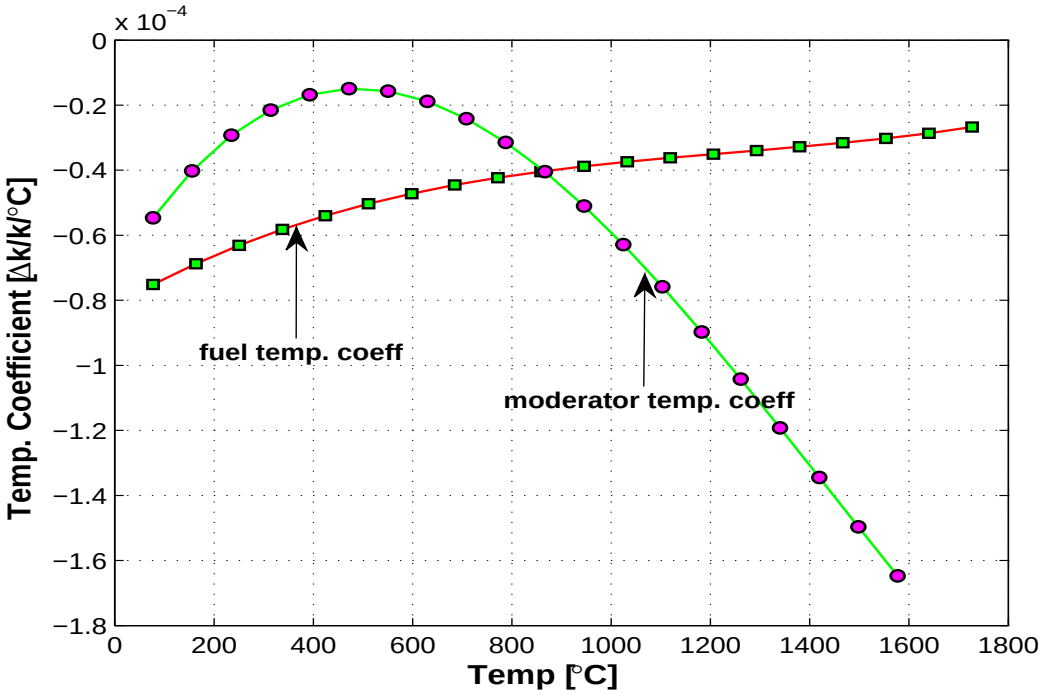

Figure 6.1: Temperature coefficient for PBMR-400 reactor

6.2.2 Neutronics/Thermal-hydraulics coupling

In order to get the neutronics/thermal-hydraulics feedback, the thermal-hydraulic program is coupled with a neutronics program. In our case, TH3D was coupled with a point kinetics model. This is an internal coupling where point kinetics model is implemented inside the TH3D program. Point kinetics model is widely used for reactor kinetics analysis due to its simplicity. Sometimes, point kinetics model is coupled initially for a basic test of coupling with more sophisticated models which considers both space and time. If the coupling does not succeed with a point kinetic model which considered the whole reactor as one point or region, it is very unlikely to succeed with models considering the reactor with many regions.

The point kinetics model is a system of coupled linear ordinary differential equations described in the section 6.1. This model describes the rate of change of neutron flux and precursor's density with time depending on the time dependent reactivity. One of the important properties of this system of equations is the stiffness which makes the numerical solution problematic. In our model, we implemented an explicit multi step Runge-Kutta method with step size control [3]. Since it is an explicit method, time step was maintained very small to get the desired accuracy. We have also implemented the numerical solution of an integral form of kinetic equation which is know as recursion equation [16] and checked the validity of Runge-Kutta method or vice versa.

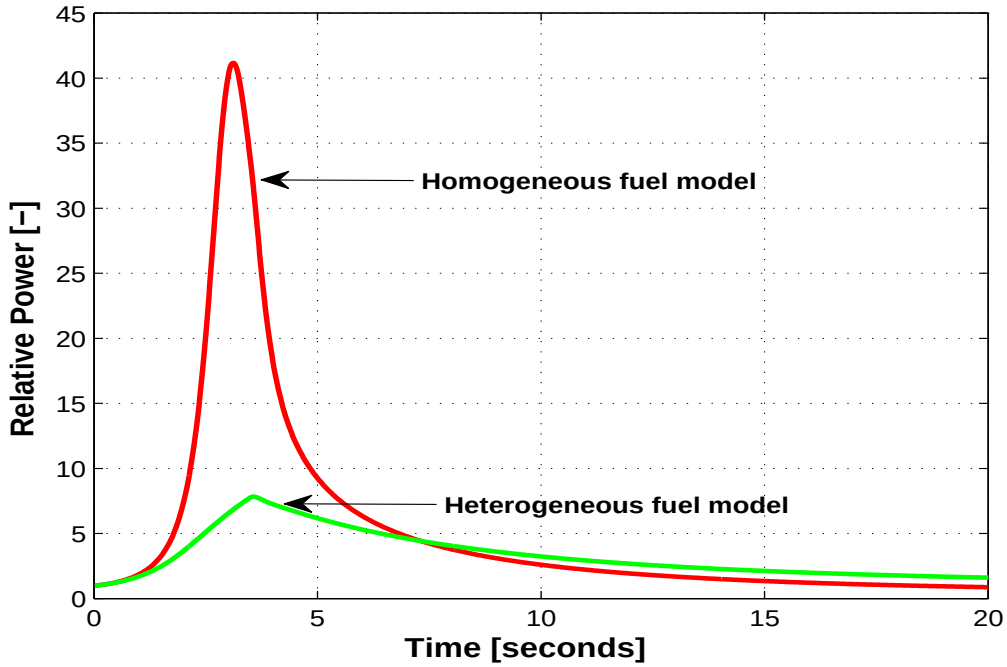

Figure 6.2: Relative power during fast transient accident simulation.

In the coupling process, the power and the temperature profile need to be exchanged between the neutronics and the thermal-hydraulics program. The data flow and the time step is controlled from a master program (In our case, TH3D is the master program) while the other program is called at each time step from the master program. A steady state condition of the reactor need to be reached in order to start the transient calculation. For our calculations, the steady state power density is either calculated by ZIRKUS program system or obtained from a benchmark definition. At the beginning of the transient (time =0), steady state temperature profile is used for calculating the reactivity co-efficient of fuel, moderator and reflector. The relative power change due to the change of reactivity is calculated from the point kinetics model. The new power profile is supplied to thermal hydraulic code TH3D for calculating the corresponding temperature profile. For the next time step, this changed temperature profile is used for calculating the reactivity coefficients. This process continues up to the end of a transient calculation. The negative reactivity insertion from Xenon build-up which is important for a slow transient is also considered by solving the simplified depletion chains of Xenon and Iodine.

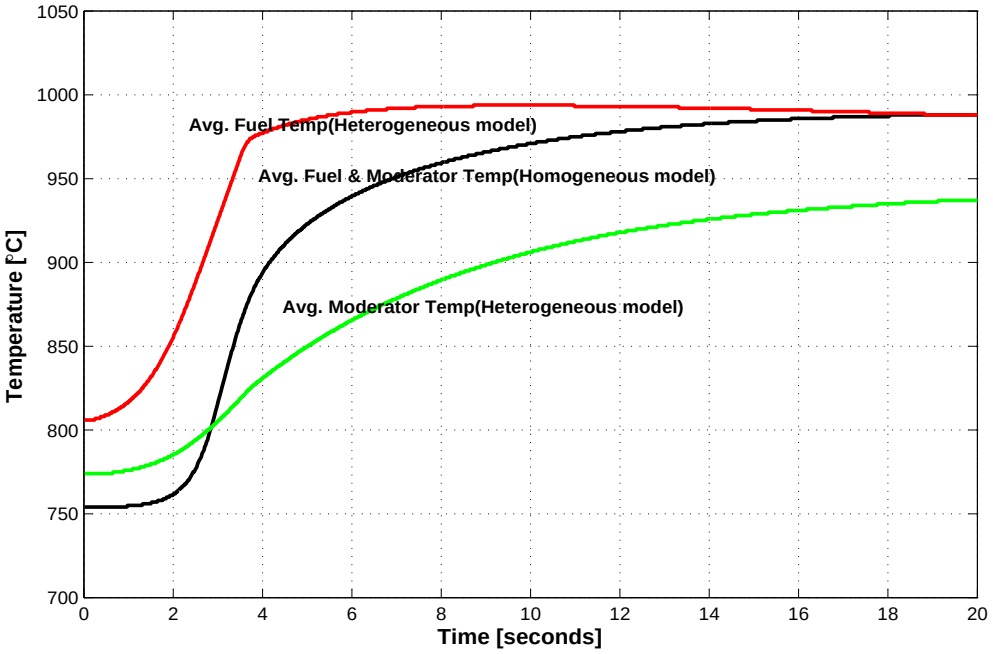

Figure 6.3: Temperature profile during fast transient accident simulation.

6.2.3 Simulation of a Fast Transient Case

A situation of fast reactivity insertion was simulated by withdrawing all control rods quickly. Though the situation is not realistic, it was done to show the capability of the code to couple with a neutronics system for simulating fast transients. In this case, all control rods were withdrawn with a velocity of 1 m/s to the end position of the control rod. It takes 3.5 sec and inserts 1.2% reactivity gradually to the system by this time. It was assumed that scram signals were not activated when power or temperature was increased beyond a limit during this withdrawal process and the the control rods system continued to be withdrawn up to the top position instead of getting down and the coolant flow was reduced by controlling the blowers.

Figure 6.2 shows the the relative power change during reactivity insertion simulation. The relative power starts to increases with increasing reactivity inserted by withdrawing the control rods. The temperature of the fuel as well as the moderator increases with relative power and due to the negative temperature reactivity coefficient, negative reactivity is inserted into the system. Initially, the positive reactivity inserted by control rods dominate over negative reactivity inserted by temperature reactivity coefficient and the relative power reaches some peak value. But after a few seconds when the temperature becomes very high, negative reactivity starts to dominate and relative power starts to decrease gradually. It shows

huge difference between the results obtained from a homogeneous and a heterogeneous assumption of the heat production inside the pebble fuel. For the case of the homogeneous assumption, the peak of the relative power is much higher since the fuel temperature does not show any significant change at initial few seconds and the negative reactivity due to temperature difference is small. But with the heterogeneous fuel model, the fuel kernel becomes very hot immediately after the insertion of the positive reactivity and the negative reactivity due to the temperature difference starts to dominate earlier. Figure 6.3 shows the temperature excursion profile during this fast transient. This temperature profile corresponds the power profile showed in figure 6.2. In the heterogeneous temperature model, fuel temperature is changed immediately with power and power excursion is restricted by negative temperature coefficient. But, in the homogeneous temperature model, the fuel temperature does not show any significant change for the initial few seconds and the power profile peak is much higher in this case.

Chapter 7

Validation against Experimental Benchmark

In order to validate TH3D against an experimental benchmark problem, an IAEA CRP-5 benchmark problem oriented to HTR-10 reactor is performed. This is an experimental benchmark performed with the HTR-10 reactor and regarded the steady state temperature distribution for a full power initial core as well as the loss of primary flow without scram and all control rods withdrawal without scram. The description of the benchmark and the calculated results with comparisons will be discussed in the coming sections.

7.1 HTR-10 Benchmark

The 10MW pebble bed high temperature gas-cooled reactor (HTR-10) was initially designed by SIEMENS and later on constructed and operated by the Institute of Nuclear Energy Technology (INET) [13]. This is an experimental reactor which is built for the purposes of gathering experiences on HTGR technology, irradiation testing of fuel elements, verifying inherent safety features of modular HTGRs. Figure 7.1 shows a vertical section of the primary loop. HTR-10 represents all main design and safety features of the modular high temperature gas-cooled reactor. The reactor core and steam generator are placed side-by-side and are installed into two separate pressure vessels which are connected by a connecting vessel in which a coaxial gas duct is placed. Inert helium is used as coolant and spherical fuel elements with coated particles are used as fuel. Fuel elements pass the core in a multi-pass pattern [13]. In order to control the reactor during operation, 10 control rods containing B4C are placed into the control rod channels at the side reflector and can be operated (can be inserted/withdrawn) either to maintain the reactor power level or to shutdown the reactor. An additional emergency shutdown system with small absorber balls known as SAS (Small Absorber Sphere) is available. These small balls are placed at the top of the reactor core and can be

dropped on demand by gravity into channels designed for these balls. Major design features are listed in Table 7.1.

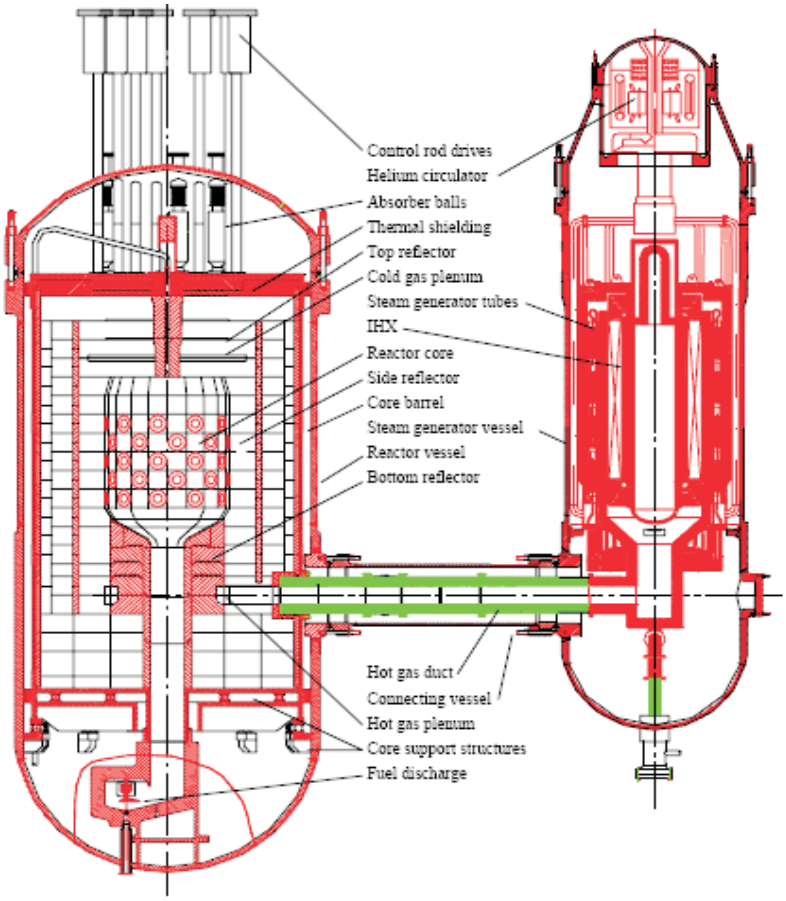

Figure 7.1: Axial section of HTR-10 reactor pressure vessel, steam generator, and connecting vessel [17].

7.1.1 Nominal Operation Case

The purpose of this benchmark is to calculate the HTR-10 reactor at nominal operation and compare the temperature distribution with experimental data. This case regards the temperature distribution of the pebble bed, the surrounding solid materials and the maximum temperature values of the main components. In this case, the initial core was composed of a mixture of fuel balls and dummy balls (containing only graphite) in a ratio of $57 : 43$ [12] and the reactor was operated at full power. The coolant helium enters at the inlet plenum with a mass flow rate of 4.32 kg/s. The average inlet temperature and the pressure of helium were 250°C

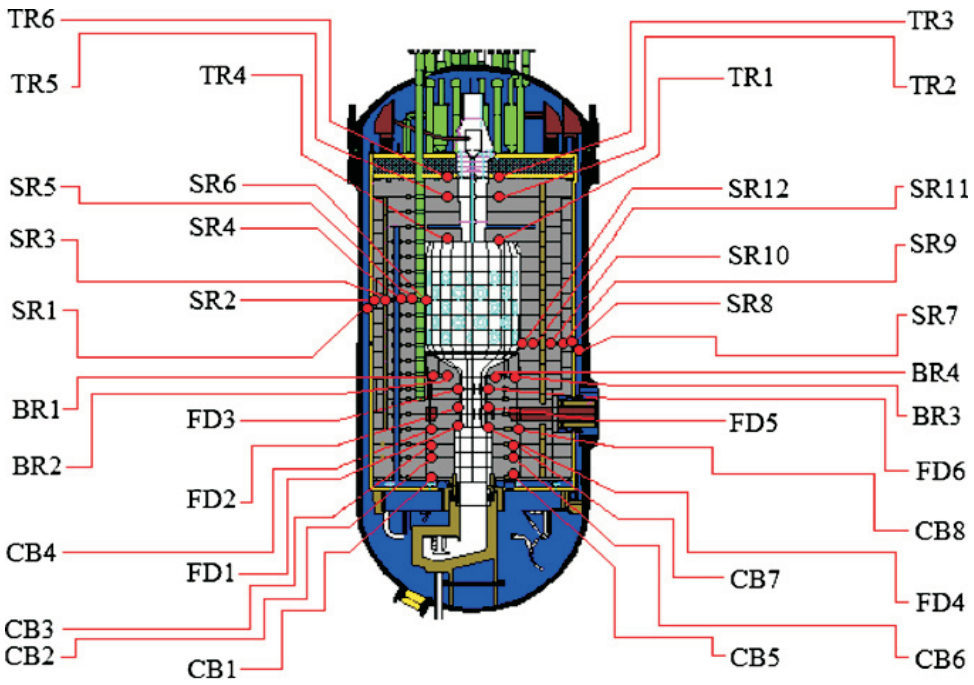

Figure 7.2: Axial cross-section of HTR-10 showing temperature measuring points [10].

Table 7.1: Main design parameters of the HTR-10 [17].

Description	**Unit**	**Value**
Reactor thermal power	MW	10
Reactor electric power	MW	3
Primary helium pressure	MPa	3
Reactor core diameter	cm	180
Average core height	cm	197
Average inlet coolant temperature	°C	250
Average outlet coolant temperature	°C	750
Helium mass flow rate at full power	kg/s	4.32

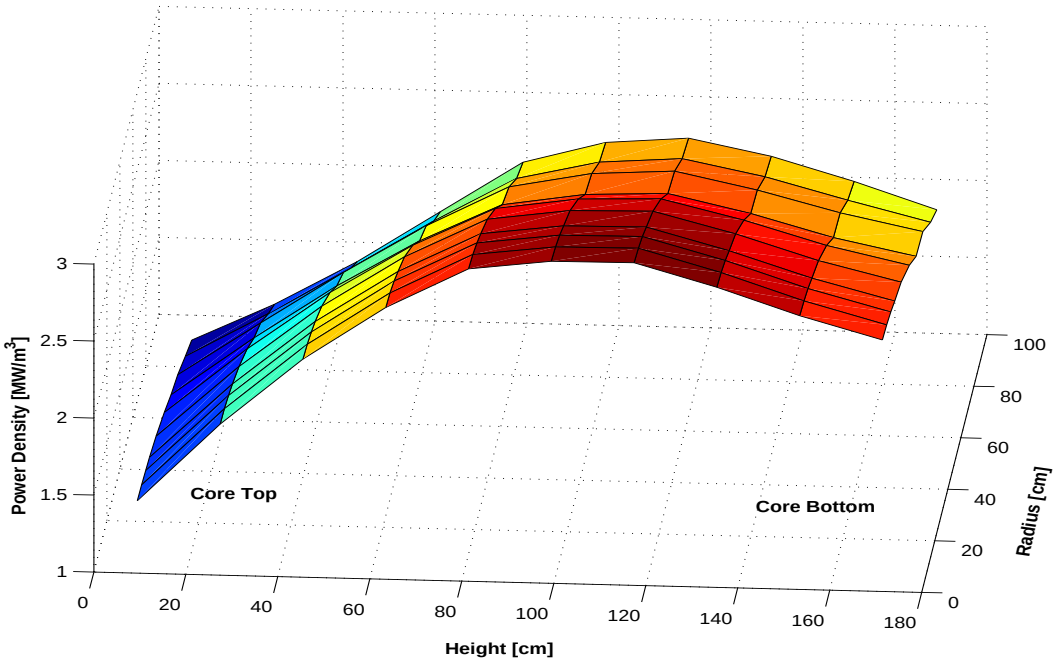

Figure 7.3: Steady state power density profile calculated by ZIRKUS code.

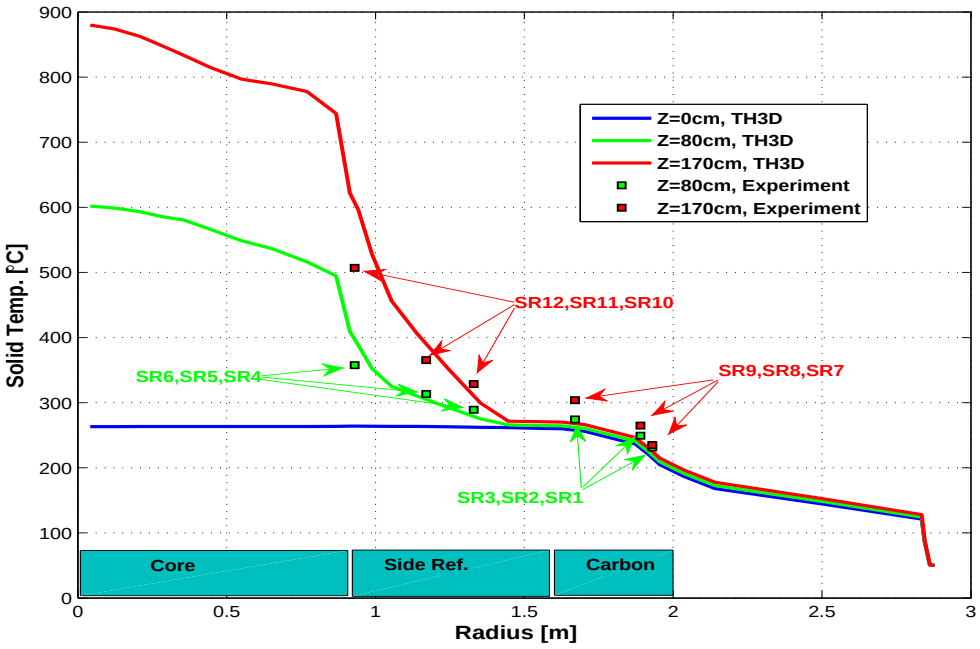

Figure 7.4: Radial solid temperature profile at nominal operation.

and 30 bar respectively and helium leaves the outlet plenum with an average temperature of 700C°. Figure 7.3 shows the power distribution calculated by ZIRKUS [7] according to the benchmarks definitions.

After entering the reactor pressure vessel (RPV), helium flows downwards through the annular gap in between RPV and core barrel. At the bottom of the RPV, flow direction is changed and flows upwards. In the thermal hydraulic calculation, all leakages and by-passes are considered according to the benchmark definition. It is assumed in benchmark that 1% of total coolant flow (1% of 4.32 kg/s) enters at the bottom of the fuel discharging tube and meets with the core flow after cooling the fuel elements in the discharging tube [13]. Most of the coolant enters into the coolant channels placed in the side reflector after cooling the bottom support structures of the reactor. The coolant is collected in the cold coolant plenum at the top of the side reflector. From the cold plenum, 2% of total coolant flows through the control rod channels and cool the control rods. Through the control rod channels, this portion of the helium flows down to the bottom of the bottom reflector and merge with the core helium flow at the small plenum located at the bottom reflector. Some part of the helium by-passes the main flow path due to the presence of gaps among the graphite blocks. According to the benchmark, 10% of total coolant is considered as by-passes. It is assumed that mentioned 10% by-passes do not play any role for cooling the core and flow directly from cold helium entry to hot helium exit. So, only 87% of the total coolant flows (87% of 4.32 kg/s) through the pebble bed core as an effective coolant [13].

In nominal operation, almost all heat produced in the core is carried away by the coolant and only a small portion of the heat is removed by the reactor cavity cooling system (RCCS). The average water temperature in the RCCS is taken as 50°C during nominal operation according to the benchmark and set as the radial boundary condition. The concrete temperature placed at the top and bottom of the reactor is taken as 50°C and set as the top and bottom boundary condition. The material properties of helium, fuel element, reflector graphite, carbon bricks, etc are taken from benchmark definition as it is recommended. The correlation used for heat transfer coefficient and pressure drop calculation are taken from KTA standard [27] [26]. The effective heat conductivity of the pebble bed was calculated according to the Zehner and Schlünder [54] model up to 1300°C and provision for Robold [40] model was available beyond 1300°C though the maximum temperature never reached this limiting value for this calculation.

Figure 7.4 shows the radial solid temperature profile at different heights and comparison with available experimental data. In this benchmark experiment, solid temperature was measured only at some fixed points (in side reflector, bottom carbon bricks, top reflector, small hot helium plenum, fuel discharging tube) and the positions of the measured points are shown in Figure 7.2. The calculated temperature shows good agreement though there are some big differences especially at the interface of core and side reflector (SR12, SR6) and at surface of the fuel discharg-

ing tube (FD3, FD6). The maximum deviation is observed at the interface of the pebble core and the solid side reflector (SR12, SR6). The reason could be the relative higher porosity formed at the boundary between core and side reflector which is not considered in the calculation. Another reason for this variation could stem from the simulation of flow (e.g. difference in heat transfer co-efficient, pressure drop calculation, etc) in control rod and coolant channels placed in side reflector. Instead of simulating each channel explicitly, these regions are also simulated as porous media and all properties are taken by averaging over the control volume. This could be another reason for this deviation.

Figure 7.5 shows the radial solid temperature profile at small helium plenum and compared with experimental results. Calculated results show very good agreement with the experimental results. Figure 7.6 shows the axial temperature profile at radius = 50cm and comparison with experimental data measured at the bottom carbon bricks. Also in this case, calculated results show very good agreement with experiment. Figure 7.7 shows the axial solid temperature profile at radius = 26cm (at the fuel discharging tube's surface) and compared with the experimental data measured at the surface of the fuel discharging tube. Calculated results at two bottom locations (FD1/FD5, FD2/FD5) show very good agreement but the value at the top location (FD3/FD6) shows large difference with experimental value. The reason could be the difference in flow pattern at that region. It might be the case that forced cooling was partially absent at the measured location due to some blockage but in simulation it was not the case.

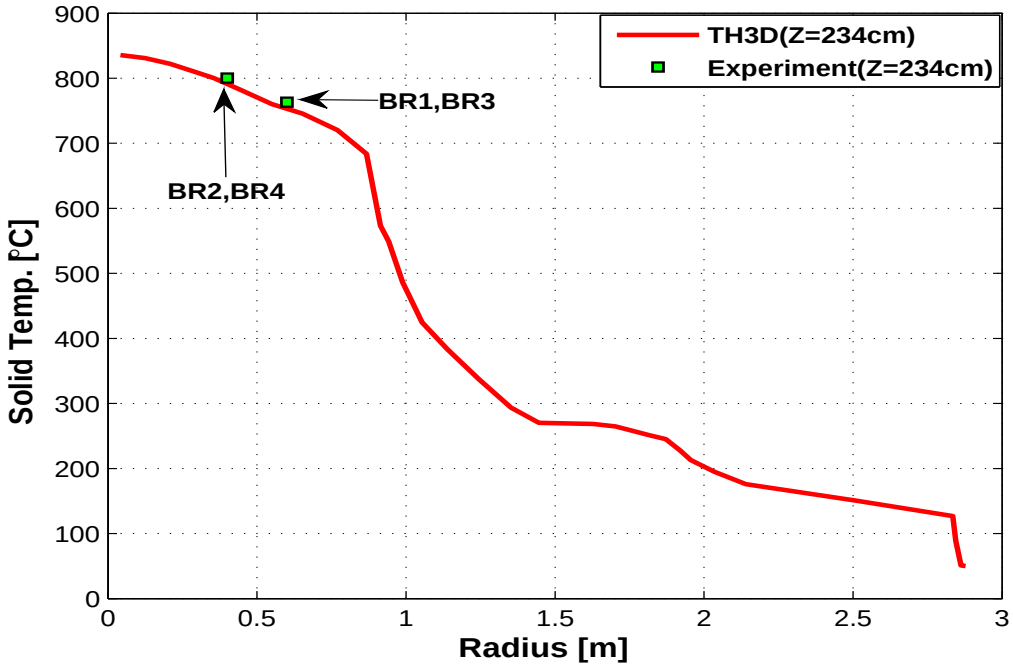

Figure 7.5: Radial solid temperature at small hot helium plenum during nominal operation.

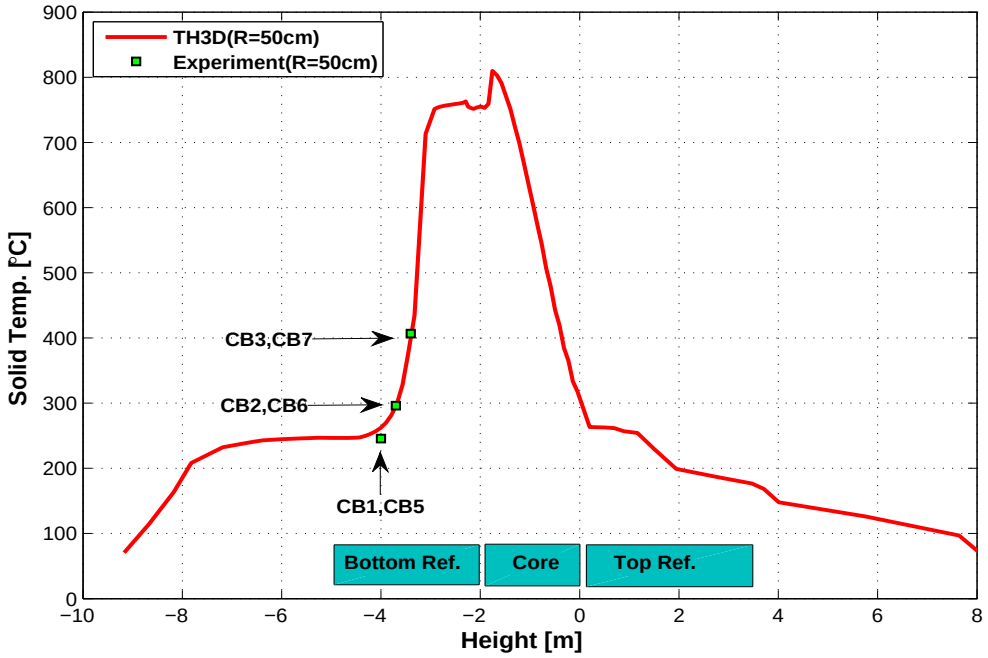

Figure 7.6: Axial solid temperature at R=50cm during nominal operation.

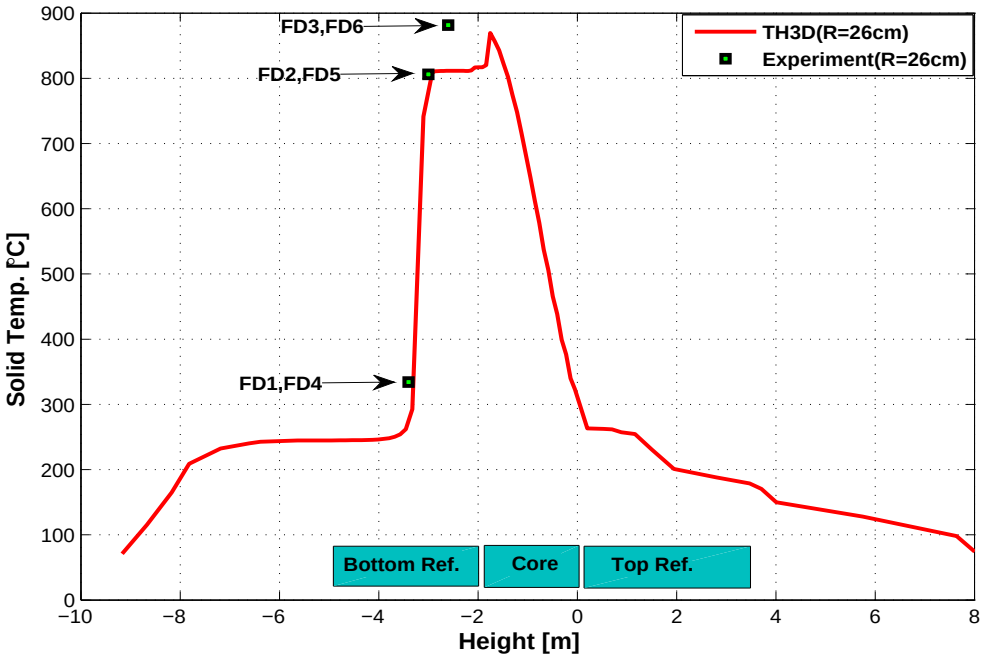

Figure 7.7: Axial solid temperature at R=26cm during nominal operation.

7.1.2 Loss Of Forced Cooling without Scram (LOFC)

This is the case where the primary loop helium blower is switched off during nominal operation. This experiment is performed to show the safety feature of the reactor in an accident case where primary coolant flow is absent but the control rods failed and remain at the nominal operational position. Before starting the experiment, the reactor is operated at a power of 30% of full power (i.e. 3MW). During nominal operation with partial load, the reactor inlet and outlet helium temperatures are 250°C and 650°C respectively and the inlet pressure is kept at 2.5 MPa [12]. According to the benchmark description, the reactor is operated for approximately 3000 MW-hour and the xenon equilibrium state is achieved before the start of the transient [12]. Nominal power density with partial load and the decay heat during transient is taken from the benchmark description [12] and the boundary condition is considered the same as it is described for nominal operation case with full power.

The transient case is started by switching off the primary helium circulator. After switching off the helium circulator, primary flow does not decrease instantly but decreases gradually due to its mechanical inertia. After 12 seconds, the reactor protection system detects a signal of ”ratio of water flow to helium flow is high” and secondary circuit is isolated from primary system by the reactor protection system. At the same time, the blower baffle was closed and primary helium flow

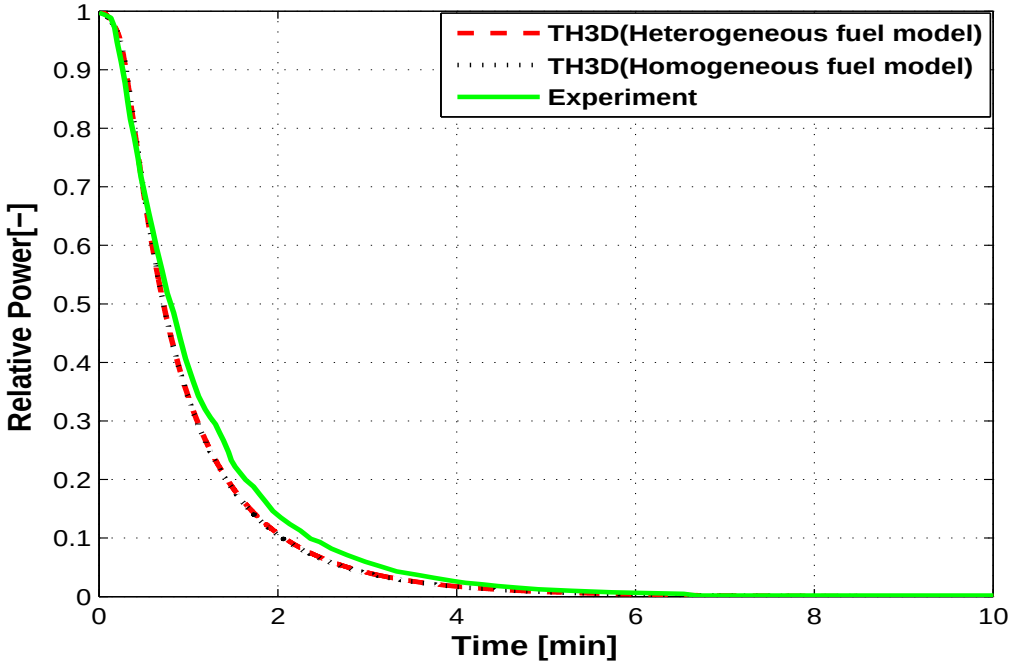

Figure 7.8: Reactor power transient response during LOFC for short time.

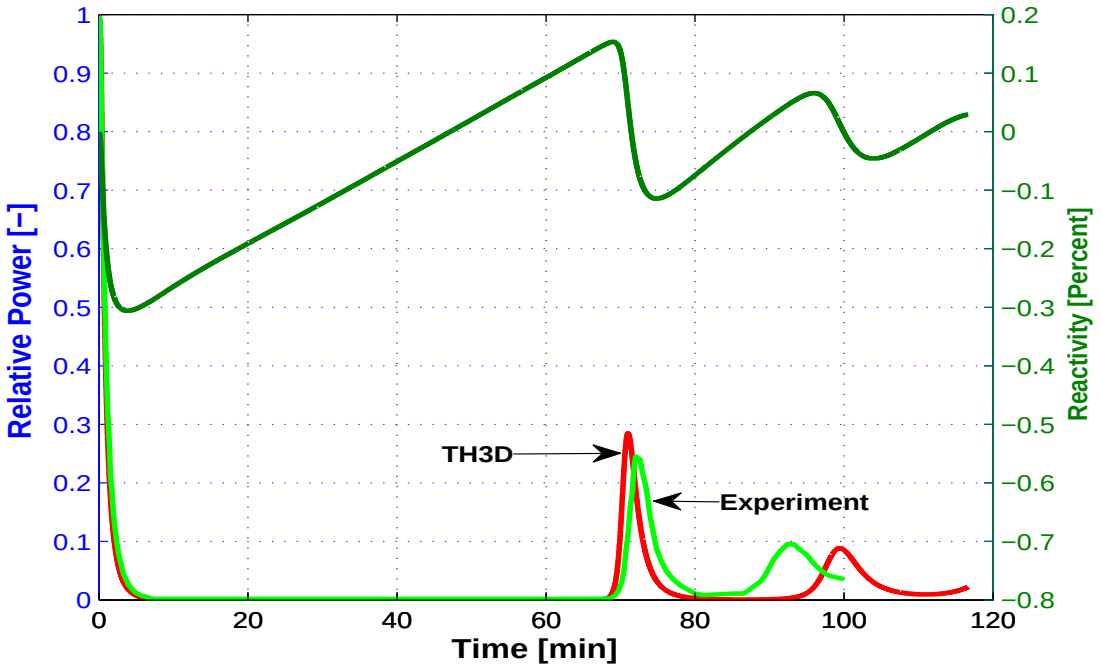

Figure 7.9: Reactor power transient response and total reactivity during LOFC for long time.

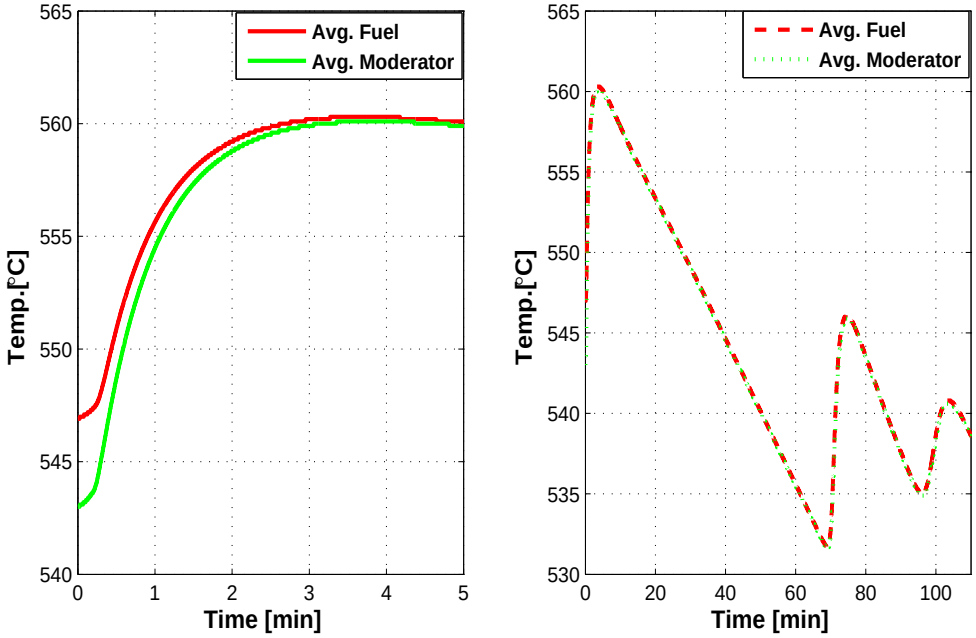

Figure 7.10: Average fuel and average moderator temperature response during LOFC for short (left) and long time.

rate was decreased to zero. It is assumed that these actions are performed very quickly. In our calculation, it is assumed that the primary helium flow for initial 12 seconds is reduced according to the blower speed [10] and stopped completely at t=20s. All neutronics parameters (e.g. fraction of delayed neutron, generation time, reactivity coefficients, etc) are taken from benchmark definition in this calculation [12]. The TH3D code was coupled with a point kinetics model for getting neutronics-thermal hydraulic feedback.

Figure 7.8 and Figure 7.9 show the reactor power transient response during LOFC accident for short and long time period, respectively. After initiation of the transient, the reactor temperature starts to increase due to the lack of forced cooling (see Figure 7.10). Reactor power starts to decrease due to the negative reactivity coefficient of fuel and moderator. At the beginning, positive reactivity coefficient of reflector does not play any role since the reflector temperature does not change within this short time. Continuous negative reactivity inserted by increasing fuel and moderator temperature drives the relative power to a very small value and after approximately 5 minutes, the decay heat is the only source of heat production.

The comparison between calculated and experimental results (Figure 7.8, Figure 7.9) shows good agreement. The small difference observed at the early stage of the transient between the results could be the effect of the mass flow rate at the initial

few seconds, material properties and point kinetics model itself. It is mentioned in benchmark description that the reactor protection system was activated at t=12 seconds and the blower baffle was closed and the primary flow in the reactor core was reduced to zero very rapidly. But how rapidly the flow in the core was reduced to zero is not available. The relative power profile initially varies strongly with the mass flow rate in the core. The time to reduce the primary mass flow to zero and its changing rate in calculation could be different from experiment and could be the reason for the differences between the results in the short time profile. Moreover, the used point kinetics model is a very simple model and therefore might not be accurate enough for getting neutronics-thermal hydraulics feedback and could produce this difference.

A detailed fuel model (heterogeneous temperature model) is available in TH3D where heterogeneity of heat production in the pebble fuel can be considered. Option is made for using either heterogeneous or homogeneous model where heat source is considered homogeneous. The detailed model and its implementation are described in chapter 4.3. For this transient case, both heterogeneous and homogeneous fuel model are used to calculate the problem. This is a slow transient in respect of reactivity change which depends on temperature change, xenon built-up, etc. The time of change of reactivity is higher than the relaxation time for the temperature adjustment between fuel kernel and its surrounding graphite. So, the fuel kernel and surrounding graphite matrix experience almost the same temperature and a detailed fuel mode (heterogeneous model) produces no difference in respect to a homogeneous model where the heat source is considered as homogeneous (see figure 7.8, figure 7.10). In the case of a fast transient, these two models produce a huge difference (see chapter 6.2.3).

At nominal operation, the bottom part of the reactor experiences higher temperature and the helium at the bottom part of the core becomes hotter and lighter. Hence, a natural convective loop is developed when primary coolant is stopped. Due to the buoyancy effect, helium gas rises up through the middle of the core, heats up the upper part of the reactor, flows downward along the boundary between the core and the side reflector blocks, releasing heat to the side reflectors. Side reflectors are cooled down by loosing heat radially. A very small part of the heat is released also in the axial direction at the top and bottom boundaries.

Since the HTR-10 is a small reactor, the reactor temperature decreases quickly which makes the reactor critical again (see figure 7.9 and figure 7.10) and produces again a significant amount of heat. During experiment, the first peak after re-criticality reaches at a maximum value at 4400 seconds (73.33 minutes) after the initiation of the test and the maximum value is 24.7% of the initial value [10]. But in our calculation, the first peak reaches at a maximum value at 4261 seconds (71 minutes) after the initiation of the test with a maximum value of 28.4% of the initial value (Figure 7.9). The re-criticality occurs much earlier than the first peak and in our calculation the re-criticality obtained at 2830 seconds (47.17 minutes).

The calculated results show very good agreement with the experiment and the small differences could be the results of the xenon built-up calculation, decay heat calculation, boundary conditions set in the calculation, material properties of the components used in the reactor, etc. Significant amount of heat produced by re-criticality increases the fuel and moderator temperature again. Increased temperature produces negative reactivity again and decreases the reactor power. The oscillation of the power peak is observed several times until it shows a quasi-steady behavior.

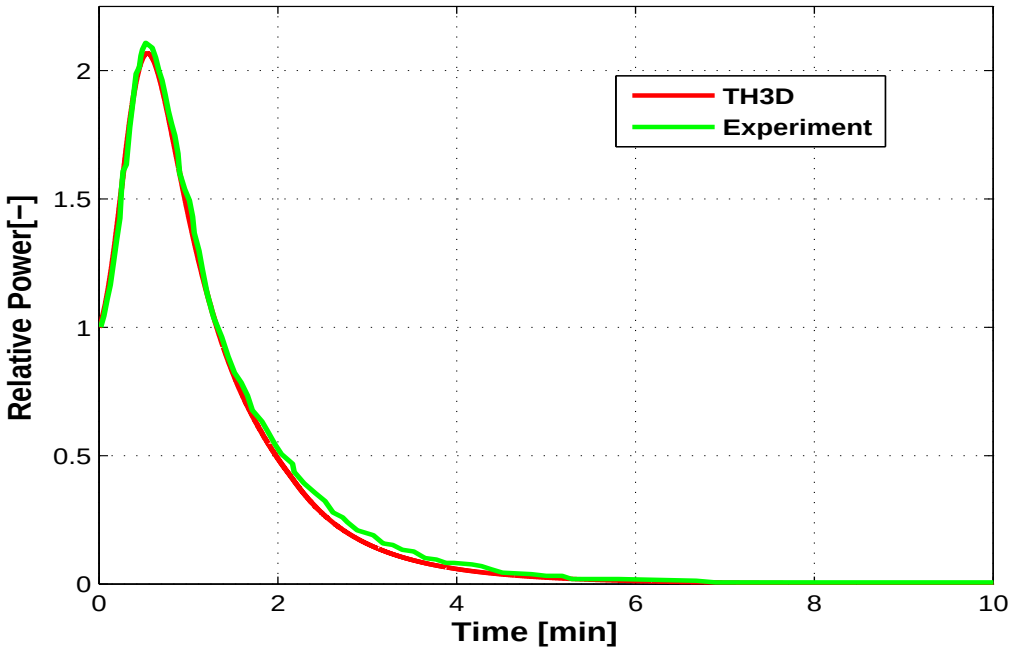

Figure 7.11: Reactor power transient response during CRW for short time.

7.1.3 Control Rod Withdrawal without Scram (CRW)

In this experiment, the reactor safety is demonstrated against reactivity insertion in the reactor by withdrawing all control rods. Also in this transient case, the reactor was operated at 30% of full power (i.e. 3MW). During nominal operation with this partial load, the reactor inlet and outlet helium temperatures are 250°C and 650°C respectively and the inlet pressure is kept at 2.5 MPa [12]. The control rods were withdrawn at operational speed (1cm/sec) [22] and inserts total reactivity $5 * 10^{-3}\Delta$k/k within 125 sec in the reactor. The reactivity insertion rate is taken from benchmark descriptions. Due to the inserted reactivity, the reactor power starts to increase and thus the fuel and moderator temperature. After 12 seconds, the reactor protection system detects a signal of "power increasing rate is high" and secondary circuit is isolated from primary system by the reactor protection system. At the same time, the blower baffle was closed and primary helium flow rate was quickly decreased to zero.

Figure 7.11 and Figure 7.12 show the transient power response during CRW-event for short and long time respectively. Increasing fuel and moderator temperature resulting from power surge inserts negative reactivity into the reactor. At the beginning, the inserted positive reactivity dominates the negative reactivity and the reactor power increases quickly. Reactor power continues to increase (initial 32 seconds) as long as the negative reactivity due to the increased temperature

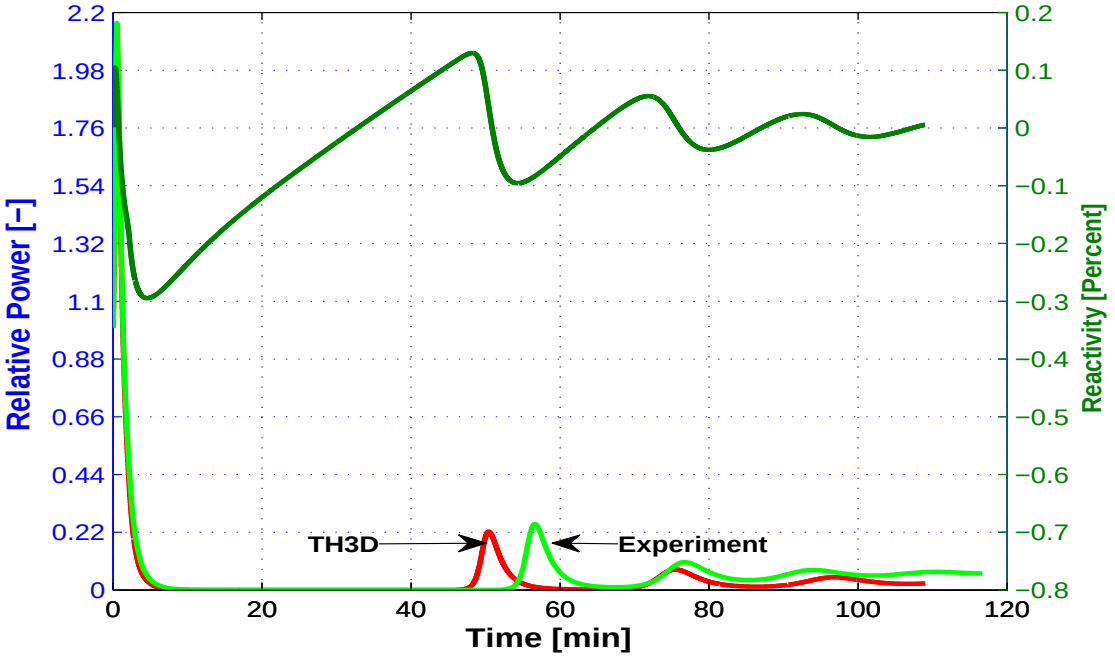

Figure 7.12: Reactor power transient response and total reactivity during CRW for long time.

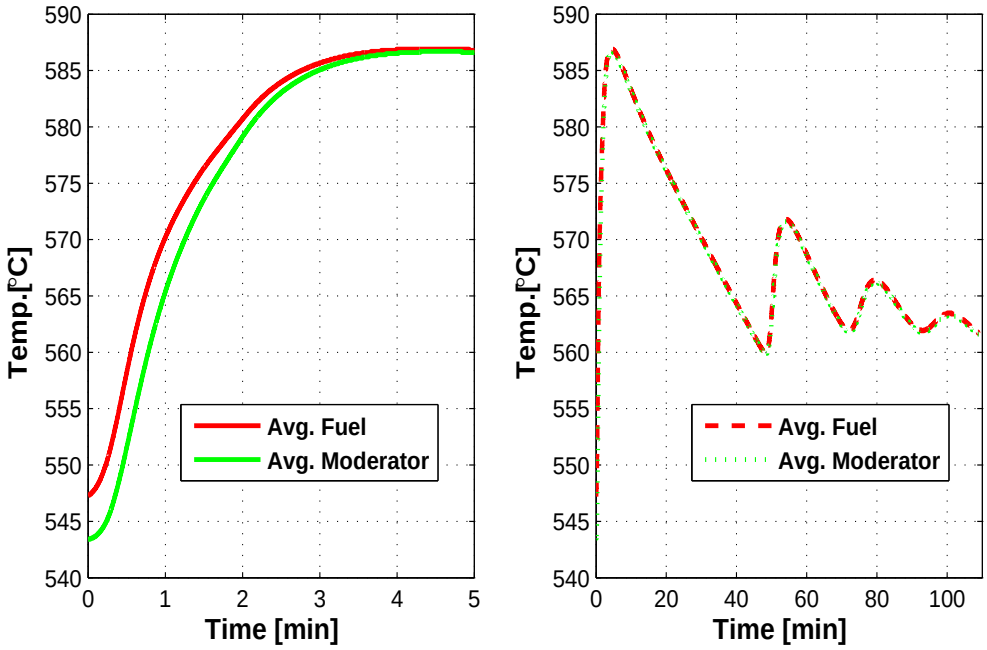

Figure 7.13: Average fuel and average moderator temperature response during CRW for short (left) and long time.

starts to dominate and reaches to a maximum value. Calculated result shows very good agreement with experimental results at the initial stage of the transient (see Figure 7.11).

After 32 seconds, the reactor power starts to decrease due to the dominance of negative reactivity and the reactor becomes sub-critical. Within less than 5 minutes, the reactor power reaches to a very small value and only decay power is the available heat producing source. Like the LOFC case, the re-criticality is observed also in this case due to the similar phenomenon described for the LOFC case. The re-criticality is observed earlier in this case than the LOFC because of the inserted reactivity by the withdrawn control rods. Calculated result shows very good agreement also for the long term transient (see Figure 7.12). Also in this case, re-criticality is observed few minutes earlier than in the experiment. This difference could be the results of the xenon built-up calculation, decay heat calculation, boundary conditions set in the calculation, material properties of the used material in the reactor.

Chapter 8

Summary and Conclusion

Due to the growing interest in nuclear energy as a viable source of energy in the total energy mix which comes from any non-greenhouse-gas-producing sources, interests are also growing for building more efficient, safe, robust reactors for future generation. Due to the inherent safety features available in modular high temperature reactors (HTRs) along with its very high outlet coolant temperature, interests are growing for this type of reactor as a source of electricity, hydrogen, etc. In order to enhance the safety features of the reactor and making nuclear energy more competitive, reliable tools need to be developed. Available tools used so far for design and safety analysis of HTRs offer 2-D thermal hydraulics. Nowadays 2-D thermal hydraulics calculation seems not adequate enough for addressing three dimensional problems arising in HTRs while available computing capacities allow us addressing 3-D situations.

The possible 3-D situations which could arise in HTRs are described in Chapter 2. It is quite clear that a 2-D cylindrical approximation of those situations could create results which are not accurate enough for designing next generation reactors. The thermal hydraulic factors which influence the reactor thermal behavior and must be addressed carefully are described in Chapter 3. For calculating the thermal hydraulic behavior, the mass flow rate, component porosity, hydraulic diameter, material properties of solid and gas, emissivity of fuel elements, neutron fluence are the most important parameters. Error in any of the mentioned factors could produce unacceptable results in thermal hydraulic calculation and thus in neutronics calculation.

Keeping the simulation time in mind and the intention to capture the possible 3-D effects, the new code TH3D is developed in the present work. Thermal non-equilibrium between solid and gas phase is considered and the physical model of this code is based on the porous media approach. Instead of considering each and every detail of a component (e.g. each pebble, coolant channel, top void, pores, etc), all properties are defined by averaging over the control volume obtained from spatial discretization of the reactor. All phases (e.g. solid, gas) are considered as continuum. The mathematical equations and the numerical procedures are

described in Chapter 3. The time dependent mass and energy conservation equations and simplified steady-state momentum conservation equation obtained from porous media approximation are solved for the coolant gas along with the time dependent energy conservation equation for the solid. The interaction between solid and gas phase is made by implementing a set of constitutive equations (e.g. heat transfer co-efficient, pressure drop, etc).

Finite volume method is used for spatial discretization of the conservation equations. The discretization of the equations can be made for 3D cartesian or cylindrical co-ordinate systems. Time marching integration is done by backward differentiation formula (BDF) method. BDF is a stable, fully implicit, multi step method which calculates the time step size automatically depending on previous convergence history. Non linear equations produced from implicit BDF method are solved by using modified Newton method. For solving the linear system of equations obtained from Newton method both direct and iterative solvers are available.

The basic capability of the program to simulate 3D situation was demonstrated by calculating a situation where three neighboring control rods were withdrawn while other rods were inserted. For the case of withdrawing three neighboring control rods, gas temperature at core exit varies around $50^{\circ}C$ in angular direction while radial variation is around $60^{\circ}C$. This angular variation could create more problems for mixing gas in the mixing zone which is already problematic with radial variation of temperature. So, a 3D calculation of HTRs for a 3D situation in any case could be justified for next generation reactor design. 3D sample calculation results show the basic capability of TH3D to capture the 3D effects which could create in HTRs though the results could not be verified due to the lack of 3D benchmarks.

In order to show the capability of TH3D for simulating pebble type fuel reactors, a 2D benchmark which was proposed by OECD/NEA/NSC and was oriented to PBMR-400 was calculated. In order to validate the results, the calculation results obtained from TH3D were compared with the results obtained from THERMIX/KONVEK for the same benchmark calculation. Comparisons of 2D results between TH3D and the well established thermal-hydraulics code THERMIX/KONVEK have shown very good agreement.

For showing the capability of TH3D for simulating block type reactors, an IAEA CRP-3 benchmark which is oriented to the Gas Turbine Modular Helium Reactor (GT-MHR), was calculated. This is also a 2D benchmark problem and several simplifications were made in the benchmark descriptions. The results obtained from TH3D for this benchmark calculation were compared with the results obtained from different countries participated in the CRP-3 benchmark program by using different code system. Also in this case, results obtained from TH3D show good agreement with other programs and shows its capability to simulate the block type

of reactor.

For getting the thermal-hydraulics/neutronics feedback, accurate fuel, moderator, and reflector temperature calculation is very essential. A detailed fuel model for pebble type fuel element is implemented where heterogeneity of heat production is considered in order to get the accurate fuel and moderator temperature. The implemented fuel model is described in Chapter 3. Though the assumption of homogeneous heat production makes little difference (around $10^\circ - 20^\circ C$ for fuel temperature) for steady state calculation, the assumption of the heterogeneous heat production makes big difference for the cases of quick transients. In order to show the capability of TH3D to couple with a neutronics program (to get the feed back of neutronics and thermal hydraulics), the program was successfully coupled with a point kinetics model. This is an internal coupling where point kinetics model is implemented inside the TH3D program. This coupling is taken as a basic test of TH3D's capability to couple with more sophisticated model which considers both space and time. In order to check the stability of the coupling, a situation of fast reactivity insertion was simulated by withdrawing all control rods quickly. The results of this coupling are described in chapter 6. It shows that TH3D is capable to be coupled with a neutronics program even in the case of a very fast transient.

In order to validate TH3D against an experimental benchmark problem, an IAEA CRP-5 benchmark problem oriented to HTR-10 reactor is performed. This is an experimental benchmark performed on the HTR-10 reactor and regarded the steady state temperature distribution for full power initial core as well as loss of primary flow without scram and control rod withdrawal without scram transients. All three cases are calculated by using TH3D and the obtained results with comparisons are presented in Chapter 7. Results show very good agreement during nominal operation as well as for transient cases. For transient, the program is coupled with point kinetics model. The results show again the capability of TH3D for simulating slow transients. It can be seen that even point kinetics gives very good neutronics feedback when thermal hydraulics behavior is well predicted.

Finally, TH3D, the newly developed 3D thermal hydraulic tool, is ready to be used for pebble bed type as well as for block type fuel reactors and can be used for simulating three dimensional problems as well as two dimensional problems. More comparison calculations for some other benchmarks are planned, as well as a coupling with a 2D/3D space kinetic neutronics tool is also planned.

Bibliography

[1] Ali Abou-Sena, Alice Ying, and Mohamed Abdou. Experimental measurements of the effective thermal conductivity of a lithium titanate (li_2tio_3) pebbles packed bed. *Journal of Materials Processing Technology*, 181:206–212, 2007.

[2] Elmar Achenbach. Druckverlust von durchströmten Kugelschüttungen bei hohen Reynolds-Zahlen. *Chem. Eng. Technol.*, 54:66–67, 1982.

[3] Uri M. Ascher and Linda R. Petzold. *Computer methods for ordinary differential equations and differential-algebraic equations*. Society for Industrial and Applied Mathematics, Philadelphia, 1998.

[4] J. Banaschek. *Berechnungsmethoden und Analysen zum Dynamischen Verhalten von Kraftwerksanlagen mit Hochtemperaturreaktor*. Dissertation, RWTH Aachen, Germany, 1983.

[5] S. Becker and E. Laurien. Three-dimensional numerical simulation of flow and heat transport in high-temperature nuclear reactors. *Nucl. Eng. Des.*, 222:189–201, 2003.

[6] R. F. Benenati and C.B. Brosilow. Void fraction distribution in beds of spheres. *A.I.Ch.E.J.*, 8(6):233–236, 1962.

[7] W. Bernnat and W. Feltes. Models for reactor physics calculations for HTR pebble bed modular reactors. *Nucl. Eng. Des.*, 222:331–347, 2003.

[8] L. Binkele, O. Hartleib, and W. Biergans. *Waermeleitfähigkeit und spez. el. Widerstand neutronenbestrahlter Graphite in Abhaengigkeit von der Temperatur*. Internal report, KFA-IRW-IB-13/75, first edition, June 1975.

[9] P.C. Carman. Fluid Flow through Granular Beds. *Trans. Inst. Chem. Engrs.*, 15:150–166, 1937.

[10] F. Chen, Y. Dong, Z. Zhang, Y. Zheng, L. Shi, and S. Hu. Post-test analysis of helium circulator trip without scram at 3 MW power level on the HTR-10. *Nucl. Eng. Des.*, 239:1010–1018, 2009.

[11] D.B. Pelowitz. *$MCNPX^{TM}$ User's Manual, Version 2.5.0*. Los Alamos National Laboratories, LA-CP-06-0369, 2005.

[12] Y. Dong. HTR-10 benchmark definitio: RCM-7 of CRP-5 on evaluation of High Temperature Gas-Cooled Reactors. *Vienna, Austria, Sep. 25-29*, 2006.

[13] Y. Dong and Y. Sun. Benchmark problem of the HTR-10 steady state temperature distribution for full power initial core. *Institute of Nuclear Energy Technology, Tsinghua University, Beijing, China*, 2003.

[14] EIA. International Energy Annual 2004. *Energy Information Administration (EIA)*, 2006.

[15] D. Emendörfer and K.H. Höcker. *Theorie der Kernreaktoren, Band 1: Der stationäre Reaktor*. Wissenschaftsverlag, 1982.

[16] D. Emendörfer and K.H. Höcker. *Theorie der Kernreaktoren, Band 2: Der instationäre Reaktor*. Wissenschaftsverlag, 1993.

[17] W. K. Terry et al. Evaluation of the initial critical configuration of the HTR-10 pebble-bed reactor. *HTR10-GCR-RESR-001, NEA/NSC/DOC*, 2006.

[18] Henri Fenech. *Heat transfer and fluid flow in nuclear systems*. Pergamon Press Inc., first edition, 1981.

[19] Michael A. Fütterer. The european union's (very) high temperature reactor technology project. In *Proceedings of the ICAPP06, Reno, NV*, June 2006.

[20] H. Haque, W. Feltes, and G. Brinkmann. Thermal response of modular high temperature reactor during passive cooldown under pressurized and depressurized conditions. *Nucl. Eng. Des.*, 236:475–484, 2006.

[21] J.P. Holman. *Heat transfer*. McGraw-Hill Publication., ninth edition, 2002.

[22] S. Hu, R. Wang, and Z. Gao. Safety demonstration tests on htr-10. In *Proceedings of HTR-2004 Conference, Beijing, China*, September 2004.

[23] IAEA DOE. *Heat transport and after heat removal for gas cooled reactors under accident conditions*. IAEA, VIENNA, 2000.

[24] Tatjana Jevremovic. *Nuclear Principles in Engineering*. Springer, 2005.

[25] KTA. *Auslegung der Reaktorkerne von Hochtemperaturreaktoren, Berechnung von Heliumstoffwerten*. KTA3102.1, 1978.

[26] KTA. *Auslegung der Reaktorkerne von gasgekühlten Hochtemperaturreaktoren, Reibungsdruckverluste in Kugelhaufen*. KTA3102.3, 1981.

[27] KTA. *Auslegung der Reaktorkerne von gasgekühlten Hochtemperaturreaktoren, Waermeübergang im Kugelhaufen*. KTA3102.2, 1983.

[28] K. Kugeler and R. Schulten. *Hochtemperaturreaktortechnik*. Springer Berlin, Heidelberg, New York, first edition, 1989.

[29] M.P. LaBar and A.S. Shenoy. The gas-turbine modular helium reactor. *General Atomics, San Diego, California*, 2003.

[30] G. Lohnert. Technical design features and essential safety related properties of the HTR-module. *Nucl. Eng. Des.*, 121:259–275, 1990.

[31] G. Lohnert. How to obtain an inherently safe power reactor. *EURO Course 2007, IKE, Universität Stuttgart*, 2007.

[32] N.G. Kuzavkov. *CRP-3 Benchmark Problem Description for GT-MHR Pu Burner Accidents, Supplementary information on the benchmark problem*. OKBM, Dec. 1997.

[33] U.S. Department of Energy. *DOE fundamentals handbook, Nuclear Physics and Reactor Theory*. U.S. Department of Energy, Washington, D.C., 1993.

[34] PBMR. *CRP-5 Benchmark definition: PBMR-400 Neutronics and thermal-hydraulics description*. PBMR, South Africa, Doc. Num. 022017, first edition, Dec. 2003.

[35] K. Petersen. *Zur Sicherheitskonzeption des Hochtemperaturreaktors mit natürlicher Wärmeableitung aus dem Kern im Störfall*. Dissertation, RWTH Aachen, Germany, 1984.

[36] R.J. Price. *Review of the thermal conductivity of nuclear graphite under HTGR conditions*. GULF general atomic company, California, first edition, Sep. 1973.

[37] T. Rademer, W. Bernnat, and G. Lohnert. Coupling of neutronics and thermal-hydraulics codes for the simulation of transients of pebble bed htr reactors. In *Proceedings of the HTR-2004 Conference, Beijing, China*, page C32, Sept 2004.

[38] F. Reitsma. *PBMR Coupled Neutronics/Thermal Hydraulics Transient Benchmark the PBMR-400 Core Design*. PBMR Company Ltd., South Africa, first edition, 2004.

[39] H. Reutler and G. Lohnert. Advantages of going modular in HTRs. *Nucl. Eng. Des.*, 78:129–136, 1984.

[40] K. Robold. *Wärmetransport im Inneren und in der Randzone von Kugelschütungen*. Dissertation, RWTH Aachen, Germany, 1982.

[41] N. Ben Said, G. Lohnert, M. Buck, and W. Bernnat. The impact of design on the decay heat removal capabilities of a modular pebble bed HTR. *Nucl. Eng. Des.*, 236:648–656, 2006.

[42] Nader Ben Said. *Thermohydraulische Analysen für das Betriebs- und Nachwärmeabfuhrverhalten modularer Hochtemperaturreaktoren mit verschiedenen Kernkonfigurationen*. Dissertation, IKE, Universität Stuttgart, Germany, 2006.

[43] W. Schenk, D. Pither, and H. Nabielek. Fission product release profiles from spherical HTR fuel elements at accident temperatures. *Kernforschungsanlage Jülich*, September 1988.

[44] E.U. Schlünder. Wärme - und Stoffübertragung zwischen durchströmten Schüttungen und darin eingebetteten Einzelkörpern. *Chemie. Ing. Technik.*, 38(9):967–979, 1966.

[45] Siemens. *ZKIND Manual*. Siemens AG, Power Generation Group(KWU), first edition, 1980.

[46] S.J. Ball. *CRP-3 Benchmark Problem Description for GT-MHR Pu Burner Accidents*. Oak Ridge National Laboratory, Feb. 1997.

[47] S.J. Ball. *CRP-3 Benchmark Problem Description for GT-MHR Pu Burner Accidents, Supplementary information on the RCCS Design*. Oak Ridge National Laboratory, April 1997.

[48] E. Tsotsas and H. Martin. Thermal conductivity of packed beds: A review. *Chem. Eng. Process*, 22:19–37, 1987.

[49] U.S.DOE. *A Technology Roadmap for Generation IV Nuclear Energy Systems*. Nuclear Energy Research Advisory Committee and the Generation IV International Forum, 2002.

[50] VDI-Wärmeatlas. *Berechnungsblätter für den Wärmeübergang Auflage*. Springer Verlag, 2002.

[51] D. Vortmeyer. *Wärmestrahlung in Kugelschüttungen*. Fortschrittsbericht des VDI, first edition, March 1966.

[52] S. Yagi, D. Kunii, and N. Wakao. Studies on axial effective conductivities in packed beds. *A.I.Ch.E.J.*, 6(4):373–381, 1960.

[53] P. Zehner and E.U. Schlünder. Thermal conductivity of granular materials at moderate temperatures. *Chem. Inngr. Tech.*, 42:933–941, 1970.

[54] P. Zehner and E.U. Schlünder. Einfluß der Wärmestrahlung und des Druckes auf den Wärmetransport in nicht durchströmten Schüttungen. *Chem. Eng. Technol.*, 44(23):1303–1308, 1972.

Institut für Kernenergetik und
Energiesysteme

Universität Stuttgart

Pfaffenwaldring 31

D-70550 Stuttgart